



UNIVERSITY OF
LEICESTER

THESIS

**Decentralized Anti-Windup Compensator
Designs for Small Unmanned Aerial Vehicles**

by

Nkemdilim OFODILE

Supervisor: **Matthew C TURNER (Prof.)**

*A thesis submitted in fulfilment of the requirements
for the degree of Doctor of Philosophy*

in the

Control Systems Research Group

Department of Engineering

University of Leicester

MAY 2017

Abstract

This thesis studies the design and implementation of anti windup compensators for UAVs with magnitude and rate saturated actuators. The focus is on two types of UAVs; a Quadrotor UAV and a Fixed wing UAV. Decentralized anti-windup compensators are designed to address the problem of magnitude saturation in Quadrotor UAVs. The developed anti-windup compensators are founded on an LMI-based approach previously used in literature to provide global stability guarantees with some level of performance guarantees.

The work on the decentralized anti-windup compensators for Quadrotor UAVs are further improved on by replacing the use of LMIs in the determination of the anti windup compensator parameters with approximate linear based guidelines after a Lure-Postnikov Lyapunov function is used to provide global stability guarantees. This approach applies not only to Quadrotor UAVs but also to a wide class of systems that contain double integrators.

The developed anti-windup compensators were designed and implemented for an experimental Quadrotor UAV where both simulation results and flight test results clearly show the ability of the anti-windup compensators to reduce the effect of magnitude saturation in Quadrotor UAVs.

Finally, the thesis describes the design of decoupled multivariable anti-windup compensators to tackle the problem of rate saturation on a fixed wing UAVs. Simulation results obtained demonstrate that these anti-windup compensators are capable of managing the system responses during periods of rate saturation.

Acknowledgements

First and foremost, I will like to thank the Nigerian Air Force for their support and for granting me the opportunity to undergo this research.

I would like to extend my gratitude to AVM CN Udeagulu, Air Cdre (Dr) PO Jemitola, Gp Capt KA Ademuwagun, Gp Capt (Dr) OC Ubadike, Dr Ramey Jamil, Wg Cdr P Okonkwo, Sq Ldr GE Abbe, Sq Ldr TD Chollom, Sq Ldr SO Uguzo, Fg Offr NA Adi and Fg Offr KM Dikwal. I thank them all for their time, support and encouragement.

I thank Dr Rob Thornton, Dr Rafael Morales-Viviescas and Dr Matteo Rubagotti for the opportunities they provided me. These opportunities helped broaden my knowledge base and made my time at the University of Leicester worthwhile.

I would also like to thank my fellow colleagues on the 6th floor and 4th floor Labs (too many to mention) for the numerous insightful discussions we had and the words of encouragement.

I would like to express my deepest gratitude to my Supervisor, Prof Matthew C Turner for his patience, generous help, enthusiastic encouragement and inspiration during the period of this research. It was truly a great privilege to work with him. I am indeed indebted to him for creating numerous opportunities for me to learn and grow as a researcher.

I thank my family for their love and encouragement, especially my parents, Wg Cdr (Dr) ON Ofodile (rtd) and Dr (Mrs). Uche Ofodile. It was because of their continuous advice, prayers and unflinching support in all aspects that kept me going so far. To my siblings, Captain KA Ofodile, Chinenye Ofodile and Ikechukwu Ofodile, I thank them for all their support.

And most of all to my loving, persuasive, encouraging and patient husband, Godbless Keku for his unrelenting immense support and encouragement during my research period. Thank you for keeping me “sane” every night during this period.

Finally, *Unto the King eternal, immortal, invisible the only wise God be honour and glory forever and ever, Amen. 1 Tim 1.17*

Veni, Vidi, Deus Vicit

Contents

Acknowledgements	ii
Contents	iii
List of Figures	vi
Symbols	ix
1 Introduction	1
1.1 Motivation	1
1.2 Research Aim and Objectives	3
1.3 Thesis Organization and Contributions	3
1.3.1 Outline of Thesis	3
1.3.2 Publications resulting from this work	5
2 Background on Anti-Windup Compensation	6
2.1 Introduction	6
2.2 Actuator Saturation	6
2.3 Early forms of AW Compensation	8
2.3.1 Anti-Reset or Back Calculation	9
2.3.2 Hanus conditioning technique	10
2.3.3 Observer-based AW approach	11
2.3.4 Internal Model Control AW approach	12
2.4 Modern AW Compensators	13
2.4.1 AW Classification	13
2.4.2 Unified AW Frameworks	15
2.4.2.1 Kothare Framework	15
2.4.2.2 Weston and Postlethwaite Framework	16
2.5 Summary	17
I Anti-Windup Design for Quadrotor UAVs	19
3 Quadrotor Mathematical Modelling and Flight Control	20
3.1 Introduction	20
3.1.1 General Description	20
3.1.2 Quadrotor Models in Literature	21
3.2 Mathematical Modelling	22
3.2.1 Reference Frames	22

3.2.2	State Variable Relationships and Kinematics	23
3.2.3	Newton-Euler rigid body dynamics	24
3.2.3.1	Translational motion	24
3.2.3.2	Rotational motion	26
3.2.4	6 DOF model	27
3.2.5	Actuator Model	28
3.2.6	Forces & Torques	29
3.3	Experimental Quadrotor Platform	30
3.3.1	Platform Description	30
3.3.2	Control Architecture	32
3.3.2.1	Quadrotor Control in Literature	32
3.3.2.2	Proposed Controller	34
3.4	Summary	36
4	Design of Decentralized AW compensators for Quadrotor UAVs	39
4.1	Introduction	39
4.2	Nonlinear systems and Stability	39
4.2.1	Lyapunov stability theory	41
4.2.2	Input-Output Stability	42
4.2.3	Absolute Stability	44
4.3	Full-order AW design approach	46
4.3.1	Generic MIMO full-order AW design	46
4.3.2	Full-order AW design for SISO/SIMO systems	49
4.4	Anti-windup design for a Quadrotor system structure	51
4.4.1	Quadrotor UAV structure	51
4.4.2	Pseudo-decentralised Anti-windup Design	53
4.4.3	Channel-by-channel anti-windup design	57
4.5	Results	62
4.5.1	Simulation Results	63
4.5.1.1	Micro-Quadrotor Model (MQM)	63
4.5.1.2	Experimental Quadrotor Model (EQM)	64
4.5.2	Flight Testing	66
4.5.2.1	Flight Plan	67
4.5.2.2	Flight Test Results	69
4.6	Summary	70
5	Non-LMI based approach to AW design for Quadrotor UAVs	71
5.1	Introduction	71
5.2	The closed-loop system and AW structure	72
5.3	Tyan and Bernstein's Result	75
5.4	Stability analysis of AW design for input-coupled double integrators plants	76
5.4.1	Part 1: For a single double integrator feedback loop	76
5.4.2	Part 2: For input-coupled double integrator systems	78
5.5	Performance Consideration	79
5.6	Results	81
5.6.1	Simulation Results	81
5.6.1.1	Micro-Quadrotor Model (MQM)	81
5.6.1.2	Experimental Quadrotor Model (EQM)	83
5.6.2	EQM Flight Test Results	84
5.7	Summary	86

II	Anti-Windup Design for Fixed Wing UAVs	88
6	Fixed-Wing UAV Modelling and Control	89
6.1	Introduction	89
6.2	Fixed-wing UAV Equations of Motion	89
6.2.1	Forces and Moments acting on a Fixed-wing UAV	91
6.2.1.1	Gravitational F_{*g}	92
6.2.1.2	Propulsion F_{*th}, Mo_{*th}	92
6.2.1.3	Aerodynamic F_{*a}, Mo_{*a}	92
6.2.1.4	Nonlinear Equations of Motion	93
6.2.2	Linearized Equations of Motion	94
6.2.2.1	Small perturbation theory & Trimmed flight	94
6.2.2.2	Aerodynamic derivatives from Taylor series expansion	96
6.2.3	The Aerosonde UAV	98
6.3	Controller Design	101
6.3.1	Longitudinal Control K_{long}	103
6.3.2	Lateral Control K_{lat}	104
6.4	Summary	105
7	Decoupled AW design with application to fixed-wing UAV	107
7.1	Introduction	107
7.2	Decoupled Anti-windup design for the fixed-wing UAV structure	108
7.2.1	Typical AW design structure with rate saturation	108
7.2.2	Decoupled UAV plant-controller representation	111
7.3	Simulation Results	114
7.3.1	Longitudinal Simulation Results	114
7.3.2	Lateral Simulation Results	114
7.4	Summary	117
8	Conclusion and Future Work	119
8.1	Summary of Main Contributions	119
8.2	Future Work	121
A	Coordinate Reference Systems.	123
A.1	Reference Frame Definitions	123
A.1.1	Inertial Frame e	123
A.1.2	Body Frame b	124
A.1.3	Stability axes Frame s	124
A.1.4	Wind axes Frame w	124
A.2	Coordinate Transformation	125
A.2.1	From Inertial Frame to Body Frame	125
A.2.2	From Body Frame to Wind/Stability axes Frame	126
	References	128

List of Figures

2.1	Actuator saturation nonlinearity	6
2.2	Rate Saturation Model	7
2.3	Closed loop control system with saturation	8
2.4	Anti-Reset or Back Calculation AW structure	9
2.5	Hanus Conditioning Technique	11
2.6	Observer-based AW structure <i>where \hat{x} is the estimated state vector and L is the state feedback gain.</i>	11
2.7	Observer-based AW structure <i>where M is a static feedback gain matrix.</i>	12
2.8	Conventional IMC AW structure	13
2.9	Modified IMC AW structure [1, 2]	13
2.10	Basic Anti-Windup Structure	14
2.11	Kothare's Framework	15
2.12	Weston and Postlethwaite Framework	16
2.13	Equivalent representation of Weston and Postlethwaite framework	16
3.1	Force, Torque and States definition of a Quadrotor	21
3.2	Showing symmetric axes with point masses (m_p) and distance (l) from centre of quadrotor	26
3.3	CAD representations	30
3.4	Modified 2014 3DR Quadrotor	31
3.5	Quadrotor Hardware Schematic	31
3.6	PWM conversion	32
3.7	PD controller structure	34
3.8	Applied Control Structure for used Flight Modes	35
3.9	Nominal quadrotor simulation results	37
4.1	Input-Output System	43
4.2	Feedback Interconnected System	44
4.3	Lur'e-type system	44
4.4	Sector Bound	45
4.5	Typical Anti-windup Configuration	46
4.6	Equivalent representation of structure	47
4.7	Single-loop anti-windup structure	49
4.8	Equivalent representation of single-loop anti-windup structure	50
4.9	Full anti-windup structure	52
4.10	Decentralised AW structure	53
4.11	Equivalent representation of decentralised AW structure	54
4.12	Non-linear loop for decentralised AW	55
4.13	Applying the AW on general plant structure (MIMO)	57
4.14	Equivalent representation for channel-by-channel AW	58

4.15	Non-linear loop for channel-by-channel AW 1	59
4.16	Non-linear loop for channel-by-channel AW 2	59
4.17	MQM Pitch angle response: (a) [from left] Saturation, no AW and (b) Saturation, full MIMO AW	63
4.18	MQM Control command due to pitch response: (a) [from left] Saturation, no AW and (b) Saturation, full MIMO AW	64
4.19	MQM Pitch angle response: (c) [from left] Saturation, psuedo-decentralized AW; and (d) Saturation, channel-by-channel AW	64
4.20	MQM Control command due to pitch response: (c) [from left] Saturation, psuedo-decentralized AW; and (d) Saturation, channel-by-channel AW	65
4.21	EQM Pitch angle response: (a) [from left] Saturation, no AW and (b) Saturation, full MIMO AW	65
4.22	EQM Control command due to pitch response: (a) [from left] Saturation, no AW and (b) Saturation, full MIMO AW	65
4.23	EQM Pitch angle response: (c) [from left] Saturation, psuedo-decentralized AW; and (d) Saturation, channel-by-channel AW	66
4.24	EQM Control command due to pitch response: (c) [from left] Saturation, psuedo-decentralized AW; and (d) Saturation, channel-by-channel AW	66
4.25	Snapshot showing Mission Waypoints	67
4.26	Full Flight Pitch response: (a) [from left] Saturated No AW ; (b) Saturated, with AW (Section 4.3)	68
4.27	Focus on artificial limit flight section: (a) [from left] Nominal response ; (b) Saturated response no AW	68
4.28	Pitch angle response: (a) [from left] Saturation, full MIMO AW ; (b) Saturation, decentralised AW ; (c) Saturation, Channel-by-channel AW	69
5.1	System under consideration	71
5.2	Input-coupled system with structured anti-windup	73
5.3	Equivalent interpretation of structured anti-windup problem	73
5.4	The nonlinear loop	74
5.5	MQM Pitch angle response: (a) [from left] Nominal and (b) Saturation, no AW	82
5.6	MQM Control response: (a) [from left] Nominal and (b) Saturation, no AW	82
5.7	MQM Pitch angle response: (a) [from left] Saturation, $\omega_n = 36.51rad/s$ with AW at different ζ ; and (b) Saturation, $\omega_n = 115.47rad/s$ with AW at different ζ	83
5.8	MQM Control response: (a) [from left] Saturation, $\omega_n = 36.51rad/s$ with AW at different ζ ; and (b) Saturation, $\omega_n = 115.47rad/s$ with AW at different ζ	83
5.9	Output response:(a) Nominal; (b) Saturation, no AW	84
5.10	Control response:(a) Nominal; (b) Saturation, no AW	84
5.11	Output response:(a) Saturation, $\omega_n = 500rad/s$ with AW at different ζ ; (b) Saturation, $\omega_n = 800rad/s$ with AW at different ζ	85
5.12	Control response: [(a), (b)] Saturation, $\omega_n = 500rad/s$ and $\omega_n = 800rad/s$ with AW at different ζ	85
5.13	Pitch angle response-Artificial limit flight section: (a) [from left] Typical Nominal response ; (b) Saturated response no AW	85
5.14	Pitch angle response: (a) [from left] Saturation, $\omega_n = 500rad/s$ with AW at $\zeta = 0.5$; (b) Saturation, $\omega_n = 500rad/s$ with AW at $\zeta = 2$	86
5.15	Pitch angle response: (a) [from left] Saturation, $\omega_n = 840rad/s$ with AW at $\zeta = 0.5$; (b) Saturation, $\omega_n = 840rad/s$ with AW at $\zeta = 2$	86
6.1	The Aerosonde TM UAV [3]	99
6.2	Aerosonde UAV Layout [3]	99
6.3	Stability Augumention System	102
6.4	Full Controller Architecture	103
6.5	Inner Loop representation of controller architecture	104

6.6	Nominal closed-loop simulation results	106
7.1	Rate saturated system	108
7.2	Rate saturated system fitted with rate saturation model	108
7.3	Rate saturated system with AW structure	109
7.4	Equivalent representation of AW system in Figure 7.3	110
7.5	Pitch angle response: (a) [from left] Nominal and (b) Saturation, no AW	115
7.6	Elevator command with rate saturation: (a) [from left] Nominal and (b) Saturation, no AW	115
7.7	Pitch angle response at $V_a=25ms^{-1}$: (c) [from left] Saturation, full MIMO AW and (d) Saturation, Longitudinal AW	115
7.8	Pitch angle response at $V_a=35ms^{-1}$: (c) [from left] Saturation, full MIMO AW and (d) Saturation, Longitudinal AW	116
7.9	Elevator command with rate saturation: (c) [from left] Saturation, full MIMO AW and (d) Saturation, Longitudinal AW	116
7.10	Roll angle response: (a) [from left] Nominal and (b) Saturation, no AW	116
7.11	Aileron command with rate saturation: (a) [from left] Nominal and (b) Saturation, no AW	117
7.12	Roll angle response at $V_a=25ms^{-1}$: (c) [from left] Saturation, full MIMO AW and (d) Saturation, Lateral AW	117
7.13	Roll angle response at $V_a=35ms^{-1}$: (c) [from left] Saturation, full MIMO AW and (d) Saturation, Lateral AW	117
7.14	Aileron command with rate saturation: (c) [from left] Saturation, full MIMO AW and (d) Saturation, Lateral AW	118
A.1	Definition of Inertial and Body Reference Frames	123
A.2	Body and Stability axes Reference Frames [4]	124
A.3	Relationship between Stability axis and Wind axis [5]	125
A.4	Rotations from inertial frame through vehicle frames to body frame [5]	126

Symbols

3D	Three Dimensional
AW	Anti Windup
DOF	Degree of Freedom
SISO	Single-Input-Single-Output
MIMO	Multiple-Input-Multiple-Outputs
LMIs	Linear Matrix Inequalities
LTIs	Linear Time Invariant
PD	Proportional Derivative
PID	Proportional Integral Derivative
SAS	Stability Augmentation System
PWM	Pulse Width Modulation
FCS	Flight Control System
UAV	Unmanned Aerial Vehicle
\mathbb{N}	set of natural numbers
\mathbb{R}	set of real numbers
\mathbb{R}^n	set of n elements belonging to the set \mathbb{R}
$\mathbb{R}^{k \times l}$	set of k -by- l real matrices
\mathcal{RH}_∞	set of real asymptotically stable transfer functions of a plant
I	the identity matrix
$\mathbf{P}^{m \times m}$	set of $m \times m$ symmetric positive-definite matrices
$\mathbf{N}^{m \times m}$	set of $m \times m$ symmetric non-negative definite matrices
\mathbf{D}	set of diagonal matrices
\mathbf{X}'	the transpose of matrix X
\mathbf{X}^{-1}	the inverse of matrix X
$\text{vec}(X)$	Vectorization of matrix X
$X' = X > 0$	X is symmetric positive definite matrix
$\text{He}\{X\}$	shorthand denoting $X + X'$
\in	belongs to
\forall	for all
\implies	implies

$blockdiag(\cdot)$	block diagonal matrix
$diag(\cdot)$	diagonal matrix
\dot{x}	derivative of x with respect to time, $\frac{dx}{dt}$
$\frac{\partial f}{\partial x}$	a partial derivative of a function with respect to x
$f : A \rightarrow B$	A function f mapping a set A into a set B
γ	\mathcal{L}_2 performance gain
v	\mathcal{H}_2 optimal gain
α	angle of attack
β	sideslip angle
Va	airspeed
h	altitude
ϕ	roll angle
θ	pitch angle
ψ	yaw angle
p	roll rate
q	pitch rate
r	yaw rate
x	position along x axis
y	position along y axis
z	position along z axis
u	linear velocity along x axis
v	linear velocity along y axis
w	linear velocity along z axis
V_T	total velocity
F	Force generated
J	Tensor of Inertia

1 Introduction

1.1 Motivation

Unmanned Aerial Vehicles (UAVs) have attracted significant interest from both researchers and various industrial sectors because of their potential to replace human piloted vehicles in many cases where they may provide a much safer, cheaper and efficient solution than their manned counterparts. Similar to their manned counterparts, UAVs can be classified into two major categories, *fixed wing* and *rotary wing*. Both categories of platform possess a unique set of advantages and limitations that render them more or less suitable for different applications. In recent years, UAVs have been used extensively or have great potential to be used in a variety of applications. These applications include: *military applications* such as surveillance, air strikes, reconnaissance, intelligence gathering etc; and *civilian applications* such as search and rescue operations, professional photography & video making, university research, agriculture etc. The growing demand for UAV applications has spurred further advancement in UAV design and control technologies resulting in different types of UAVs with different levels of control for different types of applications. However, regardless of the specie of UAV, all UAVs share the need for proper actuator-sensor management and control.

Actuators in UAVs, as well as with many other physical control systems, are subject to both magnitude and/or rate limitations where the system's controller may sometimes demand an output which is greater than what the actuator can deliver. This is known as actuator saturation and the problems associated with actuator saturation occur when the controller's output can no longer fully affect the controlled variable, causing the integral components of the system to "windup". This can lead to the degradation of the system's performance and it can introduce instability to the control system [6, 7]. In piloted aircrafts, for example, actuator rate saturation is known to be a leading cause of pilot-induced-oscillations (PIOs) which has been linked to be the reason behind a number of aircraft crashes [8, 9].

There are many ways to deal with actuator saturation but a simple and straight-forward way is by avoiding the occurrence of the "windup" situation. This can be done by increasing the capacity of the actuator to handle the demands of the controller while also ensuring that the control system is designed in such a way that the input demanded by the control law stays below the saturation limits of the actuator when the system is in operation. However for most systems,

this comes with a price. It can lead to high processing and high cost requirements. In aircraft systems, this could increase aircraft mass and design/fuel costs. With cost efficiency and ease of operation as a main design driver for UAVs, a more efficient approach would be to implement the controller with additional control logic so that the controller tackles the windup situation whenever it occurs and reverts back to normal operation after the periods of saturation. These additions are sometimes termed “**Anti-Windup**” (AW) compensators/schemes.

Over the last few decades, extensive research in the field of AW theory and compensation has led to the design, analysis, and synthesis of AW compensators that can guarantee stability and provide some acceptable threshold of performance for the control systems in which they are implemented. In the more recent past, modern AW compensators have been successfully adapted to work with MIMO systems even in the presence of uncertainty and have recently begun to find their way into UAV applications.

Relevant researches that have addressed the problem of actuator saturation in UAVs in the literature include [10–18]. These researches have demonstrated the effectiveness of their solutions in theory with very few of these having applied their solutions to practical UAVs in flight situations. Many of these however, tend to provide “ad hoc” specific solutions where the system’s control law and actuator requirements are pre-designed to reduce the tendency of the system to saturate and ensure that, if and when saturation occurs, the effects are not catastrophic. Such “ad hoc” solutions may not be applicable to another UAV of the same type.

Especially relevant are researches that use AW structures and techniques to address the problem of actuator saturation in UAVs but only a few of these exist in literature [19–22]. For practical systems, control engineers generally appreciate structure, flexibility and ease of operation which as mentioned earlier, are part of the key design drivers for UAVs. However, most of the AW compensators designed to work with UAVs tend to lack structure, and may perhaps have greater levels of complexity due to the computational techniques applied to their design thus making them less flexible and difficult to tune/operate.

Also, most of the relevant researches on AW compensation in UAVs tend to use unified AW techniques which are techniques that can be applied to a large class of systems and thus they can be used on different UAV platform types with little/ no modifications to the AW compensator design process. However, it is important to note that despite the rapid development in AW compensation techniques, research on its implementation in UAV systems is still limited, with the majority concentrating on mainly theoretical application rather than the practical/real-life application. This lack of practical application is one of the key reasons that encouraged this research and it is against this backdrop, that this thesis will attempt to address the problem of actuator magnitude and rate saturation in two practical UAVs using AW techniques.

The two practical UAVs originally considered for the work in this thesis are the 3DR Quadrotor UAV by 3DR robotics and the “GULMA” Fixed wing UAV belonging to the Nigerian Air Force (NAF). However due to the difficulty in obtaining the full parameter specifications (including stability and control derivatives) of the UAV and issues regarding military confidentiality requirements, the GULMA UAV is replaced in this thesis with the Aerosonde UAV which is a closely related model to the GULMA UAV and whose model and full parameter specifications

are readily available in literature. It is hoped that the AW designs implemented on the Aerosonde UAV can be easily transferred to the GULMA UAV in a later project.

1.2 Research Aim and Objectives

The main research aim is to present Decentralized AW compensator design approaches to tackle the problem of magnitude saturation and rate saturation in Quadrotor UAVs and Fixed wing UAVs respectively for practical flight situations. The decentralization provides the system with some level of structure and flexibility that makes the system easier to operate and appealing to a practising control engineer. The decentralized AW design techniques developed here are not only applicable to UAVs alone, but can be applied or adapted to larger class of systems e.g double integrator plants. The following objectives will help to address the aim of this research;

1. To exploit the structure of a quadrotor UAV model to design decentralized AW compensators that follow the principles and structure of the full order multivariable AW compensator design approach by [23]. This full order multivariable AW compensator design approach by [23] will form the basis for all the AW compensator design techniques developed in this thesis. The quadrotor UAV model used is developed based on works by [24] using parameters and specifications of the experimental 3DR Quadrotor UAV. A suitable PD-type flight control system is also designed to accompany the Quadrotor UAV model.
2. To take advantage of the natural decoupling of a fixed wing UAV along its longitudinal and lateral dynamics in order to design decoupled AW compensators using the multivariable AW compensator design approach by [23] for each of the decoupled MIMO loop. For this purpose, an existing nonlinear 6DOF mathematical model of the Aerosonde UAV is obtained and then linearised for straight and level flight. A simple flight control system for the Aerosonde UAV platform is also designed to accompany the model.
3. Carry out simulations and flight tests¹ to validate the effectiveness of the designed AW compensators and compare results with the multivariable AW compensator design approach [23].

1.3 Thesis Organization and Contributions

1.3.1 Outline of Thesis

Chapter 2 describes the concept of actuator magnitude and rate saturation and presents, in a somewhat historical fashion, a brief description of existing AW schemes in the literature. The AW architecture and technique which forms the basis for most of the work on AW compensators in this thesis is also presented here and described in detail.

Chapter 3 begins Part 1 of this thesis and describes a mathematical approach to the modelling of quadrotor dynamics. It also contains a description of the 3DR quadrotor UAV which will be

¹Due to the fact that an experimental version of the Aerosonde UAV was not available during the research period for test flights, only simulation results will be presented for the Fixed-wing UAV

used in subsequent chapters to test the AW techniques that will be designed. A brief description of existing controller designs for quadrotors and the PD-type flight controller design structure for the 3DR quadrotor UAV are also presented here.

Chapter 4 introduces some background concepts from systems and stability theory required for the analysis and AW design approaches discussed in later sections of the chapter and subsequent chapters. This chapter proceeds to describing the full order AW compensator synthesis method by [23, 25] and the process for synthesizing globally stabilizing “pseudo” decentralized and channel-by-channel AW compensators (based on the full order AW compensator) for addressing the problem of magnitude saturation in quadrotor UAVs. The chapter concludes by showing how the AW compensators resulting from the “pseudo” decentralized and channel-by-channel synthesis methods were applied to the Quadrotor UAV and adapted for simulations and flight tests. The results of the simulations and flight tests are presented and described.

Chapter 5 briefly introduces the AW problem for saturating double integrator plants and describes the AW compensator design process and structure that will make use of the results in [26] to guarantee closed-loop global stability for the AW compensated system while showing that using some simple transparent formulae based on a simple linear approximation of the compensator’s dynamics, a well performing AW compensator can be obtained. The AW compensator design process described in this chapter eliminates the use of LMIs in the computation of AW compensator parameters and thus reduces computational complexity that may accompany the use of LMIs in any evaluation. As done in the previous chapter, AW compensators designed using the technique described in this chapter are applied to the Quadrotor UAV and the results of simulations and flight tests are presented and described. This chapter concludes Part 1 of this thesis.

Chapter 6 begins Part 2 of this thesis and briefly describes a mathematical approach to the modelling of fixed wing UAVs. It also contains a brief description of the Aerosonde UAV model and its linearized dynamics that displays the natural decoupling into longitudinal and lateral dynamics. The dynamic modes of the UAV are examined and, based on the results of this examination, a stability augmentation system (SAS) is designed for the Aerosonde UAV model. The chapter closes with the presentation of the PID-type flight controller structure implemented for the augmented Aerosonde UAV; the closed loop system containing the augmented UAV and controller will be used in the next chapter to test the MIMO AW compensators that will be designed.

Chapter 7 leads with a description of the rate saturation problem in MIMO systems using the rate saturation model presented earlier in Chapter 2. The basic AW structure used in previous chapters is applied to the rate saturated fixed wing UAV system and restructured such that parts of the rate saturation dynamics are fused with the nominal UAV plant and controller to form an extended model of the plant and controller leaving a magnitude saturation as the only nonlinear element in the system. This restructuring allows for locally stabilizing full order compensators to be designed for the decoupled UAV closed loop system. The chapter closes with a presentation of results from simulation. This chapter concludes Part 2 of this thesis.

Chapter 8 provides a summary of the work in this thesis, and presents an outline of potential areas of further research.

1.3.2 Publications resulting from this work

- **N. Ofofile**, M. Turner, and O. Ubadike, “Channel-by-channel anti-windup design for a class of multivariable systems,” presented in American Control Conference Chicago, IL, USA, 2015.
- **N. Ofofile**, M. Turner, and J. Sofrony, ”Alternative approach to anti-windup synthesis for double integrator systems,” presented in the 2016 American Control Conference (ACC), Boston, MA, USA, 2016.
- **N. A. Ofofile** and M. C. Turner, “Decentralized approaches to antiwindup design with application to Quadrotor Unmanned Aerial Vehicles,” *IEEE Transactions on Control Systems Technology*, Volume:24, no. Issue: 6, pp. 1980-1992, November 2016.
- **N. A. Ofofile** and M. C. Turner, “Anti-windup design for input-coupled double integrator systems with application to quadrotor UAV’s,” submitted to the *European Journal of Control* 2016.

2 Background on Anti-Windup Compensation

2.1 Introduction

In this chapter, the ‘windup’ phenomenon and its effects are briefly described and a review of previous works on various AW compensation techniques with the methods of synthesizing them presented. These techniques are presented in a somewhat historical outline with the discussion ending in the choice of a suitable AW compensator technique to be improved and adapted for use on the UAV platforms.

2.2 Actuator Saturation

Every physical control input or actuator in every physical system is constrained by either magnitude and/or rate limitations. When the controller demand exceeds these limits, saturation of the actuator occurs and hence a nonlinearity is added to the system. Many studies on actuator saturation in the literature focus mainly on magnitude saturation with less attention given to rate saturation. However both saturation types, if present in a system, can significantly impact the stability of the system and degrade its performance.

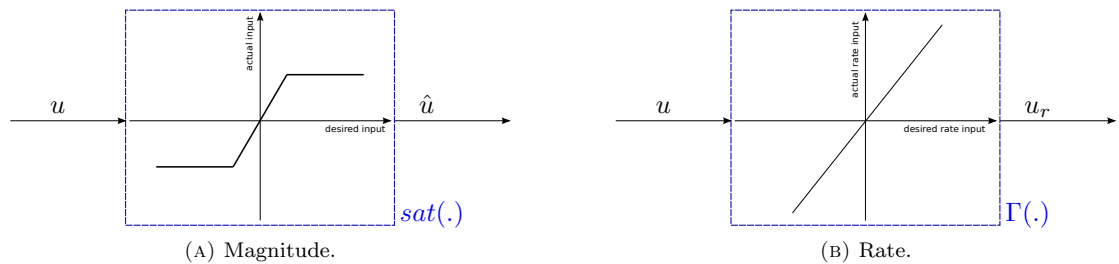


FIGURE 2.1: Actuator saturation nonlinearity

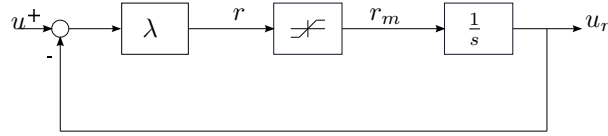


FIGURE 2.2: Rate Saturation Model

Magnitude saturation is a static nonlinearity where its limits are mapped into a range of values represented in Figure 2.1a. In the scalar case, the saturation nonlinearity is described by

$$\text{sat}(u), \hat{u} \triangleq \begin{cases} u_N, & \text{if } u \geq u_N \\ u, & \text{if } u_n \leq u \leq u_N \\ u_n, & \text{if } u \leq u_n \end{cases} \quad \text{if saturation limits are symmetric then } u_n = -u_N \quad (2.1)$$

where u_n and u_N refer to the minimum and maximum available actuator values respectively when $\text{sat}(\cdot) : \mathbb{R} \mapsto \mathbb{R}$.

In the vector case (i.e when $\text{sat}(\cdot) : \mathbb{R}^m \mapsto \mathbb{R}^m$), assuming that the saturation nonlinearity is symmetric, it is described by

$$\text{sat}(u) := [\text{sat}(u_1), \dots, \text{sat}(u_m)]'$$

where $\text{sat}(u_i) := \min\{|u_i|, \bar{u}_i\} \times \text{sign}(u_i)$.

On the other hand, rate saturation as shown in Figure 2.1b is a dynamic nonlinearity and cannot be easily represented with a “static” actuator value range allocation like the magnitude saturation. However it can be defined and modeled in a number of different ways [27, 28] that can be considered as approximations of the ideal rate saturation operation. One of such models defines rate saturation as shown in Figure 2.2. This model is a commonly used approach where a first-order lag is combined with a typical magnitude saturation block [29–32] featuring a gain λ that determines the cut-off frequency of the actuator. This model transforms the rate-saturation function into a magnitude saturation function at the risk of including extra dynamics to the receiving plant model. Based on this model, the rate saturated input signal $\Gamma(u)$ in the scalar case is represented as

$$\Gamma(u) \triangleq \begin{cases} \dot{u}_r = \text{sat}(\lambda(u - u_r)) & \text{where } \lambda = \frac{1}{\tau_c} \end{cases} \quad (2.2)$$

τ_c is the time constant of the equivalent linear actuator dynamics and is assumed to be small. This is because if τ_c is very small (i.e the actuator dynamics are very fast), this model can be considered to be a good approximation for an “ideal or “true” rate saturation and in some cases it can simply be modeled with an ideal relay instead of a saturation function as described in [33]. The model of the rate saturation in Figure 2.2 is much more appealing because it simplifies the problem by exposing the signals that go in and out of the typical magnitude saturation block (i.e r, r_m) which can replace the use of u, u_r in further analysis. This rate saturation model will form part of the rate saturation problem that will be used in this thesis.

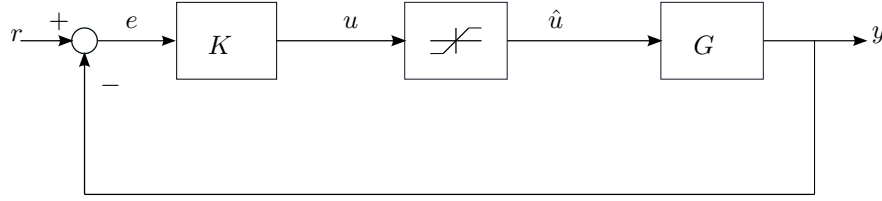


FIGURE 2.3: Closed loop control system with saturation

In the vector case, the rate saturation element $\Gamma(u)$ can be considered to be decentralized such that

$$\Gamma(u) := [\Gamma(u_1), \dots, \Gamma(u_m)]'$$

Thus, the gain λ is also decentralized i.e $\lambda = \text{diag}[\lambda_i]$ and the rate constrained values r_m which are a direct consequence of the magnitude saturation function are defined as

$$r_m = \text{sat}(r) := \text{diag}[\text{sat}(r_i)] \quad (2.3)$$

$$\text{sat}(r_i) \triangleq \min\{|r_i|, \bar{r}_i\} \times \text{sign}(r_i), \quad \forall i \in [1 \dots, m] \quad (2.4)$$

where \bar{r}_i is the saturation level for the i^{th} actuator.

The “windup” phenomenon caused by actuator saturation was initially observed in systems controlled by conventional PI/PID controllers as roughly illustrated in Figure 2.3 where u is the unsaturated control signal, $\hat{u} \in \mathbb{R}^m$ is the plant input (saturated control signal), r is the reference, y is the plant output, K is the nominal PI/PID controller and G is the plant. Here, the saturation causes the integrator in the PID controller to drift to undesirable values as the integrator will integrate over a longer period of time due to the persistence of the tracking error. In modern times, the definition of “windup” has broadened considerably and is now taken to mean any form of performance degradation which occurs due to a saturated control signal.

The effects of actuator saturation on control systems vary from negligible to catastrophic. Common effects that may arise from the failure of the actuator to meet the demands of the controller include; long rise and settling times, change of direction/phase shifts, large output overshoots and long periods of actuator saturation (actuator “lock-up”). Saturation may also lead to instability in certain systems depending on the characteristics of the system in question. Therefore, it is practically imperative that for any real life application, a scheme should be set in place to either avoid or prevent the occurrence of the ‘windup’ problem.

2.3 Early forms of AW Compensation

As earlier mentioned in the previous chapter, a simple, straight forward way of addressing the windup problem is to increase the actuator capacity in order to accommodate larger demands of the controller while also ensuring that the control law requires the input to stay below the saturation limits of the actuator when the system is in operation. This resulted in increase in the size of the systems (bulky systems), increase in processing requirements and increased design costs.

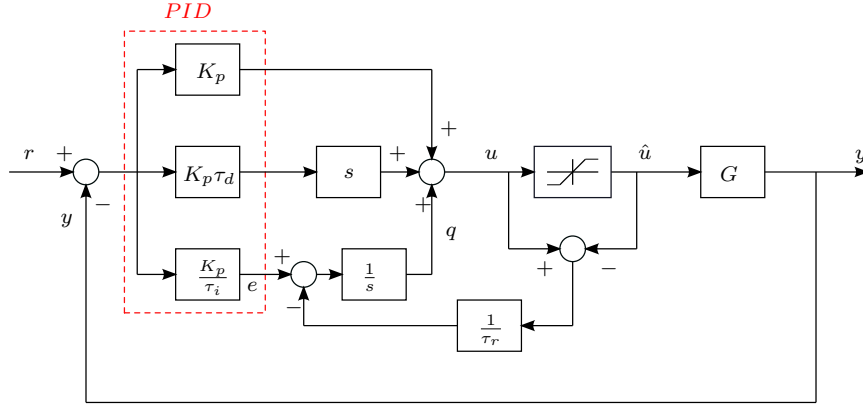


FIGURE 2.4: Anti-Reset or Back Calculation AW structure

It was later observed that instead of the unnecessary increase in the design requirements associated with the so-called ‘simple, straight forward way’, the controller could be augmented with a strategy that could minimize the nonlinear effects brought on by the saturation limits and still maintain its original design. These augmentations became later known as the so-called AW compensators.

Many of these approaches to AW compensation were developed in industry as quick solutions to the windup problem. These were rarely equipped with stability guarantees or design guidelines and were not easy to tune. As researchers began to understand more about the windup problem, design techniques were improved and stability guarantees added.

2.3.1 Anti-Reset or Back Calculation

One of the earliest forms of AW compensation that attempted to solve the PI/PID controller windup is generally referred to as the *anti-reset windup* or *back calculation and tracking* [34]. This method formed an extra feedback path from the error between the controller output u and the plant input \hat{u} (see Figure 2.4). When $\hat{u} \neq u$, the extra feedback $\frac{1}{\tau_r}$ attempts to drive the error $e = \hat{u} - u$ to zero pushing the system towards the linear region. However, when $\hat{u} = u$, the normal PI control takes effect. The integral state q in the feedback region can be written as;

$$q \triangleq \begin{cases} e, & \text{if } u = \hat{u} \\ e - \frac{1}{\tau_r}(u - \hat{u}), & \text{if } u \neq \hat{u} \end{cases} \quad (2.5)$$

Since the integral action is the major culprit here, it can simply be switched on or off such that it acts as a reset action for the integral state, hence the *anti-reset case*;

$$q \triangleq \begin{cases} e, & \text{if } u = \hat{u} \\ 0, & \text{if } u \neq \hat{u} \end{cases}$$

According to [35], it was suggested that the time constant τ_r be chosen based on the condition $\tau_d < \tau_r < \tau_i$, where τ_i and τ_d are the integral and derivative time constants of the controller

respectively. It was later identified by [36] that, the controller K need not have integrators to produce windup. Doyle in [36] termed the earlier windup described above as “*Integrator Windup*” and stated that a controller merely needs relatively slow or unstable modes that are driven by the error when the system is in saturation to cause windup problems. In fact, it is quite difficult to exactly determine which systems will exhibit susceptibility to windup effects and a complex analysis may be required.

2.3.2 Hanus conditioning technique

A significant extension and improvement of the anti-reset windup case resulted in the “*Conditioning technique*” by Hanus [37, 38] which applies to all bi-proper controllers (must have an invertible “ D ” state space matrix and stable zeros). Here, a hypothetical *realizable* reference is introduced such that if it is applied to the controller instead of the original reference input, it would result in a control input u equal to the plant input \hat{u} obtained with the original reference input and hence the saturation limits are not activated. Supposing the controller state space realization is given as

$$K(s) \sim \left[\begin{array}{c|c} A_c & B_c \\ \hline C_c & D_c \end{array} \right] \quad (2.6)$$

and according to Figure 2.5, the controller can be represented with respect to the *realizable* reference r^r as

$$\dot{x}_c = A_c x_c + B_c (r^r - y) \quad (2.7)$$

$$\hat{u} = C_c x_c + D_c (r^r - y) \quad (2.8)$$

While the controller output due to the original reference is given as

$$u = C_c x_c + D_c (r - y) \quad (2.9)$$

The difference between the saturated and non-saturated input to the plant $\hat{u} - u$ can then be used to calculate the *realizable* reference r^r

$$\hat{u} - u = D_c (r^r - r) \quad (2.10)$$

$$r^r = r + D_c^{-1} (\hat{u} - u) \quad (2.11)$$

The conditioning scheme is a simple, straightforward AW scheme, but despite this, a number of drawbacks are evident;

- (i). There are no parameters with which the designer can tune performance
- (ii). There are no guarantees of closed loop stability
- (iii). The “ D ” matrix used as a static gain (D_c) must be non-singular which means that the controller must be square and bi-proper. This is achievable with standard PI controllers but not always the case for state-space based controllers (e.g. LQR, \mathcal{H}_∞ etc) [39]

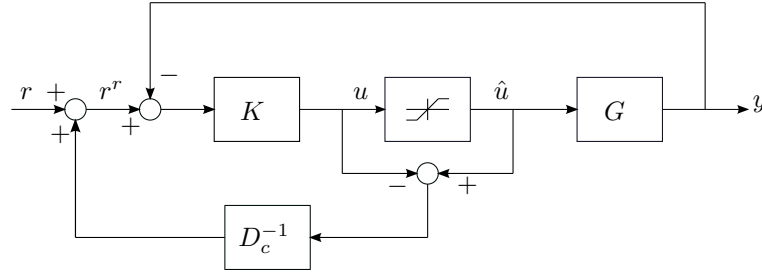


FIGURE 2.5: Hanus Conditioning Technique

Further extensions of this method [40] tried to address some of its drawbacks by including a filter to the system and conditioning on a filtered reference. This provided an avenue for tuning filter variables, but was still severely handicapped in how design parameters could be influenced to guarantee stability and closed loop performance.

2.3.3 Observer-based AW approach

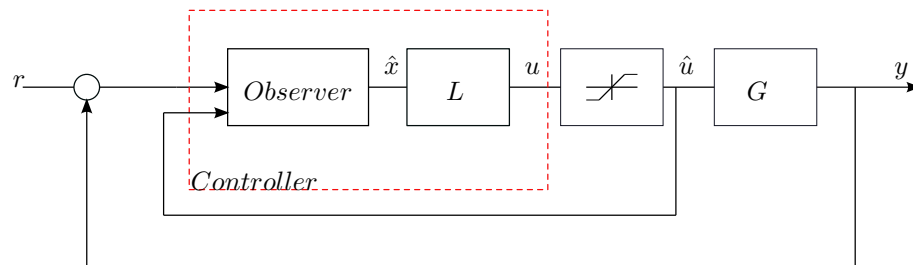
Observer-based AW approaches were then introduced to estimate the states of the controller and hence rectify the irregularities between the saturated control signal \hat{u} and the states of the controller [35, 41]. This is done by feeding back the saturated control signal \hat{u} to the observer (with a parameter) rather than the control output u as can be seen in Figure 2.6. According to [41], not all controllers need be partitioned into an observer and a state feedback, but a more general structure as in Figure 2.7 can be used with a constant high frequency gain. Again, supposing the controller state space realization is given as in equation (2.6) and according to Figure 2.7, the controller can be represented with respect to the difference between the saturated and non-saturated input to the plant $\hat{u} - u$ such that

$$\dot{x}_c = A_c x_c + B_c (r - y) + M(\hat{u} - u) \quad (2.12)$$

$$= (A_c - M C_c) x_c + (B_c - M D_c)(r - y) + M \hat{u} \quad (2.13)$$

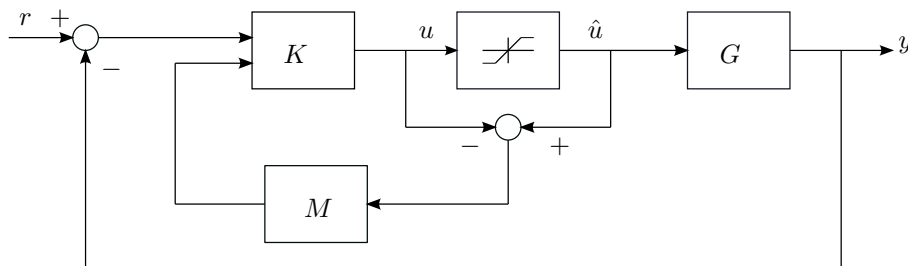
$$\hat{u} = C_c x_c + D_c (r - y) \quad (2.14)$$

Provided the M matrix is chosen such that $A_c - M C_c$ is Hurwitz¹.

FIGURE 2.6: Observer-based AW structure where \hat{x} is the estimated state vector and L is the state feedback gain.

This method allows that when $\hat{u} = u$, the controller returns back to nominal operation as in equation (2.6). It has been established that the Hanus Conditioning technique is a special case

¹Hurwitz matrix is a structured real square matrix that has stable eigenvalues

FIGURE 2.7: Observer-based AW structure where M is a static feedback gain matrix.

of these observer based approaches [42]. This method though flexible in allowing the choice of M , focuses on the choice of M from a stability point of view and does not necessarily mean that an acceptable performance can be obtained or guaranteed. Note also that “stability” must be interpreted as stability of the matrix $A_c - MC_c$ not the stability of the overall system, which was not addressed until later (see [43]).

2.3.4 Internal Model Control AW approach

The Internal Model Control (IMC) structure is based on the Internal Model Principle which states that [44]

Control can be achieved only if the control system encapsulates, either implicitly or explicitly, some representation of the process to be controlled.

This means that if the controller has been developed based on an exact replica of the plant, then perfect control is theoretically achievable [45]. The IMC structure was introduced as an AW scheme in [1, 46, 47] using the conventional IMC AW approach shown in Figure 2.8, where G is the actual plant, G_m is the known plant model, and K is the IMC linear controller designed for the linear system at $u = \hat{u}$.

According to [1, 23], if $G = G_m$ (i.e there is no mismatch between the plant and its known model), then the stability of G and K guarantees global stability of the unsaturated closed loop system. However when saturation occurs, the closed loop stability is still guaranteed but the nonlinear performance may deteriorate, especially if the plant G contains some slow or lightly damped poles. This is because the controller K does not receive any information on when the plant input saturates.

The modified IMC AW structure [1] shown in Figure 2.9 was introduced to deal with this performance deterioration associated with the conventional IMC structure by ensuring that the controller K is fed with input containing information on the saturating control actions so that the input the controller sees during saturation is the same as that of the plant model G_m during linear behaviour.

This AW compensator is relatively easy to design and can easily be manipulated but the success of the approach largely depends on the choice K_1 and K_2 in K bearing in mind the trade off between performance and stability. Modern variants and extensions of this approach exist in literature [2, 48–51]; many of which propose different methods of assigning K_1 and K_2 to K to ensure stability and achieve good nonlinear performance.

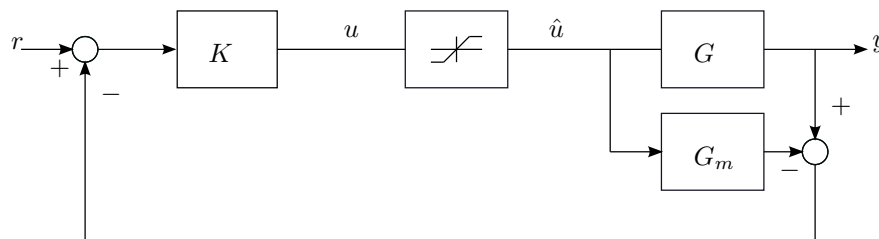


FIGURE 2.8: Conventional IMC AW structure

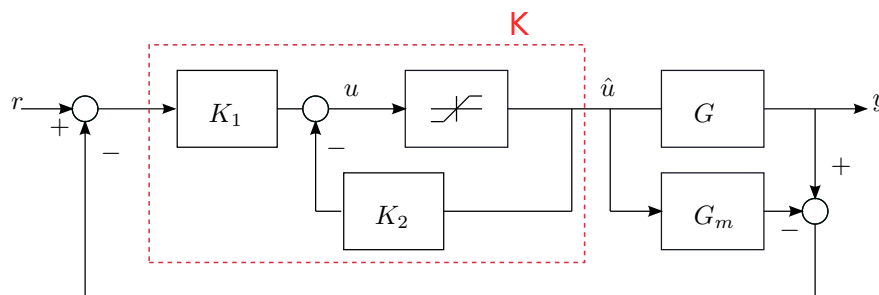


FIGURE 2.9: Modified IMC AW structure [1, 2]

2.4 Modern AW Compensators

All the AW techniques stated earlier were mainly demonstrated on linear SISO systems or considered specific cases or class of cases of linear/nonlinear systems and can be considered as *ad-hoc* solutions to industrial and/or practical problems. A generic framework for AW will be of great benefit to control engineers because it will make AW handling a process common to all situations. Modern AW techniques began with these generic AW frameworks and graduated from the problem specific solutions, to complex and sophisticated methods which are in the literature today. There are many modern AW approaches in the literature which have been classified based on different criteria related to the designer's preferred stability and performance objectives and these classifications have been presented in a number of books [52–54] and tutorials [55, 56]. In this section, a number of these AW classifications will be briefly examined.

2.4.1 AW Classification

Most AW frameworks have the generic structure shown in Figure 2.10², however the component plants, controllers and AW compensators can either be linear or nonlinear and can therefore result in different AW problem formulations. These AW problem formulations can be arranged into many classes (see [55] for some detailed AW classifications) some of which include;

- a. **Plant properties:** This classification is made by investigating the signal time-base and the closed-loop stability properties of the plant under consideration. Based on the plant's signal time-base, most AW compensators are designed for continuous-time plants such as [25, 58–61] but there are a few AW compensators that are designed for discrete-time plants as well [62–65]. The discrete-time AW compensators have equivalent properties to their continuous-time

²Some anti-windup schemes do not fall into the general structure of Figure 2.10. For example, the Model Predictive Control (MPC) based AW schemes [57]

counterparts, but the stability proofs associated with them are usually different. Considering, the closed-loop stability properties of the plant, AW schemes can be classified as:

- (i). Exponentially stable (ES) plants. Examples of AW schemes for this plant type are in [25, 59–62, 66]. AW schemes applicable to these plants are those that provide global exponential stability, global asymptotic stability and global \mathcal{L}_2 performance.
 - (ii). Marginally stable/unstable (MS) plants. Examples of AW schemes for this plant type are in [67–69]. For these systems (i.e. systems with one or more poles on the imaginary axis), it is only possible for AW compensators to provide global asymptotic stability and regional exponential stability.
 - (iii). Exponentially unstable (EUS) plants. Examples of AW schemes for this plant type are in [70–73]. In this case, the best an AW compensator can provide is local asymptotic stability with local performance properties. These systems will always exhibit instability for sufficiently large initial conditions/reference/disturbances whatever the AW compensator.
- b. **Compensator schemes synthesis methods:** Most modern AW schemes and algorithms are synthesized using Linear Matrix Inequalities (LMI) [43, 58, 66, 74]. However other notable synthesis methods are Linear Quadratic Regulator (LQR) [7, 75] and Lyapunov Equation Solution [76, 77].
 - c. **Compensator guarantees (Global/local):** Compensator stability guarantees are often associated with the closed loop stability of the plant-controller-compensator interconnection. Any compensator which seeks results that hold for either all initial conditions or all exogenous inputs is said to have global stability guarantees. A globally stabilizing AW compensator is one which ensures internal stability of the origin regardless of the location of the initial condition. Whereas, any compensator that seeks non-global results so that good performance can be achieved for reasonably sized signals is said to have *local* or regional stability guarantees. A locally stabilizing AW compensator can guarantee stability and/or performance in a certain region of the state space but not the entire state space.
 - d. **Compensator Linearity (Linear/Non-linear):** It is known that saturation effects are nonlinear and a well-posed nonlinear compensator will provide reasonable performance and maintain some level of stability. It is due to this fact that the study and synthesis of nonlinear AW schemes are of great importance. However, these nonlinear AW schemes are usually complex and difficult to synthesize and implement [70, 78, 79]. Hence, the trend of designing

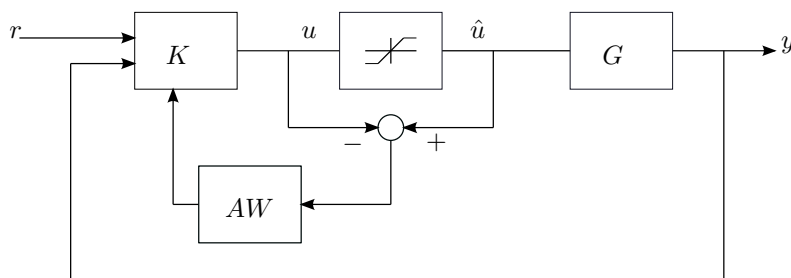


FIGURE 2.10: Basic Anti-Windup Structure

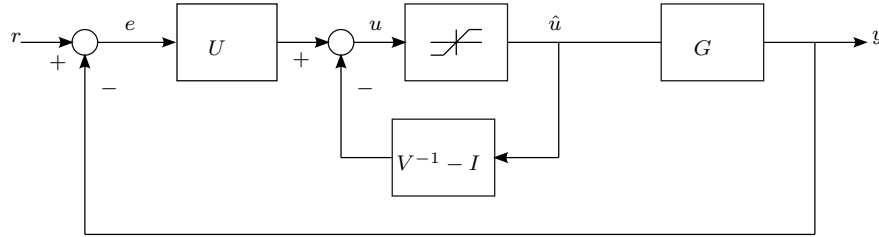


FIGURE 2.11: Kothare's Framework

linear schemes which are normally easier to implement and computationally simpler [25, 59, 80]. The choice of whether to use a linear or nonlinear compensator is a decision often based on a trade-off between computational complexity and stability/performance guarantees.

2.4.2 Unified AW Frameworks

It is important to note that AW compensators described in Section 2.3, may provide solutions to some specific cases especially for the practical engineer, but they do not capture the studies of stability and performance of the systems holistically. Some of the generic AW schemes have resulted in a number of unified AW frameworks that include the studies of stability and performance in great detail.

2.4.2.1 Kothare Framework

A notable example of a unified framework is the **Kothare** framework [40]. It is a general theoretical framework for studying plant input nonlinearities. A parameterization of the AW compensator is presented in terms of two constant matrices as opposed to the one parameter of the observer based approach.

In this framework (see Figure 2.11), the AW compensator is formed from the factors of a left coprime factorization of the controller $K(s)$ which has been conditioned using two static matrices (H_1 and H_2). The left coprime factorization of the controller as outlined in [81] is given as $K(s) = V^{-1}(s)U(s)$. If the state space realization of the controller is given as

$$K(s) \sim \left[\begin{array}{c|c} A_c & B_c \\ \hline C_c & D_c \end{array} \right]$$

then the state space realizations of $U(s)$ and $V(s)$ are given such that

$$U(s) = \left[\begin{array}{c|c} A_c - H_1 C_c & B_c - H_1 D_c \\ \hline H_2 C_c & H_2 D_c \end{array} \right] \quad V(s) = \left[\begin{array}{c|c} A_c - H_1 C_c & -H_1 \\ \hline H_2 C_c & H_2 \end{array} \right]$$

To ensure the internal stability of the feedback loop, H_1 is chosen so that $A_c - H_1 C_c$ is Hurwitz and H_2 must be invertible. The choices of the parameters (H_1 and H_2) as described in [81, 82] can be fashioned to fit many of the early forms of AW compensation methods making it arguably the first true "Unified AW" scheme; for example, it bears some resemblance to the hanus conditioning scheme when H_1 and H_2 are chosen as $H_1 = B_c D_c^{-1}$ and $H_2 = I$. However, even though this

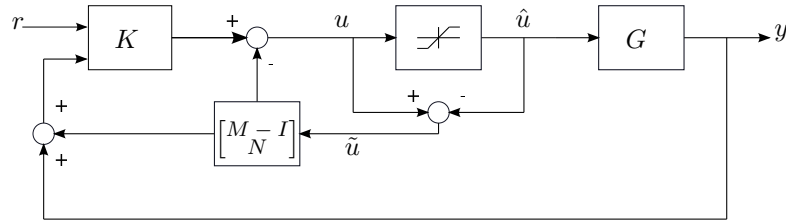


FIGURE 2.12: Weston and Postlethwaite Framework

method lays the foundation for general stability analysis, it is still quite unclear how the choice of these parameters (H_1 , H_2) can be related to the performance of the system.

A slightly extended version of the Kothare framework is the Miyamoto Method [83] where the AW compensator is synthesized by choosing an initial coprime factorization of the controller i.e. $K = V_0^{-1}U_0$ and these initial factors are then used to find a dynamic variable $W^{-1} \in \mathcal{RH}_\infty$ which can be applied to identify U and V such that $U = WU_0$ and $V = WV_0$. W is obtained by solving an H_∞ optimization problem where the closed loop stability is guaranteed while the nonlinear performance of the system is handled by using a performance index that minimizes certain transfer functions affected by the saturation nonlinearity from the plant's input to output, thereby introducing a way to determine performance measure for systems with AW compensation.

2.4.2.2 Weston and Postlethwaite Framework

Many of the previously mentioned AW compensators acted on the controller features irrespective of the plant but in [84], a framework which is similar to [40], the AW compensator can be synthesized by allowing the choice of a transfer function M which can be interpreted as a coprime factorisation of the plant. This framework presents a decoupled representation of the AW structure and was further developed in [85] often called the **Weston and Postlethwaite** (W&P) framework.

In this framework (see Figure 2.12), the effect of the plant on the AW compensator design is transparent. The design of the AW compensator involves synthesizing $M(s)$ to achieve a compromise between the system's behaviour in the nonlinear loop and in the disturbance filter

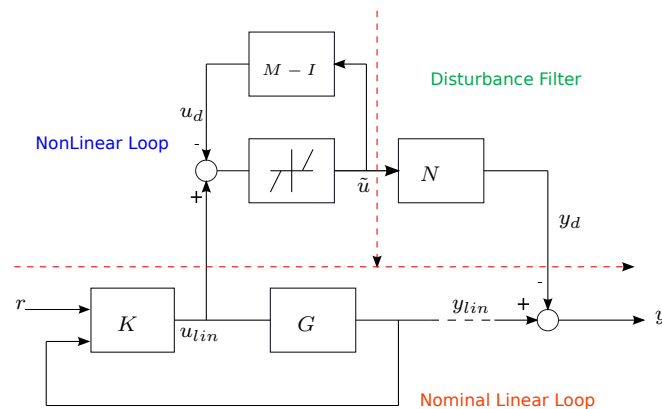


FIGURE 2.13: Equivalent representation of Weston and Postlethwaite framework

as shown in the equivalent representation of Figure 2.12 in Figure 2.13. If the state-space realisation of the plant $G(s)$ is given as

$$G(s) \sim \left[\begin{array}{c|c} A_p & B_p \\ \hline C_p & D_p \end{array} \right] \quad (2.15)$$

then $M(s)$ which is the right factor of the right coprime factorisation of the plant is given such that $G(s) = N(s)M(s)^{-1}$ where $N(s) = G(s)M(s)$ is the disturbance filter. Hence the state space realization of the $M(s)$ and $N(s)$ matrices are given as

$$\left[\begin{array}{c} M(s) \\ N(s) \end{array} \right] = \left[\begin{array}{c|c} A_p + B_p F & B_p \\ \hline F & I \\ \hline C_p + D_p F & D_p \end{array} \right] \quad (2.16)$$

where F is chosen so that $A_p + B_p F$ is Hurwitz. This method assumes that $\hat{u} = \text{sat}(u)$, is available for feedback and the interconnection between the plant $G(s)$ and the controller $K(s)$ is asymptotically stable and well-posed.

In this framework, the system functions normally during the unsaturated mode of behaviour, i.e only the nominal linear loop in Figure 2.13 is active. When saturation occurs, $\hat{u} \neq 0$ and the nonlinear loop becomes active. The signal \hat{u} also activates the disturbance filter, perturbing the output from the linear one such that $y = y_{lin} - y_d$. When the saturation ceases i.e $\hat{u} = 0$, the nonlinear loop becomes in-active and the disturbance filter is no longer forced but y_d continues to dissipate into y until it becomes negligible and the normal operation resumes. This framework allows the compensator to be added to an existing controller and plant without disturbing the implementation of the controller. To guarantee the stability or characterise the region of stability for the closed-loop system, conditions are set using theories such as small gain theorem and circle criterion to formulate optimization problems (many of which are in LMI form) to be solved while the nonlinear performance of the system is expressed using measures such as the \mathcal{L}_2 gain minimization index with the aim of minimising the deviation from linear performance during saturation and immediately after saturation. Further studies on stability and performance of this framework can be seen in [23, 58, 64, 86]. The W&P framework is an appealing one from which to view AW design because it explicitly captures the nonlinear stability problem (the nonlinear loop) while also revealing insight into the AW performance problem. This framework will be the basis for much of the AW work described in this thesis.

2.5 Summary

Over the last two decades, research on AW compensation has increased significantly and advances in computer processing technology has improved the development process, allowing for more complex design processes and solutions to be considered. This chapter has investigated some existing and popular AW compensator design techniques in a somewhat historical fashion.

Control engineers will generally consider the success of any control measure to include not only the stability of the system being designed but also how well the system performs in its operating

conditions. However, the earlier methods of AW compensation discussed did not focus on the physical interpretation of the control measures on the system to which they were applied. Also many of the earlier forms of AW compensation were application dependent and hence did not include all classes of system. These led to the works done on unified frameworks for AW compensation, some of which are also provided in this chapter. They addressed AW design for most kinds of systems, providing some sort of guarantees for both stability and performance.

In spite of significant progress in the development of AW compensators, much work remains to be done in the development of practical AW compensators for UAV systems. These AW compensators should be capable of providing guaranteed levels of performance with some level of flexibility and ease of operation that will be useful in practical real-life situations. The next chapter focuses on the mathematical and dynamical modelling and analysis of a type of rotary UAV: **The Quadrotor**. Subsequent chapters will present application of AW compensators on the UAV using the Weston & Postlethwaite structure (and recent works on this structure) as basis for the research.

Part I

**Anti-Windup Design for
Quadrotor UAVs**

3 Quadrotor Mathematical Modelling and Flight Control

3.1 Introduction

In this chapter, a general description of the quadrotor UAV is presented and its nonlinear dynamic equations of motion are derived using the Newton-Euler Formalism. The modelling approach uses linear and angular momentum to provide a set of differential equations consisting of linear and rotational motion of the UAV as well as the force and moment relation in the dynamics of the UAV. A brief description of the controller design and a detailed description of the practical platform used for flight tests are also presented.

3.1.1 General Description

The quadrotor is a rotary-wing aircraft powered by four identical motors spaced uniformly around its centre of mass (see Figure 3.1). The quadrotor motors each generate an input force and a torque when powered and the quadrotor is controlled by varying the speeds, voltage or PWM signal of each motor, thereby changing the lift force and its position and orientation in space. The quadrotor has both translational freedom, described by the position in space (x, y, z) as well as rotational freedom, described by the Euler angles (ϕ roll, θ pitch and ψ yaw). The system therefore has six degrees of freedom (6 DOF) and only four inputs, making it an under-actuated system.

The pitch movement θ is provided by one pair of motors (front and back motors) rotating in one direction and is controlled by simultaneously increasing (or decreasing) the speed of the front motor and decreasing (or increasing) the speed of the back motor thereby generating more lift on the side of the faster motor, hence pitching the aircraft. Similar to the pitch, the roll ϕ is provided by the other pair of motors (left and right motors) rotating in the opposite direction and is controlled by simultaneously increasing (or decreasing) the speed of the left motor and decreasing (or increasing) the speed of the right motor thereby generating more lift on the side of the faster motor hence rolling. The yaw movement ψ is obtained by increasing (or decreasing) the speed of the front-back group of motors while decreasing (or increasing) the same speed in the left-right group of motors. Translational motion in x, y, z direction is achieved during the

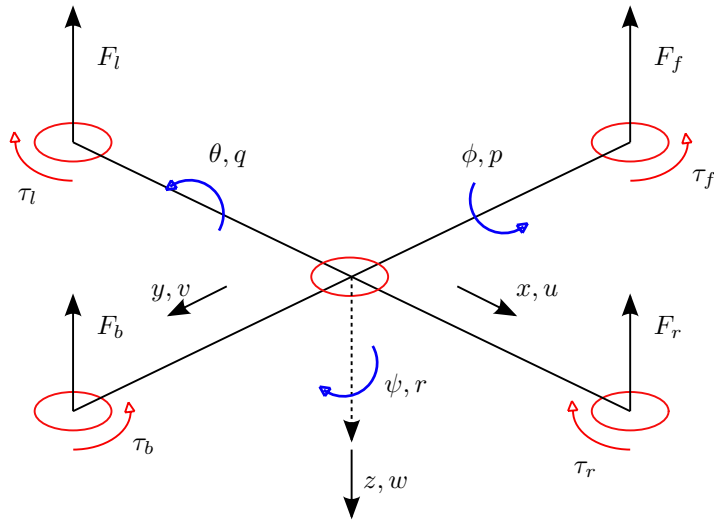


FIGURE 3.1: Force, Torque and States definition of a Quadrotor

rolling or pitching motion but there is no translational motion in the yawing motion due to the net zero force generated by the motors in yaw.

The fundamental mechanics of the quadrotor are quite simple to understand however the easy manoeuvrability of the vehicle can result in highly nonlinear behaviour arising from cross-coupling in angular velocities and may result in rapid large deviations from its stable hover position [87].

3.1.2 Quadrotor Models in Literature

There are a plethora of quadrotor models that exist in literature, many of which are dependent on a variety of conditions based on a chosen application [88–91]. However, there are some which encompass to a very large extent the complex nature of the quadrotor as a platform for performing different analyses.

The most well known of these models is Bouabdallah’s approach [92], which describes a comprehensive quadrotor mathematical model and simulator, incorporating realistic rotor and sensor models used to test a variety of control strategies. In his work [92], the two major modelling formalisms; the Euler-Lagrange formalism & the Newton-Euler formalism were used to develop the quadrotor models for a test-bench and a physical quadrotor respectively.

The Euler-Lagrange formalism makes use of the Lagrangian of a rigid body which considers the potential and kinetic energy of the system to which kinetic energy is a combination of the translational and rotational components of the system. The Newton-Euler formalism considers the linear and angular momentum of the system which allows for the easy separation of the translational and rotational components unlike in the Euler-Lagrange formalism.

Similar approaches to the Bouabdallah model are demonstrated in works such as [24, 93, 94], some of which may use just one or both of the modelling formalisms and may also contain descriptions of nonlinear rotor (motor & propeller) models. In [24], Beard derives a standard quadrotor model from Newton-Euler formalism and shows simplified models that can be used for controller design and state estimation.

The quadrotor modelling in this chapter will be derived using the Newton-Euler formalism similar to the approach in [24]. This is to allow for easy identification of the saturated actuator component to be used in subsequent chapters.

3.2 Mathematical Modelling

The model developed in this thesis assumes the following:

Assumption 3.1.

1. The structure is supposed to be rigid.
2. The quadrotor has a perfectly symmetrical structure hence the inertia matrix will be diagonal.
3. Since there are no aerodynamic lifting surfaces, it is assumed that the aerodynamic forces and moments are negligible.

The quadrotor system is a six degrees of freedom system, defined by twelve (12) states, as seen in Figure 3.1 with respect to certain fixed reference frames. These reference frames are briefly described in the next subsection. The attitude and heading of the system is characterized by six (6) states; the angles (ϕ, θ, ψ) and angular rates (p, q, r) in both the inertial and the body axes reference frames respectively. While the other six states describe the translational motion. These are the position vectors (x, y, z) in the inertial frame and the linear velocities (u, v, w) of the center of mass of the quadrotor in the body axes frame.

3.2.1 Reference Frames

Reference frames use numbers, or coordinates to uniquely define the position of a point or geometric element in space. The order of coordinates in any frame is highly significant and the use of such frames in any space definition allows problems in geometry to be translated into problems with numbers and simplified equations.

It is important to note that there are a number of reference frames used in the derivation of quadrotor dynamics, however the two major ones used are the **Inertial frame** (also known as the earth fixed frame) and the **Body axes frame** (the frame about the center of gravity of the quadrotor). In order to change from inertial reference frame to body frame and vice versa, we need to outline the rotation matrices between the inertial frame and the body frame using the rotation of the quadrotor vehicle with its origin at its center of mass through each of the rotational degrees of freedom in sequence. Each of these rotations are defined as the Vehicle's coordinate frame and the description of the vehicle's frame rotation matrices can be seen in Appendix A [24]. The resultant transformation matrix R from inertial to body frame becomes;

$$R = R_v \cdot R_{v1} \cdot R_{v2}$$

where R_v , R_{v1} and R_{v2} are the first, second and final rotations of the vehicle's coordinate frame and are given as

$$R_v = \begin{bmatrix} 1 & 0 & 0 \\ 0 & \cos \phi & -\sin \phi \\ 0 & \sin \phi & \cos \phi \end{bmatrix}, R_{v1} = \begin{bmatrix} \cos \psi & \sin \psi & 0 \\ -\sin \psi & \cos \psi & 0 \\ 0 & 0 & 1 \end{bmatrix}, R_{v2} = \begin{bmatrix} \cos \theta & 0 & \sin \theta \\ 0 & 1 & 0 \\ -\sin \theta & 0 & \cos \theta \end{bmatrix} \quad (3.1)$$

Hence, this yields;

$$R = \begin{bmatrix} \cos \psi & \sin \psi & 0 \\ -\sin \psi & \cos \psi & 0 \\ 0 & 0 & 1 \end{bmatrix} \begin{bmatrix} \cos \theta & 0 & \sin \theta \\ 0 & 1 & 0 \\ -\sin \theta & 0 & \cos \theta \end{bmatrix} \begin{bmatrix} 1 & 0 & 0 \\ 0 & \cos \phi & -\sin \phi \\ 0 & \sin \phi & \cos \phi \end{bmatrix}$$

$$R = \begin{bmatrix} \cos \theta \cdot \cos \psi & \cos \psi \cdot \sin \theta \cdot \sin \phi - \cos \phi \cdot \sin \psi & \cos \psi \cdot \sin \theta \cdot \cos \phi - \sin \phi \cdot \sin \psi \\ \cos \theta \cdot \sin \psi & \sin \psi \cdot \sin \theta \cdot \sin \phi - \cos \phi \cdot \cos \psi & \sin \psi \cdot \sin \theta \cdot \cos \phi - \sin \phi \cdot \cos \psi \\ -\sin \theta & \cos \theta \cdot \sin \phi & \cos \phi \cdot \cos \theta \end{bmatrix} \quad (3.2)$$

3.2.2 State Variable Relationships and Kinematics

The quadrotor state variables are defined in the different reference frames and are given as;

- position vectors (x, y, z) are in inertial frame
- linear velocities (u, v, w) are in body frame
- angular velocities (p, q, r) are in body frame
- yaw angle (ψ) is in inertial frame while the pitch (θ) and roll (ϕ) angles are resolved in the first and second rotation of vehicle's coordinate frame respectively all with respect to the inertial frame

Given the reference frame definitions provided by Equations (3.1) and (3.2), the linear velocities $[u, v, w]^T$ along the body axes can be described in the inertial frame and related to the position vectors $[\dot{x}, \dot{y}, \dot{z}]^T$ by the equation (3.3)

$$\begin{bmatrix} \dot{x} \\ \dot{y} \\ \dot{z} \end{bmatrix} = R \begin{bmatrix} u \\ v \\ w \end{bmatrix} \quad (3.3)$$

such that

$$\begin{bmatrix} \dot{x} \\ \dot{y} \\ \dot{z} \end{bmatrix} = \begin{bmatrix} \cos \theta \cdot \cos \psi & \cos \psi \cdot \sin \theta \cdot \sin \phi - \cos \phi \cdot \sin \psi & \cos \psi \cdot \sin \theta \cdot \cos \phi - \sin \phi \cdot \sin \psi \\ \cos \theta \cdot \sin \psi & \sin \psi \cdot \sin \theta \cdot \sin \phi - \cos \phi \cdot \cos \psi & \sin \psi \cdot \sin \theta \cdot \cos \phi - \sin \phi \cdot \cos \psi \\ -\sin \theta & \cos \theta \cdot \sin \phi & \cos \phi \cdot \cos \theta \end{bmatrix} \begin{bmatrix} u \\ v \\ w \end{bmatrix}$$

Similarly, the angular velocities $[p, q, r]^T$ along the body axes can be described in the inertial frame and related to the Euler angular rates $[\dot{\phi}, \dot{\theta}, \dot{\psi}]^T$ by the transformation matrix in equation (3.4)¹

$$\begin{aligned} \begin{bmatrix} p \\ q \\ r \end{bmatrix} &= \begin{bmatrix} \dot{\phi} \\ 0 \\ 0 \end{bmatrix} + R_v \begin{bmatrix} 0 \\ \dot{\theta} \\ 0 \end{bmatrix} + R_v R_{v2} \begin{bmatrix} 0 \\ 0 \\ \dot{\psi} \end{bmatrix} \\ \begin{bmatrix} p \\ q \\ r \end{bmatrix} &= \begin{bmatrix} 1 & 0 & -\sin \theta \\ 0 & \cos \phi & \sin \phi \cos \theta \\ 0 & -\sin \phi & \cos \phi \cos \theta \end{bmatrix} \begin{bmatrix} \dot{\phi} \\ \dot{\theta} \\ \dot{\psi} \end{bmatrix} \end{aligned} \quad (3.4)$$

By inverting equation (3.4), the euler angular rates $[\dot{\phi}, \dot{\theta}, \dot{\psi}]^T$ can be given as

$$\begin{bmatrix} \dot{\phi} \\ \dot{\theta} \\ \dot{\psi} \end{bmatrix} = \underbrace{\begin{bmatrix} 1 & \sin \phi \tan \theta & \cos \phi \tan \theta \\ 0 & \cos \phi & -\sin \phi \\ 0 & \sin \phi \sec \theta & \cos \phi \sec \theta \end{bmatrix}}_P \begin{bmatrix} p \\ q \\ r \end{bmatrix} \quad (3.5)$$

The P indicated in the above equation represents the transformation matrix for the angular rates.

3.2.3 Newton-Euler rigid body dynamics

3.2.3.1 Translational motion

The translational motion of the vehicle is obtained by considering its linear momentum using Newton's laws to describe the rigid body in inertial frame. Therefore applying Newton's second law to describe the translational motion of the quadrotor gives;

$$f_i = m \frac{dv_i}{dt}$$

where the force f_i is the rate of change of linear momentum mv_i with time in inertial frame. This force can be described in body frame by noting the transformation in equation (3.3) so that;

$$\begin{aligned} f_b &= mR^{-1}v_i = mR^{-1} \frac{d}{dt}(Rv_b) \\ &= mR^{-1}((R\dot{v}_b) + (\dot{R}v_b)) \\ &= m(\dot{v}_b + (R^{-1}\dot{R}v_b)) \end{aligned} \quad (3.6)$$

¹See Appendix A [24] for full derivation

The action of infinitesimal rotations [95, 96] allow $R^{-1}\dot{R}v_b$ to be broken down into the Coriolis² term $\omega_b \times v_b$, therefore,

$$f_b = m(\dot{v}_b + \omega_b \times v_b)^3 \quad (3.7)$$

where

- v_b is the velocity vector measured in body frame and $v_b \triangleq [uvw]^T$.
- ω_b is the angular velocity vector measured in body frame and $\omega_b \triangleq [pqr]^T$.
- f_b is the total force applied to the quadrotor in body frame.

Rearranging equation (3.7) and multiplying out the vector cross product yields;

$$\dot{v}_b = - \begin{bmatrix} u \\ v \\ w \end{bmatrix} \times \begin{bmatrix} p \\ q \\ r \end{bmatrix} + \frac{1}{m}(f_b)$$

$$\begin{bmatrix} \dot{u} \\ \dot{v} \\ \dot{w} \end{bmatrix} = \begin{bmatrix} rv - qw \\ pw - ru \\ qu - pv \end{bmatrix} + \frac{1}{m}(f_b) \quad (3.8)$$

At this stage, the forces acting on the quadrotor are the total force exerted by the motors and the force due to gravity. So from equation (3.8),

$$f_b = f_{motor_b} + f_{gravity_b} \quad (3.9)$$

The force exerted by the motors in body frame is the same in inertial frame ie $f_{motor_b} = f_{motor_i}$. The total motor force is only exerted in the z axis of the frame and it will be expressed as F hereafter ($f_{motor_b} = f_{motor_i} = F$). The force due to gravity in inertial frame is given as

$$f_{gravity_i} = \begin{bmatrix} 0 \\ 0 \\ mg \end{bmatrix}$$

and this can be expressed in body frame as

$$f_{gravity_b} = R^{-1}f_{gravity_i} = R^{-1} \begin{bmatrix} 0 \\ 0 \\ mg \end{bmatrix} \quad (3.10)$$

$$= \begin{bmatrix} -mg \sin \theta \\ mg \sin \phi \cos \theta \\ mg \cos \phi \cos \theta \end{bmatrix} \quad (3.11)$$

Substituting equations (3.9) and (3.11) in equation (3.8) yields

¹“ \times ” here represents the vector cross product

²See [97] for more information on Coriolis equation

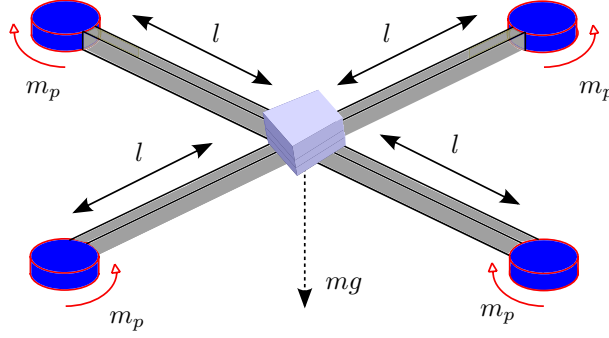


FIGURE 3.2: Showing symmetric axes with point masses (m_p) and distance (l) from centre of quadrotor

$$\begin{bmatrix} \dot{u} \\ \dot{v} \\ \dot{w} \end{bmatrix} = \begin{bmatrix} rv - qw \\ pw - ru \\ qu - pv \end{bmatrix} + \begin{bmatrix} g \sin \theta \\ g \sin \phi \cos \theta \\ g \cos \phi \cos \theta \end{bmatrix} + \frac{1}{m} \begin{bmatrix} 0 \\ 0 \\ F \end{bmatrix} \quad (3.12)$$

3.2.3.2 Rotational motion

Again applying Newton's second law to the quadrotor in rotational motion will give;

$$\tau_i = \frac{dh_i}{dt}$$

where h_i is the angular momentum and τ_i is the applied torque both in inertial frame. Recall the transformation conversion in equation (3.5) and similar to the process followed in section 3.2.3.1, the torque and angular momentum in body axes is given as;

$$\begin{aligned} \tau_b &= P^{-1} \dot{h}_b = P^{-1} \frac{d}{dt} (P h_b) \\ &= P^{-1} ((P \dot{h}_b) + (\dot{P} h_b)) \\ &= \dot{h}_b + (P^{-1} \dot{P} h_b) \end{aligned} \quad (3.13)$$

Again, the action of infinitesimal rotations allows $P^{-1} h_b \dot{P}$ to be converted to $\omega_b \times h_b$, therefore,

$$\tau_b \Rightarrow \dot{h}_b + \omega_b \times h_b^4 \quad (3.14)$$

Here, h_b is the angular momentum measured in body frame and $h_b = J \omega_b$, where J is the constant inertia matrix and it is given by

$$J \triangleq \begin{bmatrix} J_x & -J_{xy} & J_{xz} \\ -J_{xy} & J_y & -J_{yz} \\ -J_{xz} & -J_{yz} & J_z \end{bmatrix}$$

As seen in Figure 3.2 and by Assumption 3.1, since our quadrotor is symmetric about its axes, $J_{xy} = J_{xz} = J_{yz} = 0$, hence

⁴“ \times ” here represents the vector cross product

$$J = \begin{bmatrix} J_x & 0 & 0 \\ 0 & J_y & 0 \\ 0 & 0 & J_z \end{bmatrix} \quad (3.15)$$

From equation (3.14), we can then say that

$$\dot{h}_b = \omega_b \times h_b + \tau_b \quad (3.16)$$

$$= \omega_b \times J\omega_b + \tau_b \quad (3.17)$$

where

$$\dot{h}_b = \frac{d}{dt}(J\omega_b), \omega_b \triangleq \frac{1}{J} \begin{bmatrix} \dot{p} \\ \dot{q} \\ \dot{r} \end{bmatrix}$$

$$\tau_b \triangleq \begin{bmatrix} \tau_\phi \\ \tau_\theta \\ \tau_\psi \end{bmatrix} \text{ and as stated earlier } \omega_b \triangleq \begin{bmatrix} p \\ q \\ r \end{bmatrix}$$

Equation (3.17) now becomes

$$\begin{bmatrix} \dot{p} \\ \dot{q} \\ \dot{r} \end{bmatrix} = \begin{bmatrix} \frac{1}{J_x} & 0 & 0 \\ 0 & \frac{1}{J_y} & 0 \\ 0 & 0 & \frac{1}{J_z} \end{bmatrix} \left(\begin{bmatrix} p \\ q \\ r \end{bmatrix} \times \begin{bmatrix} J_x & 0 & 0 \\ 0 & J_y & 0 \\ 0 & 0 & J_z \end{bmatrix} \begin{bmatrix} p \\ q \\ r \end{bmatrix} + \begin{bmatrix} \tau_\phi \\ \tau_\theta \\ \tau_\psi \end{bmatrix} \right) \quad (3.18)$$

$$= \begin{bmatrix} \frac{J_y - J_z}{J_x} qr \\ \frac{J_x - J_z}{J_y} pr \\ \frac{J_x - J_y}{J_z} pq \end{bmatrix} + \begin{bmatrix} \frac{1}{J_x} \tau_\phi \\ \frac{1}{J_y} \tau_\theta \\ \frac{1}{J_z} \tau_\psi \end{bmatrix} \quad (3.19)$$

3.2.4 6 DOF model

The complete 6 DOF model can be summarized as follows;

$$\begin{bmatrix} \dot{x} \\ \dot{y} \\ \dot{z} \end{bmatrix} = \begin{bmatrix} \cos \theta \cos \psi & \cos \psi \sin \theta \sin \phi - \cos \phi \sin \psi & \cos \psi \sin \theta \cos \phi - \sin \phi \sin \psi \\ \cos \theta \sin \psi & \sin \psi \sin \theta \sin \phi - \cos \phi \cos \psi & \sin \psi \sin \theta \cos \phi - \sin \phi \cos \psi \\ -\sin \theta & \cos \theta \sin \phi & \cos \phi \cos \theta \end{bmatrix} \begin{bmatrix} u \\ v \\ w \end{bmatrix} \quad (3.20)$$

$$\begin{bmatrix} \dot{\phi} \\ \dot{\theta} \\ \dot{\psi} \end{bmatrix} = \begin{bmatrix} 1 & \sin \phi \tan \theta & \cos \phi \tan \theta \\ 0 & \cos \phi & -\sin \phi \\ 0 & \sin \phi \sec \theta & \cos \phi \sec \theta \end{bmatrix} \begin{bmatrix} p \\ q \\ r \end{bmatrix} \quad (3.21)$$

$$\begin{bmatrix} \dot{u} \\ \dot{v} \\ \dot{w} \end{bmatrix} = \begin{bmatrix} rv - qw \\ pw - ru \\ qu - pv \end{bmatrix} + \begin{bmatrix} g \sin \theta \\ g \sin \phi \cos \theta \\ g \cos \phi \cos \theta \end{bmatrix} + \frac{1}{m} \begin{bmatrix} 0 \\ 0 \\ F \end{bmatrix} \quad (3.22)$$

$$\begin{bmatrix} \dot{p} \\ \dot{q} \\ \dot{r} \end{bmatrix} = \begin{bmatrix} \frac{J_y - J_z}{J_x} qr \\ \frac{J_x - J_z}{J_y} pr \\ \frac{J_x - J_y}{J_z} pq \end{bmatrix} + \begin{bmatrix} \frac{1}{J_x} \tau_\phi \\ \frac{1}{J_y} \tau_\theta \\ \frac{1}{J_z} \tau_\psi \end{bmatrix} \quad (3.23)$$

3.2.5 Actuator Model

Most small quadrotors use brushless DC motors (BLDC) because they are silent and efficient at converting electrical energy into mechanical power since there are no electrical/friction losses due to brushes. BLDC motors are controlled using Electronic speed controllers (ESCs) which work as pulse width modulation (PWM) controllers, applying voltage to the motor periodically.

Propellers are connected to the motors and they spin at a given angular velocity to generate forces. Assuming that the frictional forces of the air with the blade, blade flapping and ground effect are negligible, Blade momentum theory [98, 99] shows that the force f_i and torques τ_i generated by each propeller are proportional to the squared angular velocity ω of the propeller and are defined by the equations:

$$\begin{aligned} f_i &= k_1 \omega^2 \\ \tau_i &= k_2 \omega^2 \end{aligned} \quad (3.24)$$

$$\begin{aligned} k_1 &= r_r^4 \rho \pi C_T \\ k_2 &= r_r^5 \rho \pi C_P \end{aligned} \quad (3.25)$$

where C_T, C_P are dimensionless constants of force and power, r_r is the radius of rotation and ρ is the air density.

The electromechanical interaction in the motor behaviour can be represented by the following equations based on Newton's 2nd law and Kirchoff's voltage law.

$$v = k_e \dot{\theta} + L \frac{di}{dt} + Ri \quad (3.26)$$

$$J\ddot{\theta} = k_t i - \tau_r - B\dot{\theta} \quad (3.27)$$

where k_e is the electromotive force constant, k_t is the motor torque constant, v, i is the voltage current, θ is the angular rotation of the rotor, R is the electric resistance, L is the electric inductance, J is the rotor inertia, τ_r is the resistive torque and B is the motor's viscous friction constant. A typical BLDC motor is controlled by an ESC which receives the PWM signal that drives the motor to the desired speed. Suppose we replace the voltage v in equation (3.26) with a PWM signal PWM (since most BLDCs are driven using PWM), and replace the angular

velocity $\dot{\theta}$ with ω , therefore for each motor i , equation (3.27) can be represented as

$$\frac{\omega_i}{PWM_i} = \frac{k}{(Js + B)(Ls + R) + k^2} \quad (3.28)$$

where $k = k_e + k_t$ represents both the electromotive force constant and the motor torque constant. This equation (equation (3.28)) shows an accurate representation of the motor model but it is however very difficult to obtain all the parameters represented therein from manufacturer technical data. Hence the model can be simplified to a simple first order system characterized by

$$\frac{\omega_i}{PWM_i} = \frac{k_g}{\gamma s + 1} \quad (3.29)$$

where k_g is the motor's dc gain and γ is the motor's time constant. These values are available in most BLDC motors manufacturer datasheets.

3.2.6 Forces & Torques

According to Figure 3.1 and 3.2, each motor produces an upward force F and a torque τ . These motors can be labelled as the front (f), back (b), left (l) and right (r) motors. The total force and torques exerted by the motors on the quadrotor is given by

$$\begin{aligned} \text{Lift force } F &= F_f + F_r + F_b + F_l \\ \text{Roll torque } \tau_\phi &= l(F_l - F_r) \\ \text{Pitch torque } \tau_\theta &= l(F_f - F_b) \\ \text{Yaw torque } \tau_\psi &= \tau_r + \tau_l - \tau_f - \tau_b \end{aligned} \quad (3.30)$$

where l is the distance between the motor location and centre of mass. Recall the forces and torques generated by the propellers given in equation (3.24), hence it is assumed that for each propeller

$$F_* = k_1 \delta_* \quad (3.31)$$

$$\tau_* = k_2 \delta_* \quad (3.32)$$

where k_1 and k_2 are constants that need to be determined experimentally and δ_* is the motor command.

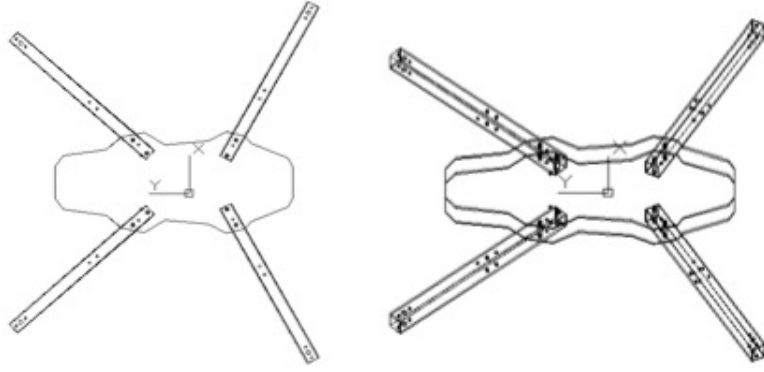


FIGURE 3.3: CAD representations

Therefore, the forces and torques on the quadrotor can be rewritten in matrix form with respect to the actual motor commands as:

$$\begin{bmatrix} F \\ \tau_\phi \\ \tau_\theta \\ \tau_\psi \end{bmatrix} = \underbrace{\begin{bmatrix} k_1 & k_1 & k_1 & k_1 \\ 0 & -lk_1 & 0 & lk_1 \\ lk_1 & 0 & -lk_1 & 0 \\ -k_2 & k_2 & -k_2 & k_2 \end{bmatrix}}_X \begin{bmatrix} \delta_f \\ \delta_r \\ \delta_b \\ \delta_l \end{bmatrix} \quad (3.33)$$

The matrix indicated as X in the equation (3.33) is invertible and constant and its inverse X^{-1} can be considered as a control allocation matrix.

3.3 Experimental Quadrotor Platform

3.3.1 Platform Description

The test platform is a 2014 3DR quadrotor [100], a DIY quadrotor kit equipped with the Ardupilot Mega (APM 2.6) programmable flight controller board whose firmware has been modified to allow for testing and validation. Figures 3.3 and 3.4 shows the CAD representation and actual prototype of the 3DR quadrotor. The hardware components of the 3DR quadrotor include;

Frame: The 3DR quadrotor frame is a combination of carbon fibre plates and aluminium struts intended to provide a balance between impact strength and weight. Impact strength is required because the frame may take a few hard landings and potential crashes during tests. The central carbon fibre plate is large enough to place components and makes it easier to attach and detach any components easily for troubleshooting purposes.

Core Avionics & Sensors: This quadrotor consists of the following sensor and avionics components: (1) four UT2212 850kV brushless DC motors, (2) a Quattro 4in1 20A electronic speed controller (ESC) which control the rate at which each motor spins at any given time, (3) four 12" two-bladed propellers, (4) a Ublox LEA-6H GPS with compass kit (5) a pair of 3DR 433MHz



FIGURE 3.4: Modified 2014 3DR Quadrotor

transceiver telemetry kit (6) an AR6200 6-channel DSMX receiver (7) and a Floureon rechargeable lithium-polymer, 11.1V, 5500mAh battery with a power module that supplies variable voltages to the different sections of the quadrotor. See Figure 3.5 for a block architecture of the interconnections of all these components.

Flight Controller: The Ardupilot Mega (APM 2.6) is based on the Arduino ATmega2560 microcontroller. It provides a large number of I/O pins for its sensors which include magnetometers, barometric pressure sensors and the inertial measurement unit (IMU) sensor consisting of a three-axis accelerometer and a three-axis gyroscope. The firmware for this system is open source and has much support on cross platform application and programming making it relatively simple to understand and modify.

Ground Control Station (GCS): The GCS is a computer that runs the software that communicates with the quadrotor remotely via the telemetry system. It helps monitor the quadrotor's

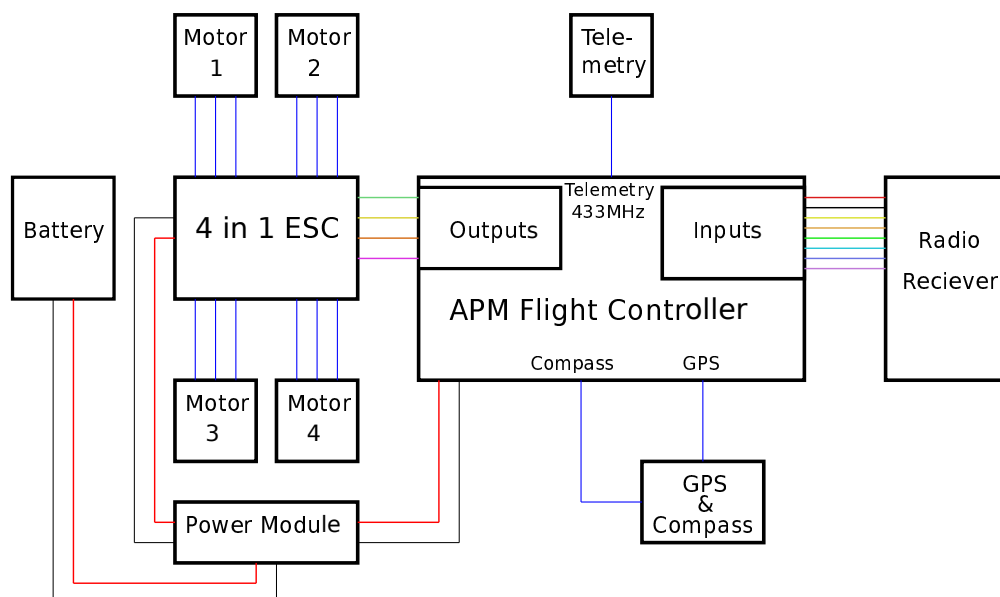


FIGURE 3.5: Quadrotor Hardware Schematic

TABLE 3.1: Approximate values of 3DR Quadrotor parameters

Parameters	Description	Values	Units
g	Gravity	9.81	ms^{-2}
m	Mass	2.1	kg
d	Distance	0.3	m
k_1	Force constant	0.89	
k_2	Torque constant	0.11	
J_x	Pitch Inertia	2.85×10^{-3}	kgm^{-2}
J_y	Roll Inertia	2.85×10^{-3}	kgm^{-2}
J_z	Yaw Inertia	1.81×10^{-3}	kgm^{-2}

performance and status. The GCS software has a heads-up display (HUD), moving maps showing the UAV's position and a host of indicators that help enhance flight performance.

Taking into account elements such as UAV size, proven performance, coding flexibility, easy detachability and ready availability of components in the market, the 2014 3DR quadrotor was chosen as the UAV model for testing. The rotational and translational dynamics of this system is similar to the complete nonlinear dynamics of the quadrotor in Section 3.2, however the motor model was further simplified from that obtained in equation (3.29) using direct measurements from the UT2212 850kV brushless DC motor such that there is a linear relationship between the motor's PWM input and the angular velocity represented as shown in figure 3.6. A summary of the quadrotor's basic parameters are shown in Table 3.1.

3.3.2 Control Architecture

3.3.2.1 Quadrotor Control in Literature

Different approaches to quadrotor control are found in the literature, including both linear and nonlinear methods. A key consideration in controller design is the ability to handle uncertainties from sensors and actuators that may not occur during simulation, however the controller design may also depend on the objectives and the level of control required by the designer of the system. These controllers work with sensor feedback devices such as (i) Inertial Measurement Units (IMUs) containing accelerometers, gyroscopes and magnetometers used in measuring linear accelerations and angular rates, (ii) Ultrasonic sensors used in measuring distances to the ground at low altitudes, (iii) Barometer measures humidity and pressure to work out the distance to ground at high altitudes, (iv) Visual or Infrared Cameras, (v) Ground Positioning System (GPS) modules. In general, the control strategies implemented in the control of a quadrotor may contain the use of only one type of controller [99, 101, 102] or a combination of different types of controllers [92] and some of these control strategies may seek to only control the orientation

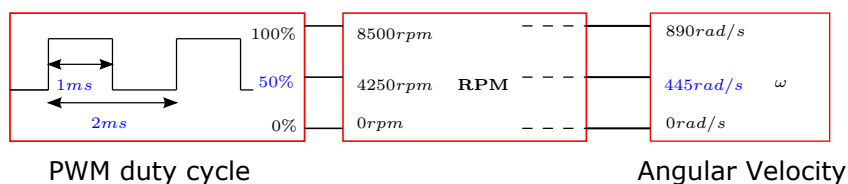


FIGURE 3.6: PWM conversion

of the vehicle, and others may seek to control orientation and position. Some of the controllers used in quadrotor control include;

- (a). **Linear Proportional-Integral-Derivative (PID):** A classical Proportional, Integral, Derivative (PID) controller uses the proportional to provide basic feedback, the integral to eliminate steady state error and the derivative to provide damping to the control. PID controllers can be used solely as in [92] or in conjunction with other control schemes to achieve better results; for example, adding *backstepping* as used in [92]. However, it may not on its own be able to stabilize the quadrotor in the presence of very strong perturbation and disturbances. Some other examples of the use of this controller include [99, 103, 104]. Other variants of this controller used on quadrotors include the **proportional-integral (PI)** [102] and the **proportional-derivative (PD)** [101, 105].
- (b). **Linear Quadratic Regulating (LQR) controllers:** The LQR is an optimal control solution that minimizes a certain cost function to achieve control of a system. In [106], an LQR controller was successfully used to control a quadrotor UAV while subsequent tuning was carried out to minimize roll and pitch angle oscillations during hover position. Other examples include [107–109]
- (c). **Backstepping:** Backstepping controllers are used when some states of a system are controlled through other states as can be seen in the case of the quadrotor dynamics. In backstepping, the control law is designed using the Lyapunov stability criteria where a virtual control law is determined by undergoing a step back through the system to find a control law [89, 110].
- (d). **Feedback Linearization and Dynamic Inversion:** In feedback linearisation control, the known nonlinear system is transformed into an equivalent linear system, through a change of variables and a suitable control input. A specific case of feedback linearization is known as nonlinear dynamic inversion, where the nonlinear model is linearised and inverted. This linearised system is placed as an inner control loop and an outer control loop is added to control this inner loop. In [110], a feedback linearisation controller for the quadrotor is designed in a number of ordered design procedures. The outer loop is designed with a classical polynomial control law. In addition, a higher-order sliding mode observer is designed to find the additional states from the position and the yaw angle to control the “*inversion*”. Other examples include [111] [87].
- (e). **Adaptive and Semi-adaptive schemes:** In [112], an adaptive controller based on a nonlinear function approximator known as the Cerebellar Model Arithmetic Computer (CMAC) and its application to a quadrotor UAV was presented. This method relies on an alternate set of weights to guide the training of the weights used in the controller CMAC. The alternate set of weights is trained online to approximate the same output with the weights clustered closer to the mean. A test on the quadrotor showed that appropriate robust controller parameters can be picked such that it prevents adaptive weights drift and bursting. Other adaptive schemes include [113–115]

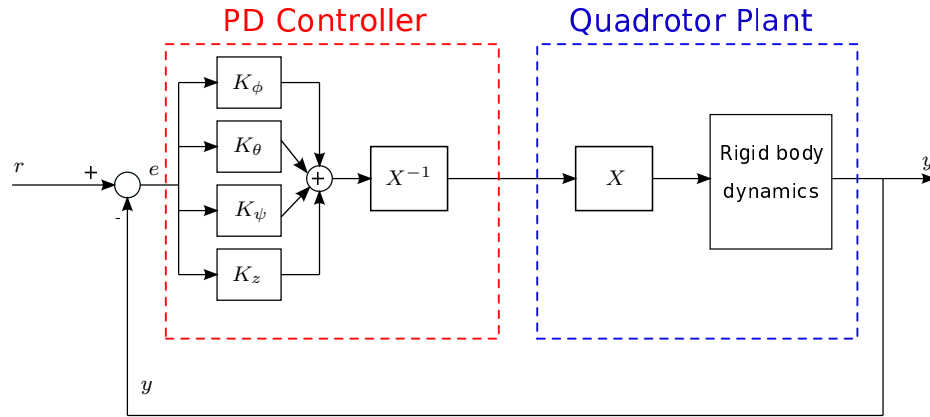


FIGURE 3.7: PD controller structure

3.3.2.2 Proposed Controller

As earlier mentioned, there are twelve states in the quadrotor, but only four control inputs (the angular velocities of the four rotors) hence it is underactuated and this could make the controller design quite difficult. However, the key considerations for the controller design in this research are;

1. To control only orientation and altitude (ϕ, θ, ψ , and z) of the quadrotor and handle the UAV's maneuvers with satisfactory performance results,
2. It should not introduce extra dynamics that could facilitate the “windup” situations,
3. To be simple (no computationally complex procedures) and yet flexible in design and implementation,
4. It should allow for a decoupled design structure.

The chosen control scheme based on the above considerations is the PD controller. In classical control theory, derivative control when added to the proportional control, provides high sensitivity (improves the transient response) and corrective responses to the rate of change of the actuating error before the magnitude of the error becomes too large and therefore increases the stability of the system. It also adds damping to the system and thus permits the use of larger values of the proportional gain, which will result in an improvement in the steady-state accuracy.

The quadrotor dynamics, defined by equations (3.20-3.23) and (3.30), together with the static matrix X described in equation (3.33), imply that there is a complex relationship between the Forces and Torques generated by the motors and the resulting quadrotor motion. Furthermore, these equations imply a highly coupled multivariable system. To simplify the controller design, the matrix X can be inverted and placed “upstream” of the control inputs (see Figure 3.7). This matrix then, to a large extent, decouples the system, allowing one to design a set of SISO controllers for the individual ϕ, θ, ψ , and z control loops such that we have a single PD controller for each individual control loop as seen in figure 3.7. This decoupling and its simplification process are described in greater detail in the next chapter.

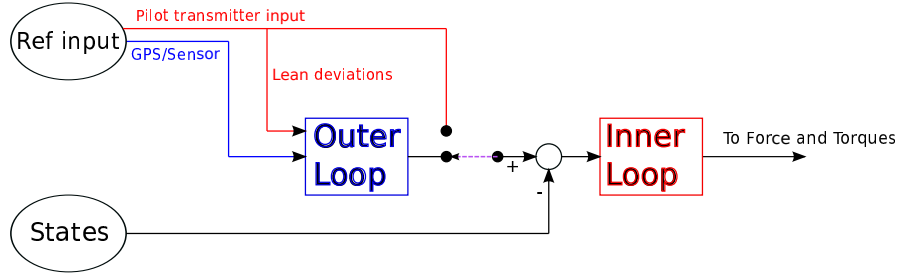


FIGURE 3.8: Applied Control Structure for used Flight Modes

The standard Ardupilot flight controller (APM) firmware for quadrotors (also known as ArduCopter) employs the use of PWM signals (between $1ms$ and $2ms$ long) derived from a translation of the rotors' angular velocities/sensor inputs and fed into a pair of cascading PID control loops in order to control the UAV's flight modes. The inner loop controllers make use of its onboard sensors to find the UAV's attitude and altitude while the outer loop controllers use GPS waypoints to calculate the UAV's desired attitude and altitude. The inner loop controllers also convert the attitude and altitude errors into actual rotor commands. The quadrotor is mostly controlled using one or more flight modes with some level of autonomy. These flight modes are sometimes GPS dependent and are generally in the outer loop control (which in turn affect the inner loop controllers). Flight modes such as STABILIZE, ALTHOLD or POSHOLD, automatically maintain the position or altitude of the quadrotor or both while others such as LOITER, RTL, AUTO, follow a set mission path of coordinates, incorporating the earlier mentioned flight modes in the process. The pilot can input transmitter control to generate desired angle deviations and headings in many of these modes. Figure 3.8 shows the interconnection of these modules in the applied control structure.

This thesis focuses only on the inner loop attitude control of the quadrotor during the AUTO flight mode maneuvers i.e the stabilization of the outer loop containing the AUTO mode is modified along with the inner loop controllers but this will not be discussed in detail, only the inner loop controllers will be considered here. The inner loop controllers consists of the following;

- (a). **Attitude and Heading Controllers:** The quadrotor is symmetrical about its centre and therefore the pitch and roll can be considered independent of each other. The following control law is used for the roll and pitch control respectively.

$$\frac{U_{\phi}(s)}{[r_{\phi} - y_{\phi}](s)} = K_{\phi,P} + sK_{\phi,D} \quad (3.34)$$

$$\frac{U_{\theta}(s)}{[r_{\theta} - y_{\theta}](s)} = K_{\theta,P} + sK_{\theta,D} \quad (3.35)$$

The yaw has very minimal direct effect on the quadrotor's pitch and roll response and hence can be tuned independent of the other controls. It is important to note that disturbances have a relatively small effect on yaw, so only small gains yaw control are required. The PD control law for yaw is given as:

$$\frac{U_{\psi}(s)}{[r_{\psi} - y_{\psi}](s)} = K_{\psi,P} + sK_{\psi,D} \quad (3.36)$$

TABLE 3.2: Approximate values of 3DR Quadrotor PD Gains

Parameters	Description	Values	Units
$K_{\phi,P}$	Proportional gain	0.22	
$K_{\theta,P}$		0.22	
$K_{\psi,P}$		0.4	
Throttle via $K_{z,P}$		6	
$K_{\phi,D}$	Derivative gain	0.004	
$K_{\theta,D}$		0.004	
$K_{\psi,D}$		0.003	
Throttle via $K_{z,D}$		0.001	

(b). **Altitude controller**

The vertical position is the height at which the quadrotor maintains. To remain at constant height, the control output must be able to drive its signal to counteract the effects of gravity and hence the PD controller is added to stabilise the motion in z direction. The control law can be described as:

$$\frac{U_z(s)}{[r_z - y_z](s)} = K_{z,P} + sK_{z,D} + \frac{g}{s} \quad (3.37)$$

In equations (3.35) - (3.37), $K_{*,P}$ is the proportional gain, $K_{*,D}$ is the derivative gain, U_* is the control input, r_* is the desired reference, y_* is the system output⁵ and g is acceleration due to gravity.

The arducopter APM firmware provides standard PID controllers but these are easily converted to PD controllers by setting the integral to zero. Tuning control gains for the inner loop controllers were typically done using Matlab/Simulink simulations in order to ensure that the controller design meets desired tracking performance while the outer loop controllers were tuned based on flight tests and simulated flights⁶ using trial and error method guides on resources such as *DIYDrones.com*. A summary of the inner loop controller gains are shown in table 3.2.

Figure 3.9 shows responses of the nonlinear quadrotor UAV model when a step reference signal of 0.4rad was commanded on the pitch, roll and yaw with reference of 1m commanded on the z axis during nominal operation.

3.4 Summary

In this chapter, the quadrotor dynamics was derived from the Newton Euler formalism and presented in a structure that links the forces and torques generated by the motors with an invertible matrix “X”. The criteria for controller design were stated and it culminated in the choice of PD type controller for the quadrotor UAV. It also considered the MIMO controller design for the system which uses the earlier defined “X” matrix to allow the MIMO controller to have a decoupled structure of PD type controllers such that each control loop for the quadrotor is controller by a single PD type controller.

⁵* represents ϕ, θ, ψ, z

⁶No system identification gain tuning methods were used to determine any of the control gains used in the flights or simulations conducted for this thesis.

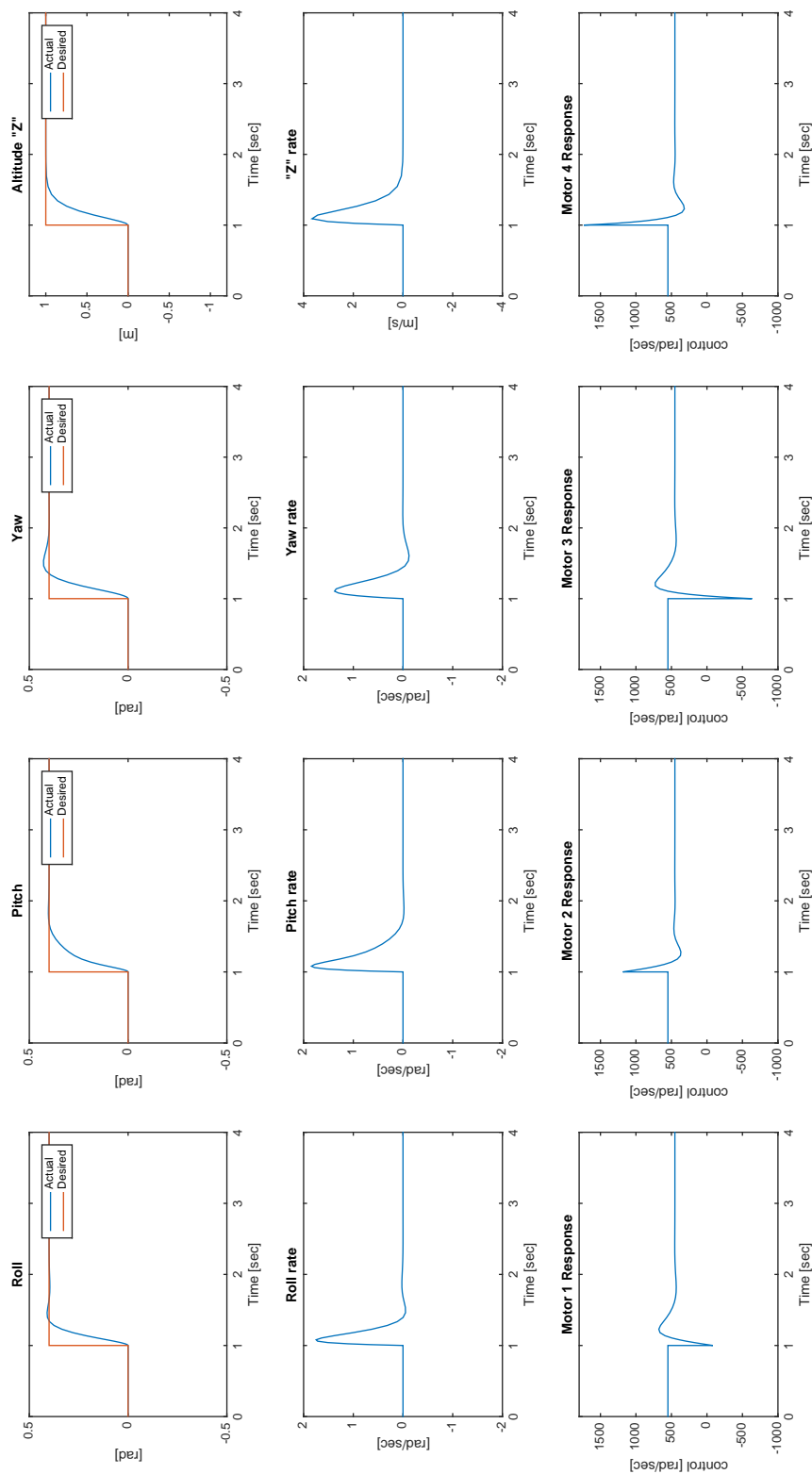


FIGURE 3.9: Nominal quadrotor simulation results

The experimental quadrotor platform, a 3DR quadrotor, was also described along with its flight controller design structure. The design structure and parameters provided for the experimental UAV are used for flight tests and simulation tests in subsequent chapters. In the next chapter, the design and application of a MIMO AW compensator and decentralized AW compensators are presented as applied to the quadrotor described in this chapter.

4 Design of Decentralized AW compensators for Quadrotor UAVs

4.1 Introduction

This chapter details the design of decentralized AW compensators for Quadrotor UAVs with actuators/rotors which are subject to saturation. Two different decentralized AW design approaches are presented here; both AW design approaches exploit the structure of the quadrotor plant and are offshoots of the principles and structure of the AW compensator design approach by [23]. The first approach attempts to impose an AW compensator whose structure is in a certain sense, decentralised: this is referred to as the *pseudo-decentralised* AW compensator in this chapter [116]. The second approach shows how several SISO AW compensators for each single-loop interconnection of the controller-plant model can be designed separately and combined to form a general “stabilizing” MIMO AW compensator: these compensators are referred to as the channel-by-channel AW compensators [117, 118] in this chapter. These AW compensators are applied to the quadrotor model presented in the previous chapter. Results of the implementation of these compensators are also presented and compared to the MIMO anti-windup design method of [23] in both simulated models and the actual UAV’s flight test performance.

4.2 Nonlinear systems and Stability

The AW design methods presented here have rigorous guarantees of nonlinear stability. It is therefore, vital to have some appreciation of certain nonlinear control concepts. This section will present a brief description of the necessary and relevant technical concepts regarding the study of nonlinear dynamical system stability under the topics of Lyapunov stability, Input-Output stability and Absolute stability. It is important to note that this is by no means an exhaustive account but rather a preamble to the stability and performance considerations used in the AW design approaches that will be presented in later sections and chapters of this thesis.

Consider a system $y(t) = F(x(t))$, where $x(t)$ represents the system’s input and $y(t)$ represents the system’s output and x and y are elements of some appropriately defined vector space, then system is considered linear if it has the superposition property given as

$$\begin{aligned} \text{Homogeneity property} \quad & F(ax(t)) = aF(x(t)) \\ \text{Additive property} \quad & F(x_1(t) + x_2(t)) = F(x_1(t)) + F(x_2(t)) \end{aligned}$$

where a is a scalar. There are several tools that are used to easily analyse stability in linear systems [119–124]. However, this thesis primarily focuses on nonlinear systems since the saturation of actuators effectively makes the standard control system feedback loop become nonlinear. Linear analysis tools may not be sufficient alone to analyse the entire nonlinear system but if linear analysis tools are to be used, the nonlinear system initially has to be linearized at a particular equilibrium point before such tools can be used. This can only provide us with information about the behaviour of the nonlinear system at that equilibrium point but not the behaviour of the entire nonlinear system therefore, more advanced techniques are required to help us analyse the entirety of the nonlinear system behaviour. These techniques include, but not limited to, Lyapunov stability theory, Input-Output stability (specifically, the concept of \mathcal{L}_2 Gain and Small Gain theorem) and Absolute stability theory (specifically, Circle theorem). Before these stability theories are introduced, we will present some key definitions on the concept of stability.

Definition 4.1 ([125, 126]). Given the autonomous system with function $f : \mathbb{R}^n \mapsto \mathbb{R}^n$ such that

$$\dot{x}(t) = f(x(t)), \quad (4.1)$$

A particular state x_{es} is called an equilibrium point if $f(x_{es}) = 0$ for all time $t > t_0$ where t_0 denotes initial time.

This definition not only describes an equilibrium point, but also captures the attributes of the system that will be used throughout this section (unless otherwise stated).

Definition 4.2 ([125, 126]). An equilibrium point x_{es} of the system (4.1) is said to be stable if for every $\epsilon > 0$ there exists a $\delta(\epsilon) > 0$ such that if $\|x(t_0) - x_{es}\| < \delta$, then $\|x(t) - x_{es}\| < \epsilon$ for every $t > t_0$. The equilibrium is globally stable if there exists a finite constant $\gamma > 0$ for any initial conditions t_0 and $x(t_0)$ such that $\|x(t) - x_{es}\| \leq \gamma \|x(t_0) - x_{es}\|$ exists at every $t > t_0$.

A system satisfying the above definition is sometimes said to be “Lyapunov stable”. The term ”globally” refers to the fact that Lyapunov stability holds regardless of the initial conditions and if it does not hold, it can be referred to as being “locally” stable. Lyapunov stability implies that solutions around a ”close vicinity” of the equilibrium point will remain “close” at any time in solution.

Definition 4.3 (Asymptotic stability [125–127]). An equilibrium point x_{es} of the system (4.1) is said to be asymptotically stable if it is Lyapunov stable and there exists a $\delta > 0$ such that if $\|x(t) - x_{es}\| < \delta$, then $\lim_{t \rightarrow \infty} \|x(t) - x_{es}\| = 0$. If the assumptions hold globally, the origin will be globally asymptotically stable

Definition 4.4 (Exponential stability [125–127]). The system (4.1) at equilibrium point x_{es} ($\dot{x}_{es} = 0$) is said to be exponentially stable if there exists a $\gamma > 0$, $\lambda < 0$ and $\delta > 0$ such that if $\|x(t_0) - x_{es}\| < \delta$, then,

$$\|x(t) - x_{es}\| \leq \gamma (\|x(t_0) - x_{es}\|) e^{\lambda t}, \quad (4.2)$$

for all $t \geq 0$. If equation 4.2 holds for all $x \in \mathbb{R}^n$, then the system is said to be globally exponentially stable.

Asymptotic stability implies that the solutions around the "close vicinity" of the equilibrium point will not only remain "close" but will also eventually converge at that equilibrium point while exponential stability implies that the solutions will not only converge at that equilibrium point but will do so with at least the rate of $\gamma(\|x(t_0) - x_{es}\|)e^{\lambda t}$.

4.2.1 Lyapunov stability theory

Lyapunov theory was developed in the late 19th century by the Russian mathematician and physicist Aleksandr Lyapunov. He developed two methods but his second (also known as the "direct") method is the most commonly used nonlinear stability tool developed for determining the stability of system equilibria without explicitly solving a differential equation and analyzing its trajectory. While investigating the concept of the "energy" of a system represented by a function $V(x(t)) : \mathbb{R}^n \rightarrow \mathbb{R}$, Lyapunov observed the time derivative $\dot{V}(x(t))$ and determined that if the energy in the system is not increasing, it follows that the solutions can not grow boundless and if the energy is strictly decreasing, then solutions must approach an equilibrium asymptotically.

Theorem 4.1 (Lyapunov Second Method [125, 126, 128]). Given the equilibrium point $x_{es} = 0$ for the system (4.1), a continuously differentiable function $V(x(t)) : \mathbb{R}^n \rightarrow \mathbb{R}$ is called a Lyapunov function, if

- $V(x(t)) = 0$ at $x(t) = 0$,
- $V(x(t)) > 0$ at $x(t) \neq 0$ (positive definite) and
- $\dot{V}(x(t)) \leq 0$.

Moreover, if $\dot{V}(x(t)) < 0$ then $x_{es} = 0$ is asymptotically stable and if $\|x(t)\| \rightarrow \infty \Rightarrow V(x(t)) \rightarrow \infty$, then the conditions are hold globally.

This theorem states a sufficient rather than a necessary condition for stability, but there are no claims on how to construct this Lyapunov function or even if a stable system has a Lyapunov function. As a result, Lyapunov functions of quadratic nature were introduced to clearly give them a structure. For a linear time invariant system

$$\dot{x}(t) = Ax(t), \quad A \in \mathbb{R}^{n \times n} \quad (4.3)$$

having an equilibrium point x_{es} at the origin, consider the quadratic Lyapunov function

$$V(x(t)) = x'(t)Px(t), \quad P = P' \in \mathbb{R}^{n \times n} \quad (4.4)$$

whose time deriative given as

$$\begin{aligned} \dot{V}(x(t)) &= x'(t)P\dot{x}(t) + \dot{x}'(t)Px(t) \\ &= x'(t)PAx(t) + (Ax(t))'(t)Px(t) \\ &= x'(t)(PA + A'P)x(t) \end{aligned} \quad (4.5)$$

It can be seen that if the matrix $PA + A'P$ is negative definite, then the system is stable. Therefore, if there exists a positive definite matrix $P > 0$ and another positive definite matrix $Q > 0$ such that

$$-Q = PA + A'P \quad \text{Lyapunov equation,} \quad (4.6)$$

we can draw some conclusions about the stability of the system in equation (4.3). This is summarized in the theorem below

Theorem 4.2. The system (4.3) is asymptotically stable about $x_{es} = 0$ if and only if there exists a positive definite symmetric matrix $P = P'$, $P > 0$ and a positive definite symmetric matrix $Q = Q'$, $Q > 0$ such that $-Q = PA + A'P$. However,

- If $P = P'$, $P > 0$ and $Q = Q'$, $Q \geq 0$, then the system is *Lyapunov stable*
- If $P = P'$, $P > 0$, $Q = Q'$, $Q \geq 0$, and (Q, A) are observable, then the system is asymptotically stable

It is important to note that for a linear system such as in equation (4.1), the conditions of Theorem 4.2 for the Lyapunov function are necessary and sufficient. However for a nonlinear system, the conditions of Theorem 4.2 are only sufficient. Thus, if the conditions of Theorem 4.1 are not satisfied, it does not necessarily mean that the nonlinear system is unstable, it only tells us that stability cannot be determined using the chosen Lyapunov function. Also, Lyapunov functions do not need to strictly take the form of the equation 4.4, but can be constructed as the designer so wishes, provided the conditions itemized in Theorem 4.1 are satisfied (see examples at [26]).

4.2.2 Input-Output Stability

Unlike the Lyapunov stability, input-output stability analyzes the stability of a system without requiring any knowledge of the internal state structure of the system. It considers a system as a mapping from its input signal to its output signal and defines stability in terms of whether the system output is bounded whenever the input is bounded (i.e finite-energy inputs maps to finite-energy outputs). Signals of a system are bounded in a space \mathcal{L}_p which can be considered as a measure of the "size" of the signal and is given by

$$\|u\|_{\mathcal{L}_p} = \left(\int_0^\infty \|u(t)\|^p dt \right)^{\frac{1}{p}} \quad (4.7)$$

where p is an integer, $p \geq 1$ and $\|u\|_{\mathcal{L}_p}$ is the norm of the signal $u(t) \in \mathcal{L}_p$ - space. The norm of a signal may be infinite however, the case of the $p = 2$ norm is of particular interest since this corresponds to signals with bounded energy. This space (i.e the \mathcal{L}_2 space) will be considered extensively in this chapter.

Consider a system H with input and output signals $u \in \mathcal{L}_2$, $y \in \mathcal{L}_2$ shown in Figure 4.1, we can now define input-output stability in \mathcal{L}_2 space as

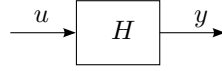


FIGURE 4.1: Input-Output System

Definition 4.5 (\mathcal{L}_2 gain [129, 130]). A mapping $H : \mathcal{L}_2 \rightarrow \mathcal{L}_2$ is said to be \mathcal{L}_2 stable if there exist a monotone non-decreasing function α and a constant β such that,

$$\begin{aligned} \|Hu\|_{\mathcal{L}_2} &\leq \alpha(\|u\|_{\mathcal{L}_2}) + \beta \quad \forall u \in \mathcal{L}_2 \\ \|y\|_{\mathcal{L}_2} &\leq \alpha(\|u\|_{\mathcal{L}_2}) + \beta \quad \forall u \in \mathcal{L}_2 \end{aligned}$$

where β is a bias term included to account for systems whose output $y \neq 0$ when the input $u = 0$. Furthermore, it is finite gain \mathcal{L}_2 stable if there exists a constant factor $\gamma > 0$ such that,

$$\|y\|_{\mathcal{L}_2} \leq \gamma \|u\|_{\mathcal{L}_2} \quad \forall u \in \mathcal{L}_2 \quad (4.8)$$

For simplicity, the bias term β has been omitted here since for our system, we consider that $y = 0$ if $u = 0$ (see [131] for more details).

The \mathcal{L}_2 gain is a very important performance indicator given that if it is made as small as possible, it will help attenuate the energy in the plant output performance, restraining the influence of disturbance for system's performance as much as possible.

In addition to being a measure of performance, the \mathcal{L}_2 gain can be used to establish stability properties for an interconnection of systems, such as that depicted in Figure 4.2. The interconnection is said to be stable if $y_1, y_2 \in \mathcal{L}_2 \mapsto u_1, u_2 \in \mathcal{L}_2$. It transpires that by bounding the gain of each subsystem, as indicated by equation (4.8), it can lead to a useful way of inferring the stability of the system in Figure 4.2. This is formalised in the Small Gain Theorem presented below.

Theorem 4.3 (Small Gain Theorem (SGT) [126, 131]). Consider the closed loop system shown in Figure 4.2, if H_1 and H_2 are both finite gain \mathcal{L}_2 stable with \mathcal{L}_2 gains $\gamma_1 > 0$ and $\gamma_2 > 0$, a sufficient condition for finite gain \mathcal{L}_2 stability of the feedback loop from inputs u_1 and u_2 to outputs y_1 and y_2 is given by

$$\gamma_1 \gamma_2 < 1 \quad (4.9)$$

This theorem is especially useful in systems with a known "nominal" part and an uncertain part where the uncertainty is modelled as an isolated nonlinearity. This approach is relatively simple in analysing stability in the systems described earlier, however, it is considered to be overly conservative [132–134] as it only provides sufficient conditions for stability and not necessary conditions. Other alternatives to the SGT exists, some of which include the passivity theorem which makes use of candidate Lyapunov functions (See [126]) and absolute stability theories.

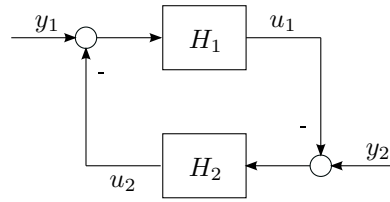


FIGURE 4.2: Feedback Interconnected System

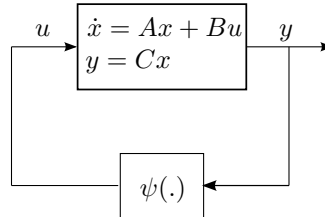


FIGURE 4.3: Lur'e-type system

4.2.3 Absolute Stability

The majority of the studies on absolute stability have been dedicated to nonlinear systems that can be modelled as a feedback connection of a linear system and a “static” nonlinearity (such as saturation, backlash, deadzone etc) as shown in Figure 4.3. This type of systems are generally called Lur’e-type systems. SGT can also be used to conduct stability analysis on this type of system but in order to reduce the conservatism of the stability criterion in the SGT, more information about the nonlinearity can be used. Absolute stability theories characterize these nonlinearities by placing constraints on them in order to have an approximate information about the nonlinearity. These approximate information are summarized in the following definitions;

Considering the feedback system in Figure 4.3 with the state space representation given as

$$\begin{aligned}\dot{x}(t) &= Ax(t) + Bu(t) \\ y(t) &= Cx(t) \\ u(t) &= \psi(y(t))\end{aligned}\tag{4.10}$$

with state $x(t) \in \mathbb{R}^n$, input $u(t) \in \mathbb{R}^m$ and output $y(t) \in \mathbb{R}^m$.

Definition 4.6. The nonlinearity $\psi(\cdot)$ is memoryless (static), possibly time varying, locally Lipschitz continuous in y (i.e slope restricted) and satisfies a sector bound condition.

Definition 4.7 (Sector bound condition). A function $\psi(\cdot) : \mathbb{R}^m \rightarrow \mathbb{R}^m$ with $\psi(0) = 0$ is said to be in sector $[k, q]$ as shown in Figure 4.4, if $\psi(y)$ for all $y \in \mathbb{R}^m$, the following inequality holds

$$(\psi(y) - ky)'(\psi(y) - qy) \leq 0\tag{4.11}$$

where k, q are diagonal positive definite matrices (i.e $k = \text{diag}(k_1 \dots k_m)$ and $q = \text{diag}(q_1 \dots q_m)$) with $k - q < 0$.

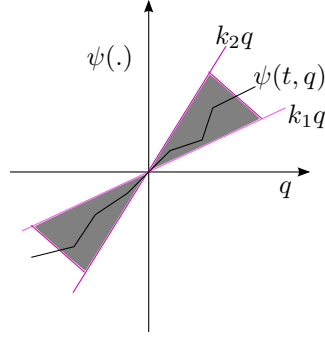


FIGURE 4.4: Sector Bound

Consider the saturation (or deadzone) nonlinearity, which corresponds to the general case when $k = 0$ and $q = I$. In this case, equation 4.11 can be written as

$$(\psi(y))'W(\psi(y) - Iy) \leq 0 \quad \forall y \in \mathbb{R}^m \quad (4.12)$$

for all diagonal positive definite matrix W (i.e $W = \text{diag}(W_1 \dots W_m)$ where $W > 0$). Recall from previous chapters that this kind of time-varying nonlinearity (saturation and deadzone) is our main focus in this thesis. The concept of Absolute Stability can now be aptly defined as

Definition 4.8. Suppose $\psi(\cdot)$ satisfies the conditions in the definitions 4.6 and 4.7. The system is absolutely stable if the equilibrium point at the origin is globally asymptotically stable for any nonlinearity in a given sector as specified in definition 4.7.

The Popov criterion and the Circle criterion are the most commonly used absolute stability theories but for the purpose of this thesis, the circle criterion is mainly used because it is a simple and convenient way to guarantee stability for arbitrarily time-varying non-linearities and it can be easily translated into flexible Linear Matrix Inequality (LMI) frameworks.

Theorem 4.4 (Circle Theorem (Multivariable) [131, 135]). Consider the closed loop system shown in Figure 4.3, whose state-space representation is given in equation (4.10), provided that A is Hurwitz and the nonlinearity satisfies the sector condition $\psi(\cdot) \in \text{Sector } [0, I]$, the origin of the system in equation (4.10) is globally absolutely stable if there exist a positive definite Lyapunov function $V(x) > 0$ and a diagonal positive definite matrix $W > 0$ which satisfy

$$\dot{V}(x) + \psi(\cdot)'W(y - \psi(\cdot)) + (y - \psi(\cdot))'W\psi(\cdot) < 0 \quad (4.13)$$

The quadratic inequality (4.4) defines a system of LMIs (which can be manipulated using techniques such as S-procedure, schur complement, congruence transformation [136] etc) whose feasibility and solutions can be determined by any of the numerous convex optimization techniques available. The Circle Theorem is the most conservative of the absolute stability theorems, given that the conditions of the Theorem 4.4 are sufficient but not necessary, similar to the SGT case. However unlike the SGT, the nonlinearity has a better defined structure hence reducing the conservatism.

4.3 Full-order AW design approach

The approach to AW design to be adopted as described briefly in Chapter 2 is the approach described in [23, 85]. This approach allows a system with AW compensation to be decoupled into an attractive structure that can be easily analysed and minimizes the deviation of the system from linear performance during and immediately after saturation. This approach concentrates on guaranteeing stability for stable plants, $(G(s) \in \mathcal{RH}_\infty)$ in the presence of input saturation and gives the assurance that there always exists an AW compensator which can globally stabilise these systems in general if the AW compensator is of the same order as the plant, i.e. a full-order AW compensator. In this section, we will review the full-order AW design approach described in [23] which lays the foundations for later sections of this chapter.

4.3.1 Generic MIMO full-order AW design

Figure 4.5 shows a typical AW configuration where $u \in \mathbb{R}^m$ is the unsaturated control signal, $u_m \in \mathbb{R}^m$ is the plant input (saturated control signal), $r \in \mathbb{R}^{n_r}$ is the reference, $y \in \mathbb{R}^p$ is the plant output, $\Theta(s)$ is the anti-windup compensator, $K(s)$ is the nominal controller and $G(s)$ is the plant and it is assumed to be stable i.e. $G(s) \in \mathcal{RH}_\infty^{p \times m}$.

The state-space realisation of the plant $G(s)$ is given as

$$G(s) \sim \left[\begin{array}{c|c} A_p & B_p \\ \hline C_p & D_p \end{array} \right] \quad (4.14)$$

where $A_p \in \mathbb{R}^{n \times n}$. The plant input u_m is defined as $u_m = \text{sat}(u)$ where the saturation function $\text{sat}(\cdot)$ (as defined in section 2.2) belongs to the sector $[0 I]$. The full-order AW compensator as stated in [25, 85] is said to have the structure

$$\Theta(s) = \begin{bmatrix} M(s) - I \\ G(s)M(s) \end{bmatrix} \quad (4.15)$$

where $M(s) \in \mathcal{RH}_\infty^{m \times m}$ is a stable transfer function matrix chosen as part of a right coprime factorisation of the plant where $G(s) = N(s)M(s)^{-1}$. For a full order AW compensator, this coprime factorisation is chosen to be equal in order to that of the plant such that the anti-windup

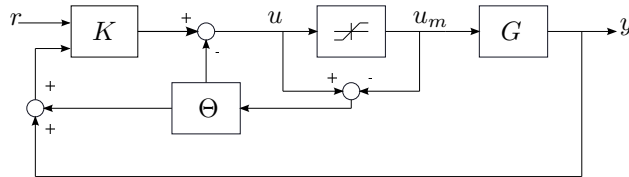


FIGURE 4.5: Typical Anti-windup Configuration

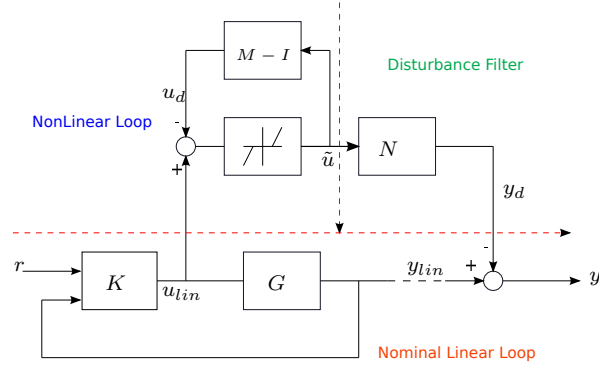


FIGURE 4.6: Equivalent representation of structure

compensator has a state-space realisation given as

$$\Theta(s) = \begin{bmatrix} M(s) - I \\ N(s) \end{bmatrix} \sim \begin{bmatrix} A_p + B_p F & B_p \\ F & 0 \\ C_p + D_p F & D_p \end{bmatrix} \quad (4.16)$$

where F is a free parameter to be chosen such that $A_p + B_p F$ is Hurwitz.

Using the above AW compensator structure, it can be shown that Figure 4.5 can be re-drawn as Figure 4.6 which exposes an attractive decoupled representation of a nominal linear system, a nonlinear loop, and a disturbance filter. If no saturation occurs ($\tilde{u} = 0$), then the nominal linear system is all that is required to determine the system's behaviour, however, if saturation occurs ($\tilde{u} \neq 0$), the nonlinear loop and disturbance filter become active.

Using this attractive representation and given that the nominal linear system is designed to stabilise the plant G with acceptable performance while $\tilde{u} = 0$, the stability of the entire system can be translated into finding out if the nonlinear loop is stable. The nonlinear loop simply makes use of the deadzone operator as seen in Figure 4.6 which is related to the saturation function via the identity $Dz(u) = u - sat(u)$.

The performance of the AW compensator can be expressed as minimising the deviation from the system's linear performance when saturation and/or the AW compensator is active. According to Figure 4.6, y_d represents the deviation of the real output (y) from the nominal linear output (y_{lin}) influenced by the effect of the control signal u_{lin} . This is expressed by the mapping $\mathcal{T}_p : u_{lin} \mapsto y_d$ and minimizing the "size" of this mapping can be achieved by minimizing its \mathcal{L}_2 gain. Hence the AW compensator can be designed in such a way that

$$\|y_d\|_{\mathcal{L}_2} \leq \gamma \|u_{lin}\|_{\mathcal{L}_2} \quad \gamma > 0 \quad \forall u_{lin} \in \mathcal{L}_2 \quad (4.17)$$

This will ensure that the closed-loop system with AW compensation is asymptotically stable and exhibits some level of performance, γ .

Assuming the state-space realisation of (4.16), the AW problem becomes that of finding a matrix F which minimizes the \mathcal{L}_2 gain of the operator \mathcal{T}_p , while also guaranteeing asymptotic stability. This is achieved essentially by combining concepts from Lyapunov stability, \mathcal{L}_2 gain minimization

and Circle criterion. In particular, the following inequality is examined

$$\underbrace{\dot{V}(x)}_{\text{Lyapunov stability}} + \underbrace{\|y_d\|_{\mathcal{L}_2}^2 - \gamma^2 \|u_{lin}\|_{\mathcal{L}_2}^2}_{\mathcal{L}_2 \text{ gain}} + \underbrace{\tilde{u}'W(u - \tilde{u})}_{\text{Sector bound condition}} < 0 \quad (4.18)$$

Evaluation of this inequality allows one to conclude that the system will be exponentially stable, with an \mathcal{L}_2 gain $\gamma > 0$. The main results from [23] on the solution to this problem are presented in the following theorem (details of the proof can be found in [23]).

Theorem 4.5 (Full order MIMO AW [23]). Assume that $G(s) \in \mathcal{RH}_\infty^{p \times m}$ and that the nominal interconnection of $K(s)$ and $G(s)$ is asymptotically stable and well-posed. If there exist matrices $Q > 0$, diagonal $U > 0$ and L , and a scalar $\gamma > 0$ such that the following linear matrix inequality

$$\text{He} \left\{ \begin{bmatrix} A_p Q + B_p L & B_p U & 0 & 0 \\ -L & -U & I & 0 \\ 0 & 0 & -\frac{\gamma}{2} I & 0 \\ C_p Q + D_p L & D_p U & 0 & -\frac{\gamma}{2} I \end{bmatrix} \right\} < 0 \quad (4.19)$$

holds, then the AW compensator (4.16) with $F = LQ^{-1}$ ensures that the system in Figure 4.6 is globally exponentially stable, well posed and such that $\|\mathcal{T}_p\|_{\mathcal{L}_2} < \gamma$.

If a measure of the \mathcal{L}_2 gain is not explicitly sought, the following corollary may be used to construct the AW compensator instead.

Corollary 4.1. Assume K and G satisfy the same conditions as in Theorem 4.5. Then the system in Figure 4.6 is globally asymptotically stable, well posed and there exists a $\gamma > 0$ such that $\|\mathcal{T}_p\|_{\mathcal{L}_2} < \gamma$ if there exist matrices $Q > 0$, L and scalar $U > 0$ such that the following linear matrix inequality holds:

$$\begin{bmatrix} QA'_p + A_p Q + B_p L + L' B'_p & B_p U - L' \\ \star & -2U \end{bmatrix} < 0 \quad (4.20)$$

If such matrices exist then an AW compensator ensuring global asymptotic stability and $\|\mathcal{T}_p\|_{\mathcal{L}_2} < \gamma$ can be constructed from (4.23) using $F = LQ^{-1}$.

The proof of this LMI (4.20) is the same as what was done by [23] for Theorem 4.5 except that the performance term $\|y_d\|_{\mathcal{L}_2}^2 - \gamma^2 \|u_{lin}\|_{\mathcal{L}_2}^2$ in the derivation is not considered.

Remark 4.1: An AW compensator designed with choosing the transfer function matrix $M(s) \in \mathcal{RH}_\infty^{m \times m}$ as a factor of the coprime factorization of the plant may result in a system with higher order extra states which may be considered "computationally expensive". Reduced states or no extra states added can be achieved by using low order and static AW compensators respectively but in these cases $M(s)$ is not chosen as part of the plant's coprime factorisation but as combination of the nominal controller and plant. However, there is no guarantee that any of these compensation schemes will globally stabilise the systems to which they serve [25].

Remark 4.2: According to [23], in a case where $G(s) \notin \mathcal{RH}_\infty$, this makes the LMI's (4.19) and thus (4.20) to become infeasible. To overcome this, a small adjustment to these LMI's can be made: if there exist matrices $Q > 0$, diagonal $U > 0$ and L such that the following LMI is

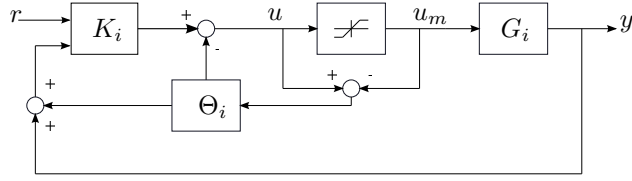


FIGURE 4.7: Single-loop anti-windup structure

satisfied

$$\text{He} \left\{ \begin{bmatrix} A_p Q + B_p L & B_p U & 0 & 0 \\ -\epsilon L & -U & \epsilon I & 0 \\ 0 & 0 & -\frac{\gamma}{2} I & 0 \\ C_p Q + D_p L & D_p U & 0 & -\frac{\gamma}{2} I \end{bmatrix} \right\} < 0 \quad (4.21)$$

then $F = LQ^{-1}$ can be used to construct the AW compensator (4.16), but this compensator no longer guarantees *global* stability. In this case, it is assumed that the standard deadzone no longer occupies the Sector $[0, I]$, but is restricted to some narrower sector, Sector $[0, \epsilon I]$ where $0 < \epsilon < 1$. Note that as ϵ approaches one, stability is closer to being administered globally. This approach, or variants thereof, has been successfully used in a number of applications, e.g. [137, 138].

4.3.2 Full-order AW design for SISO/SIMO systems

An important peculiar context to consider is the SISO/SIMO system case where the system in question has only one control input but possibly more than one output. The reason for introducing this case will become clearer later in the chapter. In a similar fashion to the MIMO case, consider the AW structure in Figure 4.7 with equivalent representation in Figure 4.8 where $G_i(s) \in \mathcal{RH}_\infty^{p_i \times 1}$ is the plant whose state-space realisation is given as

$$G_i(s) \sim \left[\begin{array}{c|c} A_i & B_i \\ \hline C_i & D_i \end{array} \right] \quad \text{where } A_i \in \mathbb{R}^{n_i \times n_i} \quad (4.22)$$

$K_i(s)$ is the controller and $\Theta_i(s)$ is the AW compensator whose state space representation (similar to equation (4.16) is given as

$$\Theta_i(s) = \begin{bmatrix} M_i(s) - 1 \\ N_i(s) \end{bmatrix} \sim \left[\begin{array}{c|c} A_i + B_i F_i & B_i \\ \hline F_i & 0 \\ \hline C_i + D_i F_i & D_i \end{array} \right]. \quad (4.23)$$

All signals including $u, u_m \in \mathbb{R}$, $r \in \mathbb{R}$ and $y \in \mathbb{R}^{p_i}$ are defined as in Section 4.3.1. The mapping $\mathcal{T}_p : u_{lin} \mapsto y_d$ is central to the AW performance and represents the deviation of the saturated behaviour of the system from its nominal linear behaviour. The following theorem is a special case of Theorem 4.5 representing the full order AW compensator design for the SISO/SIMO case.

Theorem 4.6 (Full order SISO/SIMO AW [23]). Assume that $G_i \in \mathcal{RH}_\infty^{p_i \times 1}$ and that the nominal interconnection of $K_i(s)$ and $G_i(s)$ is asymptotically stable and well-posed. If there exist matrices

$Q_i > 0$, L_i and scalars $U_i > 0$ and $\gamma_i > 0$ such that the following linear matrix inequality

$$\text{He} \left\{ \begin{bmatrix} A_i Q_i + B_i L_i & B_i U_i & 0 & 0 \\ -L_i & -U_i & I & 0 \\ 0 & 0 & -\frac{\gamma_i}{2} & 0 \\ C_i Q_i + D_i L_i & D_i U_i & 0 & -\frac{\gamma_i}{2} I \end{bmatrix} \right\} < 0 \quad (4.24)$$

holds, then the system in Figure 4.8, with the AW compensator in equation (4.23) where $F_i = L_i Q_i^{-1}$, is globally exponentially stable, well-posed and such that $\|\mathcal{T}_p\|_{\mathcal{L}_2} < \gamma$.

Again if stability is the only concern (i.e. \mathcal{L}_2 gain is not important), the following corollary may be used instead.

Corollary 4.2. Assume that $G_i \in \mathcal{RH}_\infty^{p_i \times 1}$ and that the nominal interconnection of $K_i(s)$ and $G_i(s)$ is stable and well-posed. If there exist matrices $Q_i > 0$, L_i and a scalar $U_i > 0$ such that the following linear matrix inequality

$$\begin{bmatrix} Q_i A_i' + A_i Q_i + B_i L_i + L_i' B_i' & B_i U_i - L_i' \\ * & -2U_i \end{bmatrix} < 0 \quad (4.25)$$

holds, then the system in Figure 4.8, with the AW compensator (4.23) where $F_i = L_i Q_i^{-1}$, is globally exponentially stable, well posed and there exists a $\gamma_i > 0$ such that $\|\mathcal{T}_p\|_{\mathcal{L}_2} < \gamma_i$.

Note that the inequality in equation (4.25) is also equivalent to

$$\begin{bmatrix} \hat{Q}_i A_i' + A_i \hat{Q}_i + B_i \hat{L}_i + \hat{L}_i' B_i' & B_i - \hat{L}_i' \\ * & -2I \end{bmatrix} < 0 \quad (4.26)$$

where $\hat{Q}_i = Q_i U_i^{-1}$ and $\hat{L}_i = L_i U_i^{-1}$. Thus to solve for F in this case, will result in

$$F_i = \hat{L}_i \hat{Q}_i^{-1} = \frac{L_i}{U_i} \cdot \frac{U_i}{Q_i} = L_i Q_i^{-1}$$

F_i is independent of U_i .

The choice of U_i in this case is not important in the solution of inequality (4.25) since U_i is a scalar and can be set to an arbitrary value without necessarily affecting the feasibility of the LMI (4.20) or the design of the AW compensator.

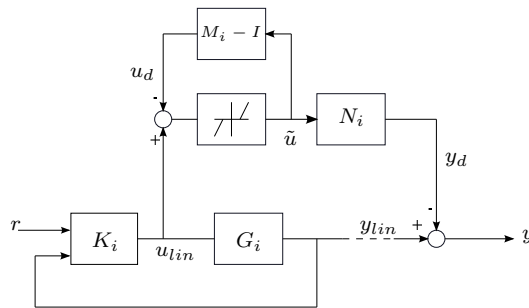


FIGURE 4.8: Equivalent representation of single-loop anti-windup structure

The Theorems 4.5 and 4.6 do not require the plant and the controller to have any particular structure and can be applied to any stabilizing plant and controller system. However, since the quadrotor system (to which we aim to design a suitable AW compensator for) has a specific structure, one would expect that simpler results and formulations can be made to these theorems to achieve some level of flexibility and simplicity.

4.4 Anti-windup design for a Quadrotor system structure

4.4.1 Quadrotor UAV structure

The quadrotor UAV dynamics presented in Section 3.2.4 can be approximately described and reduced to a system of double integrators as given in the following equations

$$\begin{aligned}
 \ddot{x} &= -(\cos\phi.\sin\theta)\frac{F}{m} \\
 \ddot{y} &= \sin\phi\frac{F}{m} \\
 \ddot{z} &= g - (\cos\phi.\cos\theta)\frac{F}{m} \\
 \ddot{\phi} &= \frac{1}{J_x}\tau_\phi \\
 \ddot{\theta} &= \frac{1}{J_y}\tau_\theta \\
 \ddot{\psi} &= \frac{1}{J_z}\tau_\psi
 \end{aligned} \tag{4.27}$$

and according to [24], the complete rotational dynamics (3.23) can be further simplified in such a way that

$$G_D(s) \sim \begin{cases} \ddot{\phi} &= \frac{1}{J_x}\tau_\phi \\ \ddot{\theta} &= \frac{1}{J_y}\tau_\theta \\ \ddot{\psi} &= \frac{1}{J_z}\tau_\psi \\ \ddot{z} &\approx g - \frac{1}{m}F \end{cases} \tag{4.28}$$

provided it is assumed that the roll and pitch angles (ϕ, θ) and the terms qr , pr and pq in the rotational dynamics equation (3.23) (also known as *Coriolis* terms) are small. Here, $\tau_\phi, \tau_\theta, \tau_\psi$ are the roll, pitch and yaw torques, F is the total lift force and m, g are the mass of the quadrotor and acceleration due to gravity respectively.

The total lift force and torques given by equation (3.30) represent the virtual control inputs to the plant G_D , however, the actual control inputs are the motor's angular velocities δ_* . As discussed in Section 3.2.6, the forces and torques generated by the motors and the actual motor

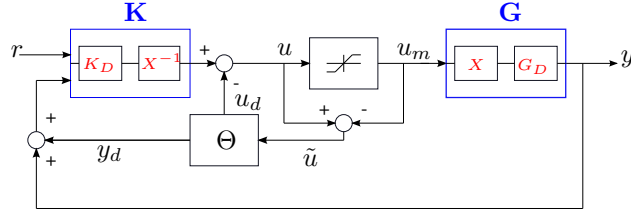


FIGURE 4.9: Full anti-windup structure

commands are related via a decoupling matrix X such that

$$\begin{bmatrix} F \\ \tau_\phi \\ \tau_\theta \\ \tau_\psi \end{bmatrix} = \underbrace{\begin{bmatrix} k_1 & k_1 & k_1 & k_1 \\ 0 & -\alpha k_1 & 0 & \alpha k_1 \\ \alpha k_1 & 0 & \alpha k_1 & 0 \\ -k_2 & k_2 & -k_2 & k_2 \end{bmatrix}}_X \underbrace{\begin{bmatrix} \delta_f \\ \delta_r \\ \delta_b \\ \delta_l \end{bmatrix}}_u. \quad (4.29)$$

where α is the distance between the centre of mass of the quadrotor and the motors. This control mapping equation (4.29) in conjunction with equation (4.28) outlines a situation where the plant can be considered to have the structure $G(s) = G_D(s)X$ as shown in Figure 4.9. With this structure, the controller can be designed to have a decoupled representation as well such that $K(s) = X^{-1}K_D(s)$ where each element of K_D is a simple PD controller for the angles ϕ, θ , and ψ and position z as described in Section 3.3.2.2

The problem of actuator saturation in quadrotors has been reported to exist in normal flight situations and extreme maneuvers by a number of researchers [139–141] and this has been included as part of our system structure as shown in Figure 4.9 where the signals and systems have the same meaning as defined in Section 4.3 with the quadrotor plant $G(s)$ and the controller $K(s)$ having the peculiar structures;

$$G(s) = G_D(s)X, \quad K(s) = X^{-1}K_D(s) \quad (4.30)$$

where $X \in \mathbb{R}^{m \times m}$ ¹ is a decoupling static invertible matrix, $G_D(s)$ and $K_D(s)$ are defined as,

$$G_D(s) = \text{blockdiag}(G_1(s), G_2(s), \dots, G_m(s)) \quad (4.31)$$

$$K_D(s) = \text{blockdiag}(K_1(s), K_2(s), \dots, K_m(s)) \quad (4.32)$$

Each element of $G_D(s)$ is assumed to be stable i.e. $G_i(s) \in \mathcal{RH}_\infty^{p_i \times 1}$ for $i \in \{1, \dots, m\}$ ² with state-space realisations the same as those given in equation (4.22)³.

With the structure of $K(s)$ and $G(s)$ given in equations (4.32) and (4.31), the unconstrained closed loop system behaves as m decoupled systems, where each $K_i(s)$ is responsible for controlling its corresponding $G_i(s)$. There is no coupling between these i control loops. However, the constrained system (when saturation occurs) no longer exhibits this decoupling into single feedback loops as observed in the unsaturated case because the decoupling matrix X is transformed

¹in this case $m = 4$

²where $\sum_{i=1}^m p_i = p$

³where $\sum_{i=1}^m n_i = n_p$

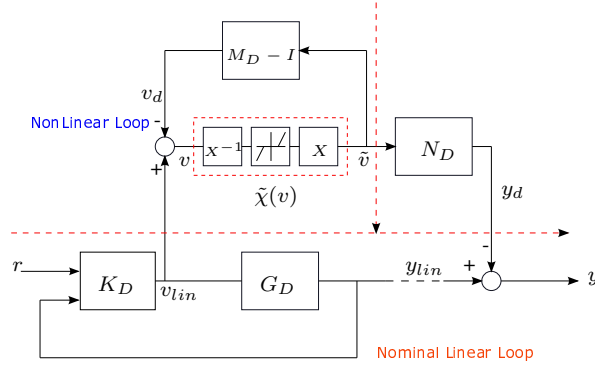


FIGURE 4.11: Equivalent representation of decentralised AW structure

system features some software induced artificial limits. Because of the way the AW compensator input \tilde{v} is portrayed, the AW compensator $\tilde{\Theta}(s)$ in this case is referred to as a *pseudo-decentralised* AW compensator and is related to the AW compensator $\Theta(s)$ in Figure 4.9 by the equation

$$\tilde{\Theta} = \begin{bmatrix} X & 0 \\ 0 & I \end{bmatrix} \Theta X^{-1}. \quad (4.36)$$

It will now be shown how the system in Figure 4.10 can be re-drawn to Figure 4.11 in a similar way to the process in Section 4.3. To enable this, it is noted that the the AW compensator input can be written as,

$$\tilde{v} = \tilde{\chi}(v) := XDz(X^{-1}v).$$

Now, according to Figure 4.10, the system output y is given as

$$\begin{aligned} y &= G_D v_m \\ &= G_D [v - \tilde{v}] \end{aligned}$$

Supposing the psuedo-decentralised AW compensator $\tilde{\Theta}(s)$ is chosen to have the structure

$$\tilde{\Theta}(s) = \begin{bmatrix} \tilde{\Theta}_1(s) \\ \tilde{\Theta}_2(s) \end{bmatrix}$$

where $v = v_{lin} + v_d$, and $v_d = \tilde{\Theta}_1 \tilde{v}$, then

$$\begin{aligned} y &= G_D v_{lin} - G_D \tilde{\Theta}_1 \tilde{v} - G_D \tilde{v} \\ &= G_D v_{lin} - G_D [\tilde{\Theta}_1 + I] \tilde{v} \end{aligned} \quad (4.37)$$

Given that, $y_{lin} = y + y_d$, $y_d = \tilde{\Theta}_2 \tilde{v}$ and if we choose $\tilde{\Theta}_1(s) = M_D(s) - I$ where $M_D(s) \in \mathcal{RH}_\infty^{m \times m}$ is some transfer function matrix, then

$$y_{lin} = G_D v_{lin} - G_D (\tilde{\Theta}_1 + I) \tilde{v} + \tilde{\Theta}_2 \tilde{v}. \quad (4.38)$$

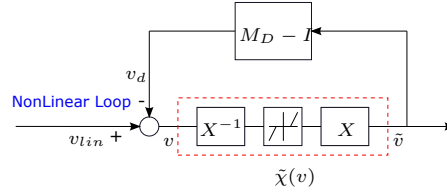


FIGURE 4.12: Non-linear loop for decentralised AW

such that for $y_{lin} = G_D v_{lin}$ and $\tilde{\Theta}_2(s) = G_D(s)M_D(s)$, the virtual AW compensator will then have the form

$$\tilde{\Theta}(s) = \begin{bmatrix} \tilde{\Theta}_1(s) \\ \tilde{\Theta}_2(s) \end{bmatrix} = \begin{bmatrix} M_D(s) - I \\ G_D(s)M_D(s) \end{bmatrix} \quad (4.39)$$

The nonlinear loop in Figure 4.11 can be redrawn and represented in Figure 4.12 where it is described by equation (4.4.2). Since $v = v_{lin} - v_d$, then

$$\tilde{v} = XDz[X^{-1}(v_{lin} - v_d)]. \quad (4.40)$$

It is important to note that, because $G_D(s)$ is block-diagonal and $M_D(s)$ is chosen to be block-diagonal as well, $\tilde{\Theta}(s)$ is considered to be decentralised from the point of view of the virtual control signals, and hence is seemingly only “pseudo”-decentralised AW structure from the point of view of the physical signals. Given that $G_D(s)$ is a block diagonal transfer function matrix with state-space realisation

$$G_D(s) \sim \left[\begin{array}{c|c} A_D & B_D \\ \hline C_D & D_D \end{array} \right] \quad (4.41)$$

where

$$A_D = \text{blockdiag}(A_1, \dots, A_m) \quad (4.42)$$

$$B_D = \text{blockdiag}(B_1, \dots, B_m) \quad (4.43)$$

$$C_D = \text{blockdiag}(C_1, \dots, C_m) \quad (4.44)$$

$$D_D = \text{blockdiag}(D_1, \dots, D_m), \quad (4.45)$$

and based on the approach in previous sections, it then follows that a full-order pseudo-decentralised AW compensator $\tilde{\Theta}(s)$ has the following structure:

$$\tilde{\Theta}(s) = \begin{bmatrix} M_D(s) - I \\ N_D(s) \end{bmatrix} \sim \left[\begin{array}{c|c} A_D + B_D F_D & B_D \\ \hline F_D & 0 \\ \hline C_D + D_D F_D & D_D \end{array} \right] \quad (4.46)$$

where

$$F_D = \text{blockdiag}(F_1, \dots, F_m). \quad (4.47)$$

The following theorem therefore gives necessary and sufficient conditions for the existence of this AW compensator guaranteeing stability and finite \mathcal{L}_2 gain.

Theorem 4.7. Let Assumption 4.1 be satisfied. Then there exists an AW compensator of the structure (4.36) such that the origin of the system in Figure 4.11 is globally asymptotically stable and $\|\mathcal{T}_p\|_{\mathcal{L}_2} < \gamma$ if there exist block-diagonal matrices $Q_D > 0$ and L_D , a diagonal matrix $U_D > 0$ and a positive real scalar γ such that the following LMI

$$\text{He} \left\{ \begin{bmatrix} A_D Q_D + B_D L_D & B_D X U_D & 0 & 0 \\ -L_D X^{-1} & -X^{-1} U_D & X^{-1} & 0 \\ 0 & 0 & -\frac{\gamma}{2} I & 0 \\ C_D Q_D + D_D L_D & D_D U_D & 0 & -\frac{\gamma}{2} I \end{bmatrix} \right\} < 0. \quad (4.48)$$

is satisfied. Furthermore, if this inequality is satisfied, a suitable $\tilde{\Theta}(s)$ achieving global asymptotic stability and $\|\mathcal{T}_p\|_{\mathcal{L}_2} < \gamma$ is obtained via the state-space equations (4.46) where $F_D = L_D Q_D^{-1}$.

Proof: Recall that the mapping \mathcal{T}_p represents the deviation of the saturated behaviour of the system from its nominal linear behaviour and to ensure that the system will be stable and give some acceptable behaviour, it is required that this deviation is kept to a minimum γ as much as possible i.e $\|\mathcal{T}_p\|_{\mathcal{L}_2} < \gamma$. In this psuedo-decentralised AW compensator, a state-space realisation of the nonlinear loop in Figure 4.12 is given by

$$\dot{x}_D = (A_D + B_D F_D)x_D + B_D \tilde{\chi}(v) \quad (4.49)$$

$$v_d = F_D x_D \quad (4.50)$$

$$y_d = (C_D + D_D F_D)x_D + D_D \tilde{\chi}(v) \quad (4.51)$$

where $\tilde{\chi}(v) = X D z[X^{-1}(v_{lin} - v_d)]$. To guarantee stability and ensure that $\|\mathcal{T}_p\|_{\mathcal{L}_2} < \gamma$, it is sufficient for the following inequality to hold for some Lyapunov function $V(x) > 0$ and some scalar $\gamma > 0$,

$$\dot{V}(x) - \gamma \|v_{lin}\|^2 + \frac{1}{\gamma} \|y_d\|^2 < 0. \quad (4.52)$$

Recall that as the deadzone inequality belongs to the Sector $[0, I]$, for some diagonal matrix $W > 0$ [125], the following inequality

$$\Omega(v) = D z(X^{-1}v)' W (v - D z(X^{-1}v)) \geq 0 \quad (4.53)$$

holds. The Lyapunov function is chosen as $V(x_D) = x_D' P_D x_D$ where P_D is a positive definite block diagonal matrix, with elements of dimensions consistent with (A_D, B_D, C_D) . By appending the sector inequality (4.53) to (4.52), we require

$$\dot{V}(x_D) - \gamma \|v_{lin}\|^2 + \frac{1}{\gamma} \|y_d\|^2 + \Omega(v) < 0. \quad (4.54)$$

Substituting for x_D , v_d and y_d from equation (4.51) and applying Schur complement ⁴ and the congruence transformation

$$\text{diag}(P_D^{-1}, W^{-1}, I, I) = \text{diag}(Q_D, U_D, I, I)$$

⁴The Schur complement lemma can be seen in [61]

to the inequality (4.54), the LMI in (4.48) is obtained.

Remark 4.2: Compared to the MIMO full-order AW synthesis method of [23], the result above is more stringent: for the existence of the pseudo-decentralised compensator described in equation (4.46) a more restrictive LMI must be satisfied (4.48): this is the price paid for a pseudo-decentralised structure. \square

4.4.3 Channel-by-channel anti-windup design

Theorem 4.7 provides conditions which enable AW compensators to be synthesized while retaining a certain “decentralized” type of structure. However, it is emphasized that the AW compensator is a multivariable AW compensator but with a decentralized structure. This section looks at an alternative approach and asks the question, is it possible to design several SISO AW compensators (one for each of the i 'th feedback loops) and then combine them for the coupled MIMO system in such a way that they retain stability? This section provides an affirmative answer to the question.

Unlike the previous case of the psuedo-decentralised AW compensator, the channel-by-channel AW compensator design considers the structure of Figure 4.13 with the AW compensator receiving its input \tilde{u} directly from the saturation function where $\tilde{u} = Dz(u)$. The equivalent representation of Figure 4.13 is shown in Figure 4.14 with the AW compensator structure given as

$$\Theta(s) = [\Theta_1(s) \quad \Theta_2(s)]'.$$

According to Figure 4.13 and similar to the process followed in Section 4.4.2,

$$\begin{aligned} y &= G_D X u_m \\ &= G_D X [u - \tilde{u}] \\ &= G_D (u_{lin} - \Theta_1 \tilde{u}) - G_D X \tilde{u} \\ &= G_D u_{lin} - G_D [\Theta_1 + X] \tilde{u}. \end{aligned} \quad (4.55)$$

Given that $y_{lin} = y + y_d$ and and if we choose $\Theta_1(s) = M(s) - X$ then

$$\begin{aligned} y_{lin} &= G_D u_{lin} - G_D (\Theta_1 + X) \tilde{u} + \Theta_2 \tilde{u} \\ &= G_D u_{lin} - G_D M \tilde{u} + \Theta_2 \tilde{u}. \end{aligned} \quad (4.56)$$

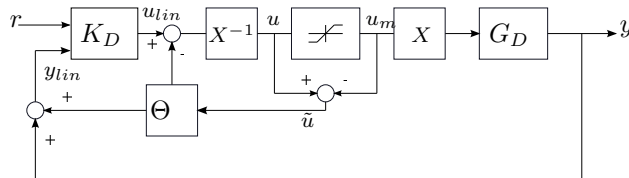


FIGURE 4.13: Applying the AW on general plant structure (MIMO)

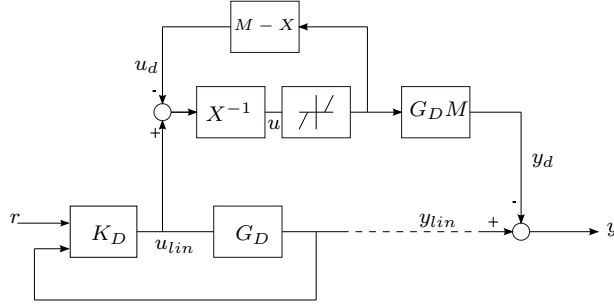


FIGURE 4.14: Equivalent representation for channel-by-channel AW

To ensure $y_{lin} = G_D u_{lin}$, we have to choose $\Theta_2(s) = G_D(s)M(s)$ so that our AW compensator $\Theta(s)$ can have the form:

$$\Theta(s) = \begin{bmatrix} \Theta_1(s) \\ \Theta_2(s) \end{bmatrix} = \begin{bmatrix} M(s) - X \\ G_D(s)M(s) \end{bmatrix} \quad (4.57)$$

where $M(s) \in \mathcal{RH}_\infty^{m \times m}$ is a free parameter to be chosen.

The diagonal transfer function matrix $G_D(s)$ consists of m $G_i(s)$ plants for $\forall i \in \{1 \dots, m\}$ and has a coprime factorization

$$G_D(s) = N_D(s)M_D(s)^{-1} \quad \text{equivalently written as,} \quad (4.58)$$

$$G_D(s) = N_D(s)X(M_D(s)X)^{-1}. \quad (4.59)$$

Now, assume that each $G_i(s)$ has the right coprime factorisation of $G_i(s) = N_i(s)M_i(s)^{-1}$ where each $N_i(s)$ and $M_i(s) \forall i \in \{1 \dots, m\}$ make up the block diagonal transfer functions $N_D(s)$ and $M_D(s)$ given as

$$\begin{aligned} N_D(s) &= \text{blockdiag}(N_1(s), \dots, N_m(s)) \\ M_D(s) &= \text{blockdiag}(M_1(s), \dots, M_m(s)). \end{aligned}$$

So if we choose $M(s) = M_D(s)X$ such that

$$M(s) - X = (M_D(s) - I)X,$$

the equations of the nonlinear loop as shown in Figure 4.15 will then take the form:

$$\tilde{u} = \text{Dz}[X^{-1}(u_{lin} - u_d)] \quad (4.60)$$

Since $u_d = (M_D - I)X\tilde{u}$, the nonlinear loop of Figure 4.15 can be redrawn and represented as Figure 4.16 such that equation (4.60) becomes

$$\tilde{u} = \text{Dz}[X^{-1}u_{lin} - (X^{-1}(M_D - I)X)\tilde{u}].$$

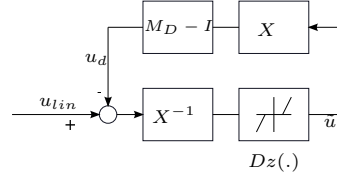


FIGURE 4.15: Non-linear loop for channel-by-channel AW 1

Therefore, the AW compensator can now be outlined as:

$$\Theta(s) = \begin{bmatrix} M_D(s) - I \\ N_D(s) \end{bmatrix} X. \quad (4.61)$$

This implies that the MIMO AW compensator $\Theta(s)$ can be considered as $\Theta(s) = \Theta_D(s)X$ where $\Theta_D(s) = \text{blockdiag}(\Theta_i(s)) \forall i \in \{1 \dots, m\}$, allowing the independent design of AW compensators for each individual channel or feedback loop, hence the name *channel-by-channel* AW compensator design.

Note that if the deadzone in the nonlinearity $\tilde{\chi}(u)$ in Figure 4.16 is considered to be in the sector $[0, I]$, it then follows that the following lemma should hold;

Lemma 4.1. Consider the nonlinearity $\tilde{\chi}(\cdot) : \mathbb{R}^m \mapsto \mathbb{R}^m$

$$\tilde{\chi}(u) := XDz(X^{-1}u) \quad (4.62)$$

where $X \in \mathbb{R}^{m \times m}$ is a nonsingular matrix. If there exist diagonal matrices $W > 0$ and $V > 0$ such that

$$V = X'WX > 0 \quad (4.63)$$

then the following inequality

$$\tilde{\chi}(u)'W(u - \tilde{\chi}(u)) \geq 0, \quad \forall u \in \mathbb{R}^m. \quad (4.64)$$

holds.

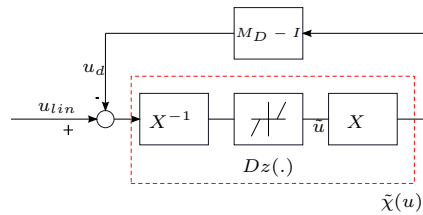


FIGURE 4.16: Non-linear loop for channel-by-channel AW 2

Proof: Since $\tilde{\chi}(u) := XDz(X^{-1}u)$, the left hand side of the inequality (4.64) can then be written as

$$\begin{aligned} \text{l.h.s.}(4.64) &= Dz(X^{-1}u)'X'W[u - XDz(X^{-1}u)] \\ &= Dz(X^{-1}u)'X'WX[X^{-1}u - Dz(X^{-1}u)]. \end{aligned} \quad (4.65)$$

Substituting $u_x = X^{-1}u$ and $V = X'WX$ in the equation above results in,

$$\tilde{\chi}(u)'W(u - \tilde{\chi}(u)) = Dz(u_x)V[u_x - Dz(u_x)]. \quad (4.66)$$

It then follows that for any u_x and any diagonal $V > 0$, the inequality,

$$Dz(u_x)'V[u_x - Dz(u_x)] > 0 \quad \forall u_x \in \mathbb{R}^m \quad (4.67)$$

holds by virtue of the deadzone's sector property. Hence, inequality (4.64) holds, if there exists diagonal matrices $W > 0$ and $V > 0$ that satisfies (4.63). \square

Provided Assumption 4.1 is satisfied, Lemma 4.1 result can be used to setup conditions to guarantee global stability of the system in Figure 4.13, as illustrated in the following theorem.

Theorem 4.8. If there exist diagonal matrices $W > 0$ and $V > 0$ such that $V = X'WX$ and there exist matrices $Q_i > 0$, L_i and scalars $U_i > 0$ such that the LMIs (4.25) are satisfied for all $i \in \{1, \dots, m\}$, then with $\Theta(s)$ designed as in (4.61) where $F_i = L_iQ_i^{-1}$, the system in Figure 4.16 is globally exponentially stable.

Proof: The state space realization of each i^{th} loop of $\Theta(s)$ in (4.61) is

$$\dot{x}_i = (A_i + B_iF_i)x_i + B_i\tilde{\chi}_i(u) \quad (4.68)$$

$$u_i = F_ix_i \quad (4.69)$$

$$y_i = (C_i + D_iF_i)x_i + D_i\tilde{\chi}(u). \quad (4.70)$$

By choosing the Lyapunov function $V(x) = x'P_Dx = \sum_{i=1}^m x_i'P_ix_i$, $\dot{V}(x)$ becomes

$$\begin{aligned} \dot{V}(x) &= x'((A_D + B_DF_D)'P_D + P_D(A_D + B_DF_D))x \\ &\quad + 2x'P_DB_D\tilde{\chi}(u). \end{aligned} \quad (4.71)$$

Using Lemma 4.1, it follows that there exists a diagonal $W > 0$ such that

$$\tilde{\chi}(u)'W(u - \tilde{\chi}(u)) \geq 0, \quad \forall u \in \mathbb{R}^m. \quad (4.72)$$

Therefore, a sufficient condition for inequality (4.71) to hold is for the inequality below to hold:

$$\dot{V}(x) \leq \begin{bmatrix} x \\ \tilde{\chi}(u) \end{bmatrix}' \text{He} \left\{ \begin{bmatrix} P_D(A_D + B_DF_D) & P_DB_D \\ -WF_D & -W \end{bmatrix} \right\} \begin{bmatrix} x \\ \tilde{\chi}(u) \end{bmatrix}. \quad (4.73)$$

Due to the diagonal nature of all the matrices, this inequality can be broken down into

$$\dot{V}(x) \leq \sum_{i=1}^m \begin{bmatrix} x_i \\ \tilde{\chi}_i(u) \end{bmatrix}' \text{He} \left\{ \begin{bmatrix} P_i(A_i + B_i F_i) & P_i B_i \\ -W_i F_i & -W_i \end{bmatrix} \right\} \begin{bmatrix} x_i \\ \tilde{\chi}_i(u) \end{bmatrix}. \quad (4.74)$$

Applying standard Schur complements and using the congruence transformation $\text{diag}(P_i^{-1}, W_i^{-1}) = \text{diag}(Q_i, U_i)$ yields the LMI (4.25). \square

Notice that in order to design m AW compensators for the structure in Figure 4.13 using the system of LMI's in (4.25), Lemma 4.1 must be satisfied so that diagonal matrices $W > 0$ and $V > 0$ exists under the condition that $V = X'WX$. The circumstance under which these matrices $V > 0$ and $W > 0$ such that $V = X'WX$ exists can be obtained by solving a linear program where

$$\text{vec}(X'WX) = \text{vec}(V) = [X' \otimes X'] \text{vec}(W) \quad (4.75)$$

$$= \begin{bmatrix} V_1 \\ 0 \\ \vdots \\ V_2 \\ 0 \\ \vdots \\ \vdots \\ V_m \end{bmatrix} = [X' \otimes X'] \begin{bmatrix} W_1 \\ 0 \\ \vdots \\ W_2 \\ 0 \\ \vdots \\ \vdots \\ W_m \end{bmatrix} \quad (4.76)$$

such that $\text{vec}(V), \text{vec}(W) \in \mathbb{R}^{m^2}$ and $X' \otimes X' \in \mathbb{R}^{m^2 \times m^2}$. Equation (4.75) uses the relationship between the $\text{vec}(\cdot)$ operator and the Kronecker product [143] where the vec operation $\text{vec}(A)$ rearranges the column vectors of $A = [a_1, a_2, \dots, a_n] \in \mathbb{R}^{n \times n}$ in the following way:

$$\text{vec}(A) = [a'_1 \quad a'_2 \quad \dots \quad a'_n]'$$

Equation (4.76) represents a linear programming feasibility problem which can be solved in straightforward manner with modern numerical softwares. It is important to note that if solutions exist to the earlier specified linear program, then AW compensators that ensure the global stability of the entire system in Figure 4.13 can be designed individually for the m control loops or channels of the MIMO system.

Remark 4.3: The channel-by-channel AW result may seem constrained in some sense due to the strong requirement for the existence of positive definite diagonal matrices, V and W satisfying $V = X'WX$. However, it offers greater flexibility than the pseudo-decentralised approach: because in the channel-by-channel case, it allows for *any* suitable SISO/SIMO AW compensator to be designed and re-designed without requiring to repeat any stability analysis for the overall system. In a practical sense, this is greatly appreciated. Also, the linear programming solution presents a transparent and efficient method of determining the diagonal matrices $V > 0$ and $W > 0$ satisfying equation (4.63). However the numerical value of V and W are not needed in

TABLE 4.1: MQM simulation table of parameters and PD Gains

Parameters	Description	Values	Units
g	Gravity	9.81	ms^{-2}
m	Mass	0.65	kg
d	Distance	0.3	m
k_1	Force constant	2.9×10^{-3}	
k_2	Torque constant	1.1×10^{-4}	
J_x	Pitch Inertia	7.5×10^{-3}	kgm^{-2}
J_y	Roll Inertia	7.5×10^{-3}	kgm^{-2}
J_z	Yaw Inertia	1.3×10^{-3}	kgm^{-2}
$K_{\phi,P}$	Proportional gain	1.2	
$K_{\theta,P}$		1.2	
$K_{\psi,P}$		1	
$K_{z,P}$		100	
$K_{\phi,D}$	Derivative gain	0.2	
$K_{\theta,D}$		0.2	
$K_{\psi,D}$		0.2	
$K_{z,D}$		20	

the design of the AW compensator, they exist only to help draw definitive conclusions about the nonlinear stability of the overall system.

4.5 Results

There are two nonlinear quadrotor models used in this thesis for simulation purposes. The first is the exact model described in the previous chapter which is a complete higher level model that represents the experimental platform (EQM) on which operational flight tests will be performed. The second is a simplified model similar to our model described in the previous chapter that captures only the main dynamics of the quadrotor and the basic controller but without the actuator (motor) dynamics. It is considered to be a micro-quadrotor (MQM) because of its low size & weight and the parameters/PD gains used for the simulation are stated in Table 4.1. The second model is used only for simulation and verification of the feasibility of designs, hence any designs with acceptable performance on the second model is also simulated on the first model before it is taken to the experimental platform for flight tests.

A linearized version of both models was also developed around hover for fixed input $u = [\tau_\phi \ \tau_\theta \ \tau_\psi \ F]'$ and outputs $y = [\phi \ \dot{\phi} \ \theta \ \dot{\theta} \ \psi \ \dot{\psi} \ z \ \dot{z}]'$. In this section, three AW compensators types are designed using the linearized model and applied to the nonlinear quadrotor models for both simulations and flight tests. These AW compensator designs are:

- The MIMO AW compensator of [23] designed for the plant $G(s) = G_D(s)X$ without taking into account the structure of $G_D(s)X$ where X is given in equation (4.29).
- The pseudo-decentralised AW compensator (Section 4.4.2) [116] where the compensator takes into account the structure of $G(s)$ but from the perspective of the "virtual" control inputs.

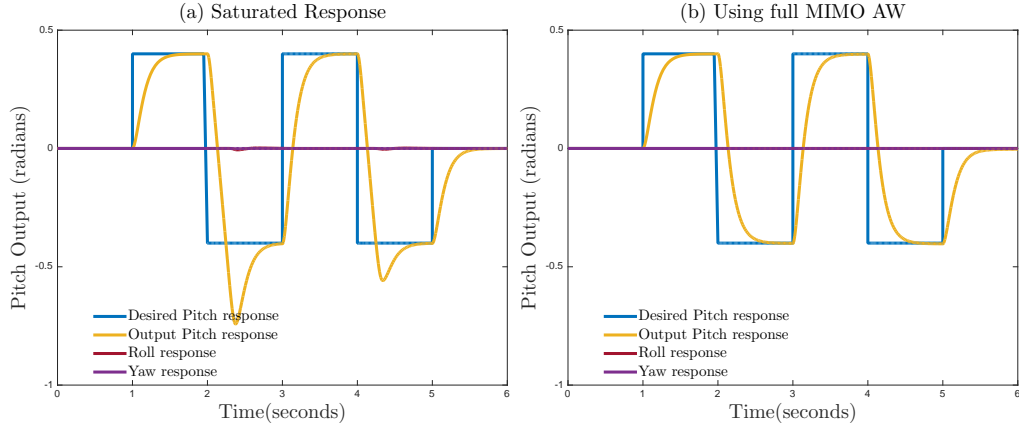


FIGURE 4.17: MQM Pitch angle response: (a) [from left] Saturation, no AW and (b) Saturation, full MIMO AW

- The combination of SISO/SIMO AW compensators referred to as Channel-by-channel AW compensators (Section 4.4.3) [116, 118] where the structure of $G(s) = G_D(s)X$ via the physical control inputs are taken into account. With the matrix X for the quadrotor system, it was verified via the solution of a linear programme that there indeed exists diagonal matrix V and W such that equation (4.63) is satisfied.

The following results show the effectiveness of these AW compensators and compares their performances.

4.5.1 Simulation Results

In these results, the effects of saturation and the attendant AW compensation will be observed on the output pitch θ attitude (angle) whose nominal response is presented in Figure 3.9 of the previous chapter. A pulse reference signal of $0.4rad$ was commanded on the pitch θ with saturation constraints applied on all control signals (motor angular velocities).

4.5.1.1 Micro-Quadrotor Model (MQM)

Figures 4.17a/4.18a shows a saturated pitch response of the system and its corresponding control response; the saturation has ruined the attractive decoupling along the individual loops giving rise to windup effects of large overshoots and longer settling times. Improvements over the uncompensated responses are observed when the full MIMO AW, pseudo-decentralized AW and channel-by-channel AW compensators are used as can be seen in Figures 4.17b/4.18b, Figures 4.19a/4.20a and Figures 4.19b/4.20b respectively. However, the performance, as measured by the induced norm of the mapping \mathcal{T}_p of , is $\gamma \approx 1.9773$ for the full MIMO AW compensator while the pseudo-decentralized AW and channel-by-channel AW compensators gave the performance indices $\gamma \approx 1.8121$ and $\gamma \approx 1.8102$ respectively.

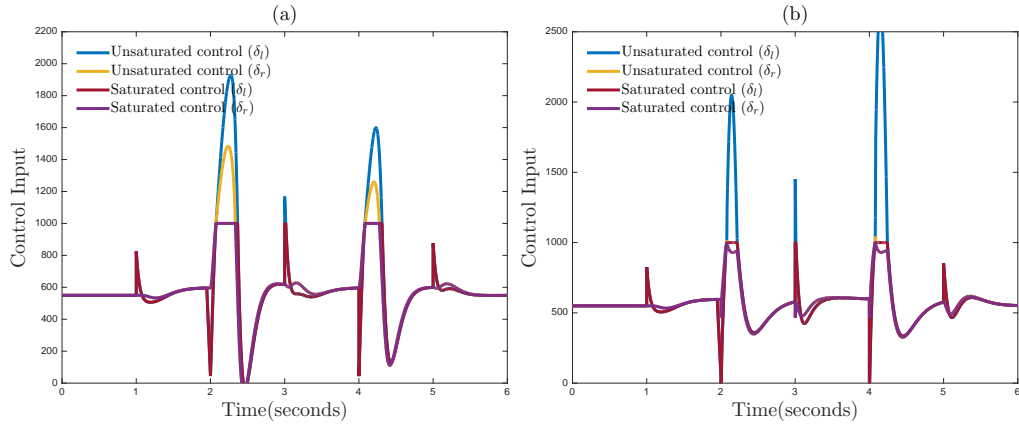


FIGURE 4.18: MQM Control command due to pitch response: (a) [from left] Saturation, no AW and (b) Saturation, full MIMO AW

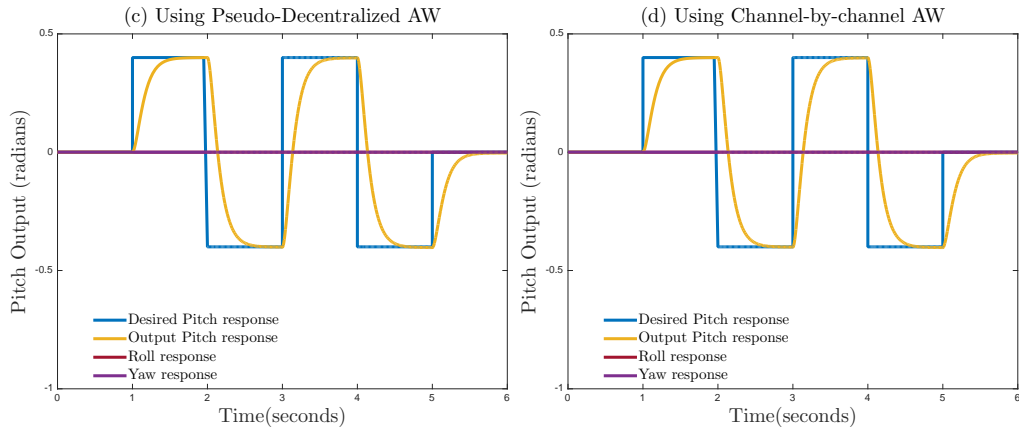


FIGURE 4.19: MQM Pitch angle response: (c) [from left] Saturation, psuedo-decentralized AW; and (d) Saturation, channel-by-channel AW

4.5.1.2 Experimental Quadrotor Model (EQM)

Figures 4.21a/4.22a show the saturated response of the system. Again, windup effects of large overshoot caused by the increasing pitch feedback error driven by slow poles in the nonlinear system are observed on the pitch and roll channels. The existence of the large overshoot observed on the roll channel even though there is no command on the roll is due to the apparent coupling between the roll and pitch channels.

Figures 4.21b/4.22b, Figures 4.19a/4.20a and Figures 4.23b/4.24b clearly show improved responses from the use of the full MIMO AW, pseudo-decentralized AW and channel-by-channel AW compensators respectively.

Note that the performance levels for the three AW compensator types are very similar here with the performance indices for the full MIMO AW, pseudo-decentralized AW and channel-by-channel AW compensators given as $\gamma \approx 1.4556$, $\gamma \approx 1.3836$ and $\gamma \approx 1.2117$ respectively, but the channel-by-channel AW compensator has much practical appeal than the others due to its simplicity and flexibility in implementation.

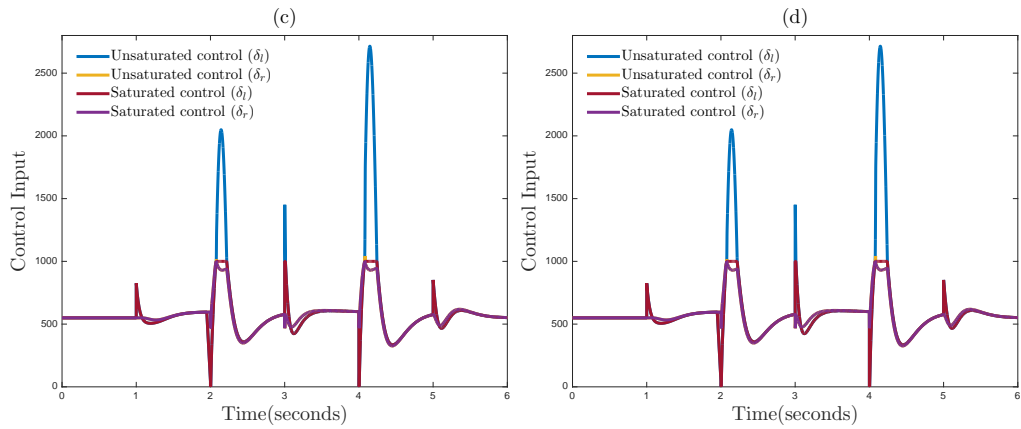


FIGURE 4.20: MQM Control command due to pitch response: (c) [from left] Saturation, pseudo-decentralized AW; and (d) Saturation, channel-by-channel AW

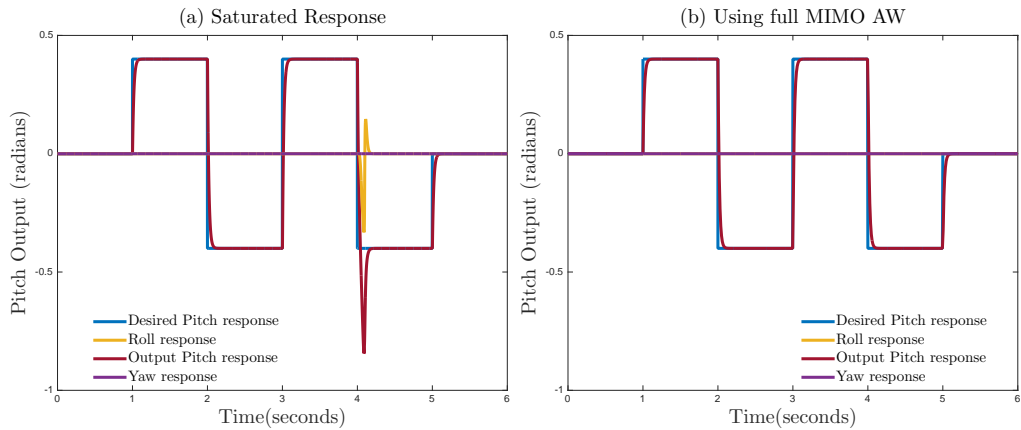


FIGURE 4.21: EQM Pitch angle response: (a) [from left] Saturation, no AW and (b) Saturation, full MIMO AW

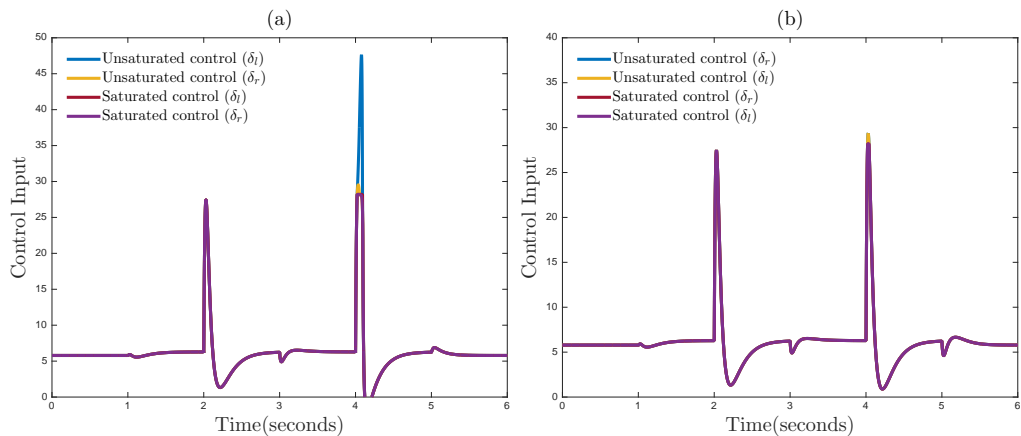


FIGURE 4.22: EQM Control command due to pitch response: (a) [from left] Saturation, no AW and (b) Saturation, full MIMO AW

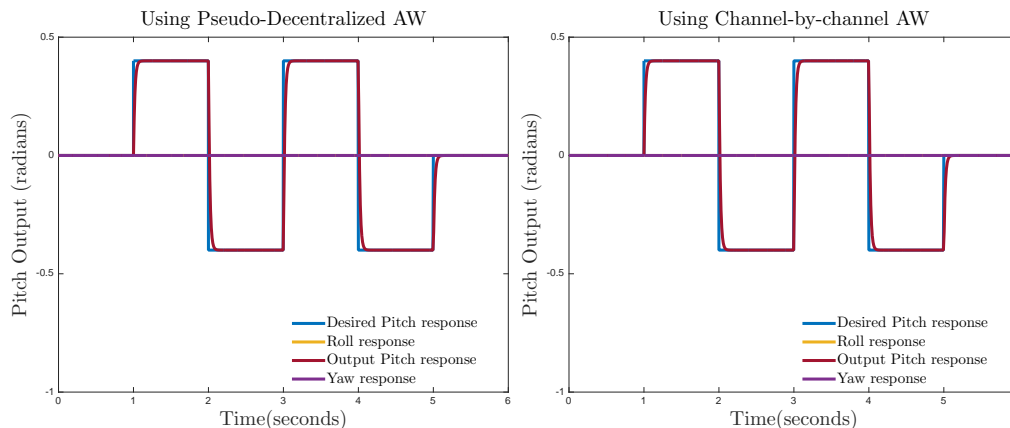


FIGURE 4.23: EQM Pitch angle response: (c) [from left] Saturation, psuedo-decentralized AW; and (d) Saturation, channel-by-channel AW

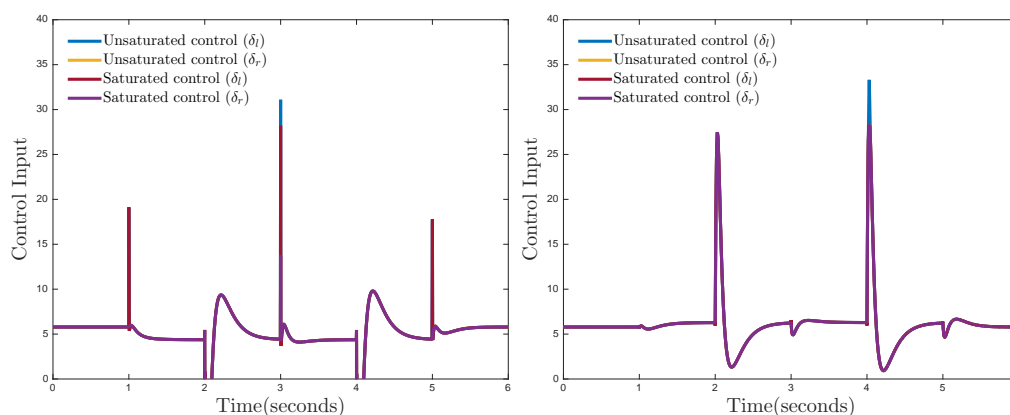


FIGURE 4.24: EQM Control command due to pitch response: (c) [from left] Saturation, psuedo-decentralized AW; and (d) Saturation, channel-by-channel AW

4.5.2 Flight Testing

To establish and maintain uniformity in gathering and collection of results data, the experimental quadrotor was first configured for a fully autonomous flight ⁵ with a constant mission. The entire flight was under the control of the onboard autopilot and Ground Control Station (GCS) with the data acquisition system measuring and recording real time sensor measurement data at various sampling rates ranging from $400Hz$ - $5kHz$. The objective of the flight tests are two-fold;

1. To identify and perform proper tuning of outer-loop controller parameters under levelled hover flight condition which is necessary for the autonomous flight demonstration and then
2. To compare and validate the performances of the AW compensators designed for the EQM

The first objective was accomplished rapidly in part, due to the insight gained from the simulations and the wide availability of manuals and troubleshooting resources available for the autopilot type. It is important to note that the AW compensator design was already scripted in

⁵The flight tests phase spanned the period January 2015 to August 2015 and were held at the large Victoria park space adjacent to the University of Leicester's Engineering Building.



FIGURE 4.25: Snapshot showing Mission Waypoints

C code and appended to the already existent controller library in the autopilot firmware code before the first objective was embarked on. The second objective was assessed based on the following autonomous flight plan;

4.5.2.1 Flight Plan

The flight plan as plotted in Figure 4.25 includes:

- a Quadrotor UAV started in manual mode with preflight checks carried out.
- b Autonomous Takeoff engaged, saved mission plan begins, UAV climbs to $20m$ heading to Waypoint 1.
- c Head to Waypoint 2, descends to $10m$.
- d Head to Waypoint 3, maintain altitude.
- e Climbs to $25m$, Loiter for 10secs-3mins at Waypoint 3
- f Autonomous Landing engaged to land at Waypoint 4

During the initial tests, the quadrotor became easily vulnerable to the effects of actuator saturation under gusty weather conditions. However, these tests were not under controlled and repeatable conditions (they were against the original aim of uniformity) and hence resulted in unreliable outcomes that made it difficult to fly the UAV safely. Therefore, to safely and consistently observe the effects of saturation, artificial limits were imposed on the system using the autopilot software and flights only took place in fairly clement weather conditions of $4 - 14mph$ winds, $2 - 15^{\circ}C$ temperature and less than 50% precipitation. This ensured that saturation effects could be recovered from safely (i.e. the limits could be restored to nominal values) to prevent the quadrotor from crashing, and also that saturation arose mainly from (repeatable) reference demands rather than (unrepeatable) disturbances.

Also in initial tests, the artificial saturation limits were set at about 50% of nominal. However, without AW, the quadrotor became highly unstable and resulted in a safe crash seconds after the

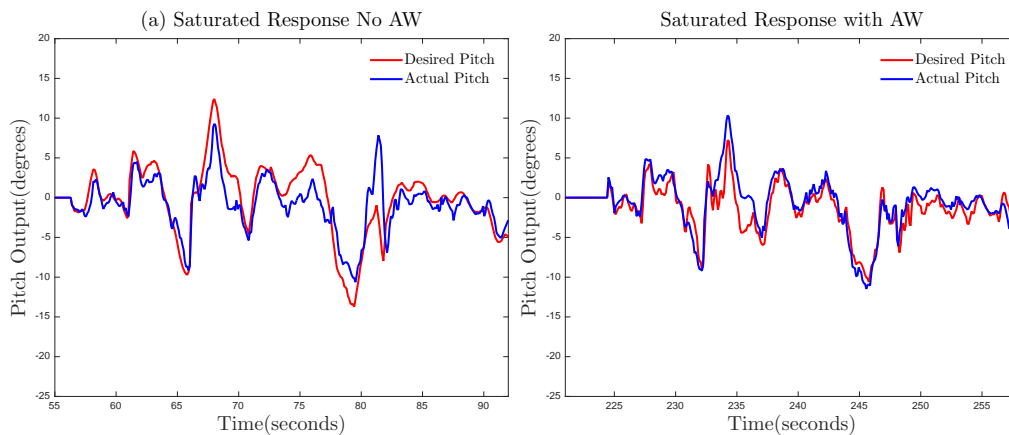


FIGURE 4.26: **Full Flight Pitch response:** (a) [from left] **Saturated No AW**; (b) **Saturated, with AW (Section 4.3)**

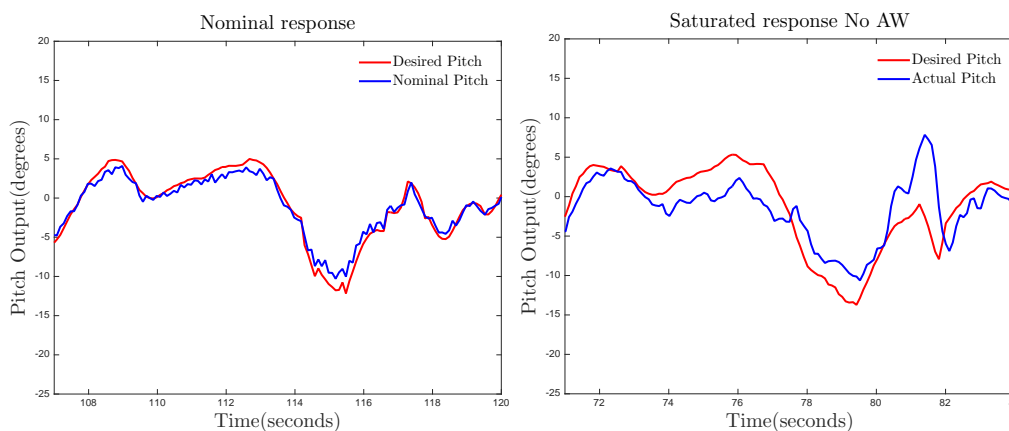


FIGURE 4.27: **Focus on artificial limit flight section:** (a) [from left] **Nominal response** ; (b) **Saturated response no AW**

artificial limits were engaged. When AW was applied with these limits engaged, the quadrotor maintained stable flight in air but with less than desirable performance. For this reason, artificial limits were degraded to a more modest 13% of nominal in all flight tests. These modest degradations still allow the differences between the UAV behaviour with and without AW compensation to be observed but the flights were less prone to disasters.

The scripted flight plan was executed in a similar fashion for each flight test with the artificial limits or artificial limits + AW compensator becoming active in the mission on the path from waypoint 2 to waypoint 3 at an altitude of 9-10 m when the quadrotor is on level flight as shown in Figure 4.25 and then the artificial limits are switched off just before it hits waypoint 3.

Note that the quadrotor is very much capable of flying at altitudes up to 140m but for the purpose of the flight tests, the quadrotor was kept within visible range at altitudes below 30m in order to clearly observe the behaviour of the UAV whenever saturation occurs.

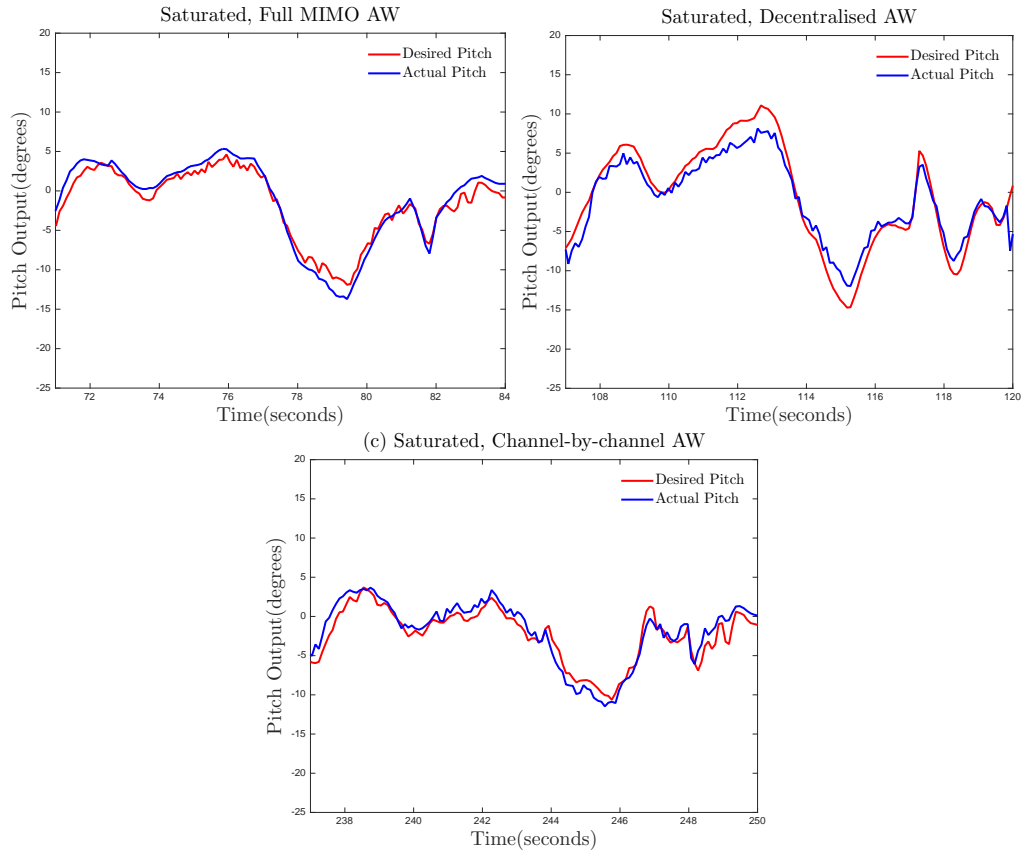


FIGURE 4.28: Pitch angle response: (a) [from left] Saturation, **full MIMO AW**; (b) Saturation, **decentralised AW**; (c) Saturation, **Channel-by-channel AW**

4.5.2.2 Flight Test Results

Figure 4.26a shows the pitch response for a full flight with artificial limits engaged but no AW compensation while Figure 4.26b shows another flight case with artificial limits and channel-by-channel AW compensation engaged.

Figure 4.27a focuses on the flight section with the waypoints where artificial limit were applied and shows the response of the system when no artificial saturation limits are imposed on the system. Note the nominal system's good performance with some good signal tracking and good settling time.

Now, Figure 4.27b shows a degraded response with the artificial saturation limits imposed. It can clearly be seen that the pitch response has large overshoots and is out of phase. Physically, the UAV is seen to jerk slightly along the pitch axis and becomes increasingly unstable with time.

Figures 4.28a, 4.28b and 4.28c show improved responses when the AW compensators are engaged using the full MIMO AW, decentralised AW and channel-by-channel AW compensators respectively. The pitch response overshoot seen in Figure 4.27b is largely reduced in all three cases of Figure 4.28 and its signals are now in phase with the desired/reference signal.

It is important to note that all flights are not exactly alike because with outdoor flights, gust, wind speed and other weather conditions are not constant and hence the differences between

each of these plots.

4.6 Summary

In this chapter, the case of structured AW compensation for a quadrotor system experiencing input saturation was tackled. Two alternative approaches to the design of structured full order AW compensators for a quadrotor plant structure was presented. Both solutions extend the use of the MIMO full order AW compensator of [23] in two novel directions where the first exploits the structure of the plant capturing the network of its “*virtual*” control inputs, thus resulting in an AW compensator which, in a certain sense, is decentralised; this is called the pseudo-decentralised AW compensator. This design is advantageous in cases where the “*virtual*” inputs of the quadrotor can be easily accessed by the design. The second shows how a set of SISO/SIMO AW compensators can be designed for each individual control channel of the quadrotor plant structure; these are referred to as channel-by-channel AW compensators and they have much practical appeal due to their transparency, flexibility (each channel can be re-designed independent of the others) and ease of monitoring.

These AW compensator designs were tested alongside the MIMO full order AW compensator of [23] on simulated quadrotor systems and then validated by application on an experimental quadrotor. Good performances were observed by all three AW compensator types both in simulation and in experiment but in experiment, the channel-by-channel AW compensator design proved superior because they allowed for reduced computational burden and simplified tuning for each channel rather than considering the tuning for the entire system.

Although the AW techniques presented in this chapter were inspired by the quadrotor application, they can potentially be applicable to a wider class of systems. For example, they can be applied to systems that can be modelled as a series interconnection of a diagonal dynamic part and a non-diagonal, but invertible, static part.

5 Non-LMI based approach to AW design for Quadrotor UAVs

5.1 Introduction

LMI techniques have been employed extensively in AW synthesis approaches [61, 62, 74, 144] in recent years. They are appealing because they, in principle, make the design of AW compensator relatively easy. Another reason for their appeal is that they allow stability and performance guarantees for the nonlinear closed loop system to be given.

In Chapter 4, a modified AW technique was proposed for a class of systems depicted in Figure 5.1, where X is assumed to be an invertible matrix. This technique exploited the plant and controllers' structures but still relied on LMIs for AW compensator synthesis. However, the use of LMIs may seem computationally excessive in the design of compensators for relatively simple systems like double integrators. The quadrotor UAV falls into this class of systems, which will be defined more precisely shortly. LMI methods typically use the \mathcal{L}_2 gain as a performance measure, this effectively requires that the performance is bounded by an affine function of the input energy. However, it may, in fact, not be an adequate measure or a reliable indicator of the nonlinear system's practical performance given the fact that the output energy may scale in a nonlinear way with the input energy in the nonlinear system [145]. Also, although LMI-based approaches make AW design systematic and tractable, the use of LMIs, would normally generate one "optimal" solution. This may not necessarily be the only solution yielding a "good" AW compensator, but rather there may exist a family of AW compensators with satisfactory performance from which the designer can choose any.

In this chapter, the AW design process will be broken down into two procedures; the stability analysis and the performance analysis. The stability analysis approach uses the method by Tyan

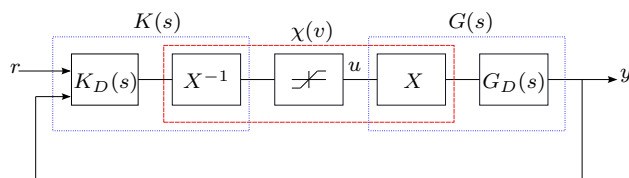


FIGURE 5.1: System under consideration

and Bernstein in [26] which employs a Lure-Postnikov Lyapunov function to generate a Popov-like sufficient condition to guarantee closed-loop global stability for the system. After stability has been guaranteed, the performance analysis will then involve formulating a state-feedback matrix which is constructed using some simple formulae based on a simple linear approximation of the compensator's dynamics and not the \mathcal{L}_2 gain conditions. Compensators designed using this method will be applied to our quadrotor model and results of this implementation will be presented and compared with the MIMO AW design method of [23] in both simulated models and the actual UAV's flight test performance.

5.2 The closed-loop system and AW structure

The results in this chapter are motivated by this quadrotor system which has already been described in previous chapters but they actually apply to a much wider class of systems. Although some of the material has been covered earlier, the essential parts are reiterated below. Now consider the system depicted in Figure 5.1 where $G(s)$ is the nominal plant, $K(s)$ is the controller, $r(t) \in \mathbb{R}^m$ is the reference signal, $y(t) \in \mathbb{R}^p$ is the output and $u(t) \in \mathbb{R}^m$ is the controller demand. The input-coupled plant and the controller have the structure;

$$G(s) = G_D(s)X \quad K(s) = X^{-1}K_D(s) \quad (5.1)$$

where $X \in \mathbb{R}^{m \times m}$ is an invertible matrix and $G_D(s), K_D(s)$ have a block-diagonal arrangement i.e.

$$\begin{aligned} G_D(s) &= \text{blockdiag}(G_1(s), G_2(s), \dots, G_m(s)) \\ K_D(s) &= \text{blockdiag}(K_1(s), K_2(s), \dots, K_m(s)) \end{aligned} \quad (5.2)$$

It is assumed that $G_D(s)$ is a parallel combination of double integrators with the state-space realisation;

$$G_D(s) \sim \left[\begin{array}{c|c} A_D & B_D \\ \hline C_D & D_D \end{array} \right] \quad (5.3)$$

$$\begin{aligned} A_D &= \text{blockdiag}(A, A, A, \dots, A) \in \mathbb{R}^{2m \times 2m} \\ B_D &= \text{blockdiag}(B, B, B, \dots, B) \in \mathbb{R}^{2m \times m} \\ C_D &= \text{blockdiag}(C_1, C_2, C_3, \dots, C_m) \in \mathbb{R}^{p \times 2m} \\ D_D &= \text{blockdiag}(D_1, D_2, D_3, \dots, D_m) \in \mathbb{R}^{p \times 2m} \end{aligned} \quad (5.4)$$

where the matrices A and B have the form;

$$A = \begin{bmatrix} 0 & 1 \\ 0 & 0 \end{bmatrix} \quad B = \begin{bmatrix} 0 \\ \beta \end{bmatrix} \quad (5.5)$$

and the matrices A_D and B_D can be equivalently written as

$$A_D = I_m \otimes A \quad (5.6)$$

$$B_D = I_m \otimes B \quad (5.7)$$

The matrices C_i are not restricted to have a particular structure apart from the fact that (C_i, A) should be observable for all $i \in \{1, \dots, m\}$. It is important to note that specifically, the G_D dynamics of our quadrotor can be essentially represented as a set of double integrators such that

$$G_D(s) = \text{diag}\left(\frac{1}{J_x s^2}, \frac{1}{J_y s^2}, \frac{1}{J_z s^2}, \frac{1}{m s^2}\right) \quad (5.8)$$

with its state-space realisation taking the form of equation (5.4) given that the A and B matrices have the form (5.5) where $\beta = 1$ and the C matrices have the form.

$$C_1 = \frac{1}{J_x} I_2 \quad C_2 = \frac{1}{J_y} I_2 \quad C_3 = \frac{1}{J_z} I_2 \quad C_4 = \frac{1}{m} I_2 \quad (5.9)$$

When saturation is absent, it is assumed that the controller $K(s)$ internally stabilises $G(s)$ and ensures the system exhibits good performance. This is equivalent to $K_D(s)$ internally stabilising $G_D(s)$ and, thus due to their block diagonal structure, each $K_i(s)$ internally stabilising $G_i(s)$ for all $i \in \{1, \dots, m\}$. Therefore, in the absence of saturation, the coupling disappears because the nonlinearity (see Figure 5.1)

$$\chi(u) = X \text{sat}(X^{-1}u) \quad (5.10)$$

is simply the identity operator. However, when saturation is present i.e $u \neq u_m$, the saturation element causes some nonlinear coupling between the system's m control loops and, unless X is diagonal, the decoupling offered by the nominal controller is lost. This coupling becomes the trigger for performance deterioration and instability in the system.

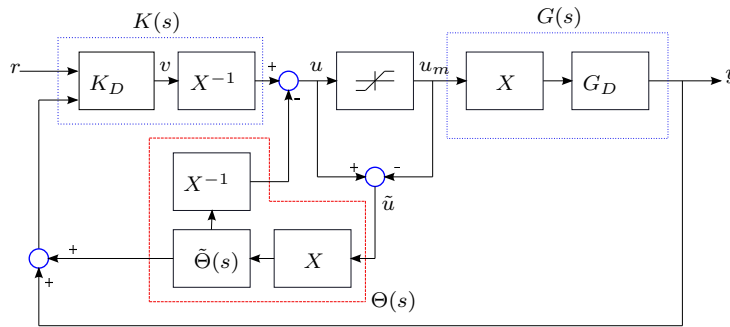


FIGURE 5.2: Input-coupled system with structured anti-windup

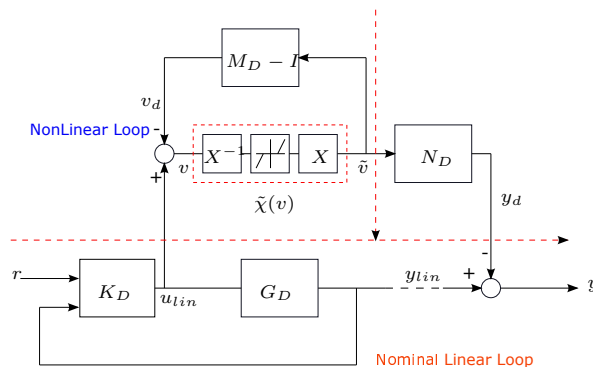


FIGURE 5.3: Equivalent interpretation of structured anti-windup problem

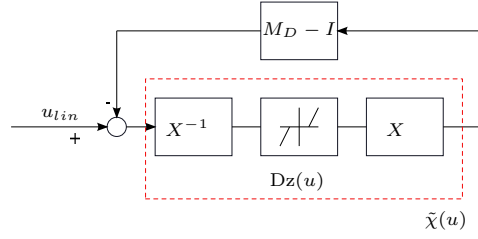


FIGURE 5.4: The nonlinear loop

Now recall the AW architecture proposed in the previous chapter as shown in Figure 5.2 where all parameters remain as described earlier except that $v(t)$ is considered as the *virtual* control input and $\Theta(s)$ is the AW compensator. This structure is exactly the pseudo decentralized AW case in Section 4.4.3 but after some equivalent transformations however, the AW compensator $\Theta(s)$ can be chosen to have the form;

$$\Theta(s) = \begin{bmatrix} X^{-1} & 0 \\ 0 & I \end{bmatrix} \hat{\Theta}(s)X \quad (5.11)$$

where

$$\tilde{\Theta}(s) = \begin{bmatrix} M_D(s) - I \\ N_D(s) \end{bmatrix} \sim \left[\begin{array}{c|c} A_D + B_D F_D & B_D \\ \hline F_D & 0 \\ C_D & 0 \end{array} \right] \quad (5.12)$$

$$N_D(s) = \text{blockdiag}(N_1(s), \dots, N_m(s))$$

$$M_D(s) = \text{blockdiag}(M_1(s), \dots, M_m(s))$$

$$F_D(s) = \text{blockdiag}(F_1(s), \dots, F_m(s))$$

and F_D is chosen such that $A_D + B_D F_D$ is a Hurwitz matrix. For each $i \in \{1 \dots, m\}$, $N_i(s)$ and $M_i(s)$ are factors in the right coprime factorization of $G_i(s)$

$$G_i(s) = N_i(s)M_i(s)^{-1} \quad N_i, M_i \in \mathcal{RH}_\infty \quad (5.13)$$

Recall from Section 4.3.1 that Figure 5.2 with the structure of equation (5.11) can be re-drawn to have the equivalent representation shown in Figure 5.3 from which the nonlinear loop is re-drawn in Figure 5.4. From Figure 5.3, it follows that if the nonlinear loop is stable, then the entire system depicted in Figure 5.2 is stable. A state-space realization of the nonlinear loop is given by

$$\dot{x} = (A_D + B_D F_D)x + B_D \tilde{\chi}(-v_d) \quad (5.14)$$

$$v_d = F_D x \quad (5.15)$$

where, as before,

$$\tilde{\chi}(v) \triangleq XDz(X^{-1}v) = v - \chi(v) \quad (5.16)$$

During normal operation (no saturation), this AW structure allows the design of AW compensators $\hat{\Theta}_i$ for each i^{th} feedback loop independently. However in the presence of saturation, the nonlinearity $\tilde{\chi}(v)$ (5.16), is not a decentralised (diagonal) function (unless X is diagonal) and this implies that even though each i^{th} feedback loop with $\hat{\Theta}_i$ is guaranteed stable (using the process in section 4.3.2), the entire non-linear system will not be stable. To ensure stability of the entire non-linear system, it was shown in Section 4.4.3 (also [116, 118]) that if each AW compensator $\hat{\Theta}_i$ was able to stabilise the i^{th} loop when considered alone and, in addition there existed two diagonal matrices, $V, W \in \mathbf{DP}^{m \times m}$ satisfying the following condition

$$V = X'WX$$

then, an AW compensator $\Theta(s)$ structured as in equation (5.11) would provide exponential stability of the nonlinear loop (and thus stability of the system in Figure 5.2).

These results however focused on the case that $G_i \in \mathcal{RH}_\infty$ for all $i \in \{1 \dots, m\}$. But in the case of our quadrotor plant structure which can be described as a system of double integrators coupled at the input by a matrix X , $G_i(s) \notin \mathcal{RH}_\infty$, and as mentioned in Remark 4.2, small changes to the design procedure can be made to enable the design of a stabilising AW compensator, but the trade-off is that the results will yield a compensator providing only local asymptotic stability. There is however an alternative where this compromise or trade-off does not need to exist. This alternative employs a method by Tyan and Bernstein [26] to achieve global stability results for double integrator plants despite $G(s) \notin \mathcal{RH}_\infty$. A summary of Tyan and Bernstein's result will be presented in the next section and this will be used in subsequent sections to describe the proposed alternative AW design for the system in Figure 5.2 such that the nonlinear loop (equations (5.14)-(5.15)) is globally asymptotically stable implying global stability of the entire system.

5.3 Tyan and Bernstein's Result

Consider a linear system with input saturation whose state-space realization is given as;

$$\dot{x}(t) = A_o x(t) + B_o \text{sat}(u(t)) \quad (5.17)$$

$$u(t) = K_o x(t) \quad (5.18)$$

where it is assumed that the state-space matrices are structured as

$$A_o = \begin{bmatrix} A_z & 0 \\ 0 & A_s \end{bmatrix} \quad B_o = \begin{bmatrix} B_z \\ B_s \end{bmatrix} \quad (5.19)$$

$A_s \in \mathbb{R}^{n_s \times n_s}$ is Hurwitz, $A_z \in \mathbb{R}^{n_z \times n_z}$ and has eigenvalues on the imaginary axis. $B_z \in \mathbb{R}^{n_z \times m}$, $B_s \in \mathbb{R}^{n_s \times m}$ and all signals are assumed to be of compatible dimensions.

According to [26], it is possible to present sufficient conditions which ensure global stability of the above system by using a Lure-Postnikov Lyapunov function that consists of a positive *semi*-definite quadratic term and an additional integral term. This result is summarized as follows.

Theorem 5.1 (Tyan & Bernstein Result [26]). Given that

$$R = \begin{bmatrix} R_z & 0 \\ 0 & R_s \end{bmatrix}, R_z \in \mathbf{N}^{n_z}, R_s \in \mathbf{N}^{n_s}, K_o = [K_1 \dots K_m]'$$

and assuming that (A_o, K_o) is observable or (A_o, K_o) is detectable and (A_o, R) is observable, if there exist matrices $R_2 \in \mathbf{DN}^m$, $N \in \mathbf{DN}^m$, $P \in \mathbf{N}^{(n_z+n_s)}$ such that the following equations and inequalities are satisfied:

$$0 = A_o'P + PA_o + R \quad (5.20)$$

$$0 = B_o'P + NK_oA_o + R_2K_o \quad (5.21)$$

$$0 < 2R_2 - (NK_oB_o + B_o'K_o'N) \quad (5.22)$$

$$0 < P + K_o'NK_o \quad (5.23)$$

then the origin of the system (5.17)-(5.18) is globally asymptotically stable and the Lyapunov function guaranteeing stability is given by

$$V(x) = x'Px + 2 \sum_{i=1}^m \int_0^{u_i=K_i x} N_i \text{sat}_i(u_i) du_i$$

The proof of Theorem 5.1 can be found in [26] and it shows that global stability can be guaranteed for the given saturated system in (5.17)-(5.18) or used to construct a stabilizing controller for the system. This result is used in the next two sections as the basis for constructing AW compensators.

5.4 Stability analysis of AW design for input-coupled double integrators plants

This section is divided into two parts; for simplicity and ease of understanding, the first part presents the proposed AW design procedure for an elementary case of the system structure (i.e. a single double integrator feedback loop) and the second part applies the logic for the AW design from the first part to the more intricate case of our quadrotor plant structure.

5.4.1 Part 1: For a single double integrator feedback loop

Let's assume that the system under consideration is a single double integrator feedback loop with $X = 1$ and the plant state-space matrices are reduced to $A_D = A, B_D = B, C_D = C \in \mathbb{R}^{p \times 2}, D_D = 0$, for $p = 1$. The nonlinearity $\tilde{\chi}(\cdot)$ simply becomes the deadzone, and the nonlinear

loop of equations (5.14)-(5.15) are then reduced to

$$\dot{x} = (A + BF)x + BDz(-v_d) \quad (5.24)$$

$$v_d = Fx \quad (5.25)$$

where $F \in \mathbb{R}^{p \times 2}$ is the state-feedback matrix used for the AW compensator design. Given that the deadzone operator $Dz(u) = u - \text{sat}(u)$, the nonlinear loop dynamics (5.24)-(5.25) can be re-written as

$$\dot{x} = Ax + B\text{sat}(v_d) \quad (5.26)$$

$$v_d = Fx \quad (5.27)$$

The following corollary provides a sufficient condition on F which ensures the nonlinear loop dynamics are globally asymptotically stable.

Corollary 5.1. Assume $F = [F_a \ F_b]$ is chosen such that $\text{sign}(F_a) = -\text{sign}(\beta)$ and $\text{sign}(F_b) = -\text{sign}(\beta)$. Then the origin of the system (5.24)-(5.25) is globally asymptotically stable.

Proof: Theorem 5.1 is applied to the system in equation (5.24)-(5.25) such that the system has the same form (5.17)-(5.18) where $A_z = A$, $B_z = B$ and $K = F$, given that $n_z = 2$, $n_s = 0$ and $m = 1$. Therefore, equations (5.20)-(5.23) from Theorem 5.1 becomes

$$0 = A'P + PA + R \quad (5.28)$$

$$0 = B'P + NFA + R_2F \quad (5.29)$$

$$0 < 2R_2 - (NFB + B'F'N) \quad (5.30)$$

$$0 < P + F'NF \quad (5.31)$$

Now let $R = 0$, $R_2 = 0$ and $N = 1$, and suppose P is partitioned such that

$$P = \begin{bmatrix} P_a & P_{b/c} \\ P_{b/c} & P_d \end{bmatrix} \quad (5.32)$$

This makes equation (5.28) become

$$\begin{bmatrix} 0 & 0 \\ 0 & 0 \end{bmatrix} = \begin{bmatrix} 0 & 1 \\ 0 & 0 \end{bmatrix}' \begin{bmatrix} P_a & P_{b/c} \\ P_{b/c} & P_d \end{bmatrix} + \begin{bmatrix} P_a & P_{b/c} \\ P_{b/c} & P_d \end{bmatrix} \begin{bmatrix} 0 & 1 \\ 0 & 0 \end{bmatrix} = \begin{bmatrix} 0 & 0 \\ P_a & P_{b/c} \end{bmatrix} + \begin{bmatrix} 0 & 0 \\ P_a & P_{b/c} \end{bmatrix}' \quad (5.33)$$

This shows that $P_a = P_{b/c} = 0$ and thus equation (5.29) can now be written as

$$\begin{bmatrix} 0 & 0 \end{bmatrix} = \begin{bmatrix} 0 & \beta \end{bmatrix} \begin{bmatrix} P_a & P_{b/c} \\ P_{b/c} & P_d \end{bmatrix} + \begin{bmatrix} F_a & F_b \end{bmatrix} \begin{bmatrix} 0 & 1 \\ 0 & 0 \end{bmatrix} \quad (5.34)$$

$$= \begin{bmatrix} \beta P_{b/c} & \beta P_d + F_a \end{bmatrix} \quad (5.35)$$

From equation (5.35), $P_d = -F_a/\beta$ and because, P_d must be positive semi-definite, it is necessary and sufficient for $\text{sign}(F_a) = -\text{sign}(\beta)$ or $P_d = 0$ and $F_a = 0$. Given the format for P as obtained above, inequality (5.30) becomes

$$0 < - \begin{bmatrix} F_a & F_b \end{bmatrix} \begin{bmatrix} 0 \\ \beta \end{bmatrix} + \begin{bmatrix} 0 & \beta \end{bmatrix} \begin{bmatrix} F_a \\ F_b \end{bmatrix} \quad (5.36)$$

$$= -2F_b\beta \quad (5.37)$$

It is important to note that for this inequality to hold, it is imperative that $\text{sign}(F_b) = -\text{sign}(\beta)$. Finally, inequality (5.31) can now be written as

$$0 < \begin{bmatrix} 0 & 0 \\ 0 & P_d \end{bmatrix} + \begin{bmatrix} F_a \\ F_b \end{bmatrix} \begin{bmatrix} F_a & F_b \end{bmatrix} = \begin{bmatrix} F_a^2 & F_a F_b \\ F_a F_b & P_d + F_b^2 \end{bmatrix} \quad (5.38)$$

For this inequality to hold also we must strengthen our conclusion to the fact that $\text{sign}(F_a) = -\text{sign}(\beta)$: it cannot be zero or only positive semi-definiteness would be proven. Hence in this case, the conditions of Theorem 5.1 are fulfilled and the system will be globally asymptotically stable. \square

5.4.2 Part 2: For input-coupled double integrator systems

Consider now the more intricate and general case of the system presented by equations (5.1)-(5.4) while noting the dynamics of the nonlinear loop (5.14)-(5.15). The following corollary provides a sufficient condition for ensuring global stability of the origin of this system

Corollary 5.2. Let $F_D = (I_m \otimes F)$ where $F = [F_a \ F_b]$ is chosen such that $\text{sign}(F_a) = -\text{sign}(\beta)$ and $\text{sign}(F_b) = -\text{sign}(\beta)$. Then the origin of the system (5.14)-(5.15) is globally asymptotically stable.

Proof: This is a simple extension of the proof of Corollary 5.1 above. Using the identity (5.16), the dynamics of the nonlinear loop (5.14)-(5.15) can be re-written as

$$\dot{x} = A_D x + B_D \chi(F_D x) \quad (5.39)$$

$$= (I \otimes A)x + (I \otimes B)\chi((I \otimes F)x) \quad (5.40)$$

$$= (I \otimes A)x + (I \otimes B)X \text{sat}(X^{-1}(I \otimes F)x) \quad (5.41)$$

We define $\bar{A} = I \otimes A$, $\bar{B} = (I \otimes B)X$ and $\bar{F} = X^{-1}(I \otimes F)$, equation (5.41) then becomes

$$\dot{x}(t) = \bar{A}x(t) + \bar{B} \text{sat}(\bar{F}x(t)) \quad (5.42)$$

Applying Theorem 5.1 to the system in equation (5.42) implies that the origin will be globally asymptotically stable if there exist matrices $\bar{P} \in \mathbf{P}^{2m \times 2m}$, $\bar{R} \in \mathbf{P}^{2m \times 2m}$, $\bar{R}_2, \bar{N} \in \mathbf{DP}^{m \times m}$ such

that the following matrix equations and inequalities hold;

$$0 = \bar{A}'\bar{P} + \bar{P}\bar{A} + \bar{R} \quad (5.43)$$

$$0 = \bar{B}'\bar{P} + \bar{N}\bar{F}\bar{A} + \bar{R}_2\bar{F} \quad (5.44)$$

$$0 < 2\bar{R}_2 - (\bar{N}\bar{F}\bar{B} + \bar{B}'\bar{F}'\bar{N}) \quad (5.45)$$

$$0 < \bar{P} + \bar{F}'\bar{N}\bar{F} \quad (5.46)$$

Now supposing

$$\bar{P} = (I_m \otimes P) \quad \bar{R} = 0 \quad \bar{R}_2 = 0 \quad \bar{N} = X'X \quad (5.47)$$

where P has the structure in equation (5.32). \bar{N} is positive definite since X is nonsingular. Equations/inequalities (5.43)-(5.46) can then be re-written as

$$0 = I_m \otimes (PA' + PA) \quad (5.48)$$

$$0 = X'(I_m \otimes (B'P + FA)) \quad (5.49)$$

$$0 < -X'(I_m \otimes (FB + B'F'))X \quad (5.50)$$

$$0 < I_m \otimes (P + F'F) \quad (5.51)$$

where the following properties of the Kronecker Product have been used

$$(A \otimes B)(C \otimes D) = AC \otimes BD \quad (5.52)$$

$$(A \otimes B)' = A' \otimes B' \quad (5.53)$$

Similar to the process followed in the proof of Corollary 5.1, equations/inequalities (5.48-5.51) are satisfied if the conditions imposed on F as stipulated in the summary statement of the corollary 5.1 are also satisfied. \square

5.5 Performance Consideration

From both Corollaries 5.1 and 5.2, it can be seen that there exist a large family of AW compensators which ensure global asymptotic stability of the origin of the AW system. This is due to the fact that the values of the state-feedback matrix F simply need to be opposite in sign to β . However, one would expect that not all values of F will perform well in the system; only a portion of these are likely to provide acceptable performance. In this section, a transparent procedure is presented for selecting suitable ranges of F for acceptable performance based on the AW compensator dynamics. Note that F_D in the AW structure 5.12 can be constructed to have the form $F_D = (I \otimes F)$ where F can be chosen individually for each double integrator feedback loop due to the structure of equation (5.1).

Since F can be chosen individually for each feedback loop, consider a single double integrator feedback loop and here, the saturation function in the AW compensator dynamics (5.26)-(5.27)

is replaced with a time-varying gain, such that the saturation function becomes,

$$\text{sat}(u) = \sigma(u)u \quad \sigma(\cdot) : \mathbb{R} \mapsto [0, 1] \quad (5.54)$$

When the time-varying gain (5.54) is applied to the nonlinear loop equations (5.26)-(5.27), they become;

$$\dot{x} = (A + B\sigma(u)F)x \quad (5.55)$$

This results in the “A”-matrix of the nonlinear loop having the form

$$A + B\sigma(u)F = \begin{bmatrix} 0 & 1 \\ \beta\sigma(u)F_a & \beta\sigma(u)F_b \end{bmatrix} \quad (5.56)$$

The matrix $A + B\sigma(u)F$ has the appearance of a time-varying “A”-matrix and although it cannot, strictly speaking, be subjected to linear analysis, we can use approximate linear analysis with some confidence: it has already been established that the system is stable providing F satisfies corollary 5.1. The idea is to use this approximate analysis to examine the system’s performance. With the above in mind, the characteristic equation of the matrix $A + B\sigma(u)F$ is given by

$$s^2 - \beta\sigma(u)F_b s - \beta\sigma(u)F_a = 0 \quad (5.57)$$

Now suppose the time varying gain $\sigma(u)$ is replaced by a constant σ_0 such that $\sigma_0 \in [0, 1]$ then the above equation becomes

$$s^2 - \beta\sigma_0 F_b s - \beta\sigma_0 F_a = 0 \quad (5.58)$$

Note that $\sigma_0 = 1$ is equivalent to that the control signal remaining within the saturation limits and thus the system is in its normal operation. $\sigma_0 < 1$ denotes that the control signal is outside the saturation limits and thus the system is in its saturated state. The standard second order characteristic equation is defined as

$$s^2 + 2\zeta\omega_n s + \omega_n^2 = 0 \quad (5.59)$$

where ω_n is the undamped natural frequency and ζ is the damping ratio. Thus comparing the coefficients of both equations 5.58 and 5.59, we can obtain expressions for ω_n and ζ as

$$\omega_n = \sqrt{-\beta\sigma_0 F_a} \quad \zeta = -\frac{F_b}{2} \sqrt{-\frac{\beta\sigma_0}{F_a}} \quad (5.60)$$

Rearranging equation (5.60) such that F_a and F_b are made subject of the formula gives

$$F_a = -\omega_n^2 / \beta\sigma_0 \quad F_b = -2\zeta \sqrt{-\frac{F_a}{\beta\sigma_0}} \quad (5.61)$$

Equation (5.61) implies that F_a is a function of the desired natural frequency ω_n of the system while F_b is a function of the selected value of F_a and the desired damping ratio ζ . Note however that both F_a and F_b depend also on σ_0 which represents the level of saturation so one could choose F such that good behaviour (damping) is observed for a range of σ_0 . For example,

choosing $\zeta = 1$ for $\sigma_0 = 1$ implies that compensator will be underdamped for $\sigma_0 < 1$ (i.e when saturation occurs) and thus poor responses are expected, but choosing $\zeta > 1$ might be expected to give better responses.

In reality however, the saturation level varies, causing σ_0 to fluctuate between the range $[0, 1]$. However, F_a and F_b could be designed by choosing a suitable value of σ_0 , possibly corresponding to some lower limit on $\sigma(\cdot)$ and then it would be expected that the compensators would have acceptable performance if the saturation did not cause $\sigma(\cdot)$ to deviate too much from this value. For example, if the control signal was expected to exceed twice the saturation limits, σ_0 could be chosen as 0.5 and hence, the AW compensator can be designed using this value.

Remark 5.1: The range of values for F obtained in this section is a much smaller set than that indicated in Corollary 5.1 and any selected F value will largely depend on the designer's requirement which may be to reduce the computational requirements on the system or to obtain very good performance bearing in mind that there is a tradeoff between computational requirements and performance expectations. \square

5.6 Results

In this section, the test models of the quadrotor used in the previous chapter (precisely Section 4.5) are used to validate the AW compensator design described in Sections 5.4 and 5.5. Each test case consists of using 2 different natural frequencies at varying damping ratios for the AW design. These are presented in detail in the following;

5.6.1 Simulation Results

In these results, the effects of saturation and the attendant AW compensation will be observed on the quadrotor's pitch θ attitude (angle). A pulse reference signal of 0.4 rad was commanded on the pitch θ with saturation constraints applied on all control signals.

5.6.1.1 Micro-Quadrotor Model (MQM)

AW compensators were designed for the quadrotor system at $\sigma_0 = 1$ with F matrices obtained for $\omega_n = 115.47 \text{ rad/s}$ and at various damping ratios as listed in the Table 5.1. A further set of F matrices were designed for $\omega_n = 36.51 \text{ rad/s}$ and various damping ratios according to the Table 5.2. Figures 5.5a shows the nominal response and Figures 5.5b indicates that the saturated

TABLE 5.1: MQM Damping Ratios and AW Gains for Simulations at $\omega_n = 115.47 \text{ rad/s}$

Damping Ratio	F_a	F_b	Remark
$\zeta = 0.1$	-100	-0.1732	$\zeta < 1$
$\zeta = 1$	-100	-1.7321	$\zeta = 1$
$\zeta = 5$	-100	-8.6603	$\zeta > 1$

TABLE 5.2: MQM Damping Ratios and AW Gains for Simulations at $\omega_n = 36.51\text{rad/s}$

Damping Ratio	F_a	F_b	Remark
$\zeta = 0.1$	-10	-0.0548	$\zeta < 1$
$\zeta = 1$	-10	-0.5477	$\zeta = 1$
$\zeta = 5$	-10	-2.7386	$\zeta > 1$

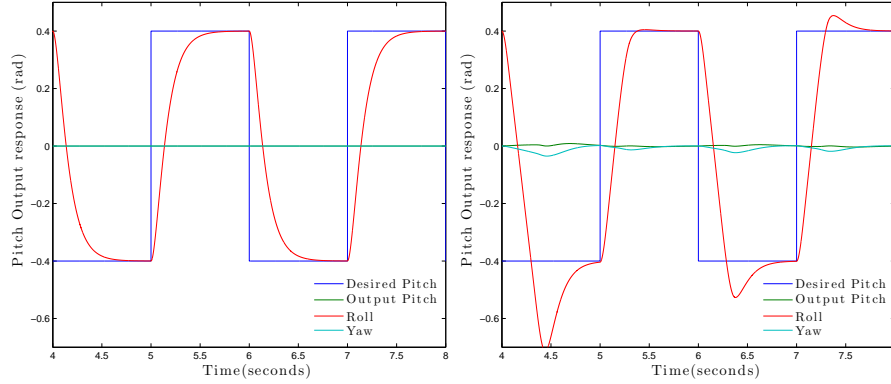


FIGURE 5.5: MQM Pitch angle response: (a) [from left] Nominal and (b) Saturation, no AW

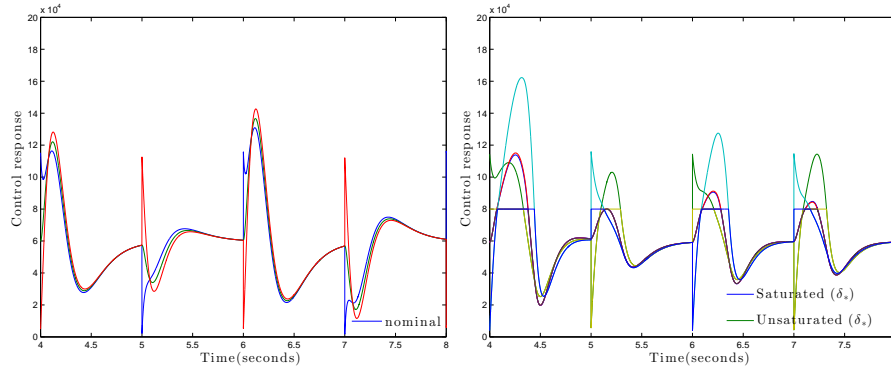


FIGURE 5.6: MQM Control response: (a) [from left] Nominal and (b) Saturation, no AW

system has poor performance. During saturation, the system loses the decoupling properties provided by virtue of the structure $G(s) = G_D(s)X$.

Figures 5.7 show the response with AW compensation. Notice that the response improves as ζ increases from 0.1 to 5 with the best response at $\zeta = 5$. Recall that the damping ratio ζ is strictly an increasing function of σ_0 , so when saturation occurs $\sigma_0 < 1$, it implies that choosing $\zeta = 1$ (critically damped) will result in an underdamped AW compensator and thus poor responses, however if the damping ratio is chosen to be overdamped ($\zeta > 1$), this improves the damping of the AW compensator and therefore results in better responses as can be seen in Figures 5.7. Note that at higher frequencies, better responses were obtained from the system and these can be seen in the difference between Figure 5.7a and Figure 5.7b. this can be seen as a consequence of the relationship between the damping ratio ζ and the natural frequency ω_n in equation (5.60), where increasing the natural frequency ω_n also improves the damping ratio ζ of the system. The All plots of Figure 5.6 and Figure 5.8 show the control signal response both at nominal and at saturation.

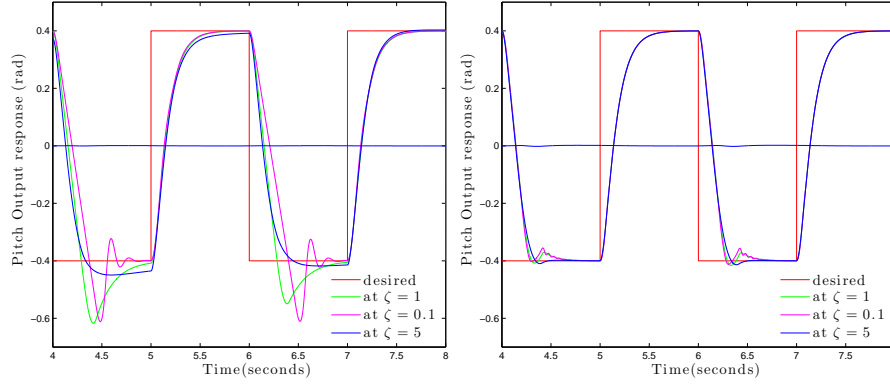


FIGURE 5.7: MQM Pitch angle response: (a) [from left] Saturation, $\omega_n = 36.51rad/s$ with AW at different ζ ; and (b) Saturation, $\omega_n = 115.47rad/s$ with AW at different ζ

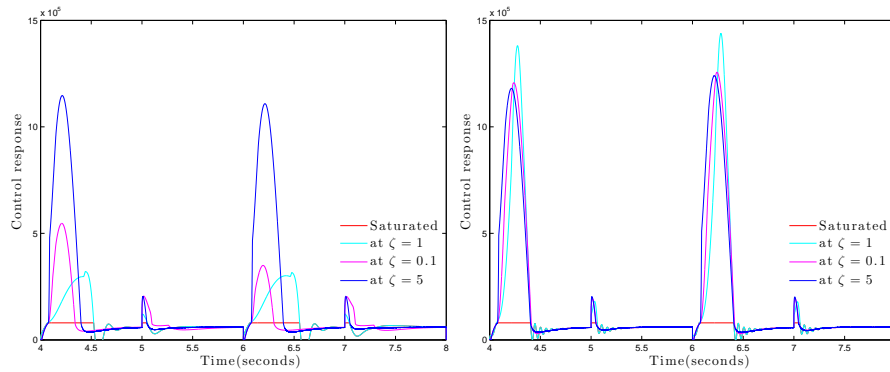


FIGURE 5.8: MQM Control response: (a) [from left] Saturation, $\omega_n = 36.51rad/s$ with AW at different ζ ; and (b) Saturation, $\omega_n = 115.47rad/s$ with AW at different ζ

TABLE 5.3: EQM Damping Ratios and AW Gains for Simulations at $\omega_n = 800rad/s$

Damping Ratio	F_a	F_b	Remark
$\zeta = 0.5$	-1.8240	-0.0023	$\zeta < 1$
$\zeta = 1$	-1.8240	-0.0046	$\zeta = 1$
$\zeta = 5$	-1.8240	-0.0228	$\zeta > 1$

5.6.1.2 Experimental Quadrotor Model (EQM)

AW compensators were designed for the quadrotor system at $\sigma_0 = 1$. The first set were designed with natural frequency of $\omega_n = 800rad/s$ and the damping ratios varied as listed in Table 5.3. A further set of AW compensators were designed using a frequency of $\omega_n = 500rad/s$ and the damping ratios varied as listed in Table 5.4.

Figure 5.9a shows the nominal response and Figure 5.9b shows the saturated system with poor performance that may become highly unstable with time.

Figures 5.11a and 5.11b show the saturated response with AW compensation. The response improves as ζ increases from 0.5 to 5 with the best response at $\zeta = 5$. Note that at higher undamped natural frequencies, better responses were obtained from the system and these can

TABLE 5.4: EQM Damping Ratios and AW Gains for Simulations at $\omega_n = 500\text{rad/s}$

Damping Ratio	F_a	F_b	Remark
$\zeta = 0.5$	-0.7125	-0.0014	$\zeta < 1$
$\zeta = 1$	-0.7125	-0.0028	$\zeta = 1$
$\zeta = 5$	-0.7125	-0.0142	$\zeta > 1$

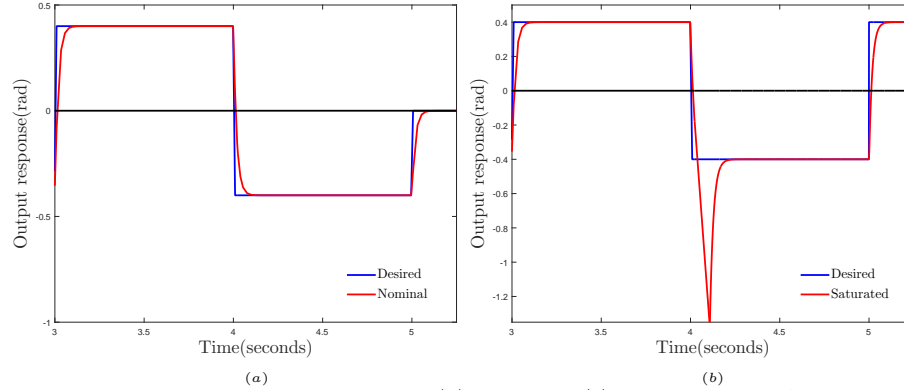


FIGURE 5.9: Output response:(a) Nominal; (b) Saturation, no AW

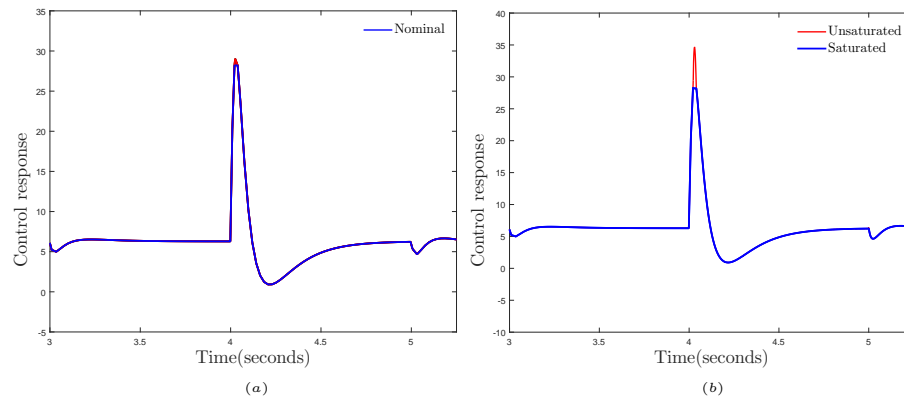


FIGURE 5.10: Control response:(a) Nominal; (b) Saturation, no AW

be seen in the difference between Figure 5.11a and Figure 5.11b. All plots of Figure 5.10 and Figure 5.12 show the control signal response both at nominal and at saturation.

5.6.2 EQM Flight Test Results

The quadrotor setup and test procedure follows the same process outlined in Section 4.5.2 so we will go ahead and present the results of the tests.

Figure 5.13a shows a typical pitch response when no artificial limits were imposed. This can be interpreted as the *nominal case*. Figure 5.13b shows a similar section of the flight, but with the artificial limits applied and no AW compensation. One can see that when the limits are imposed, the pitch response deteriorates and almost becomes unstable.

Figures 5.14a and 5.14b show the response of the system when the artificial limits are applied and the AW compensators corresponding to $\omega_n = 500\text{rad/s}$ at $\zeta = 0.5$ and $\zeta = 2$ are used. The results seem better than the saturated no AW case but with a less than desirable signal

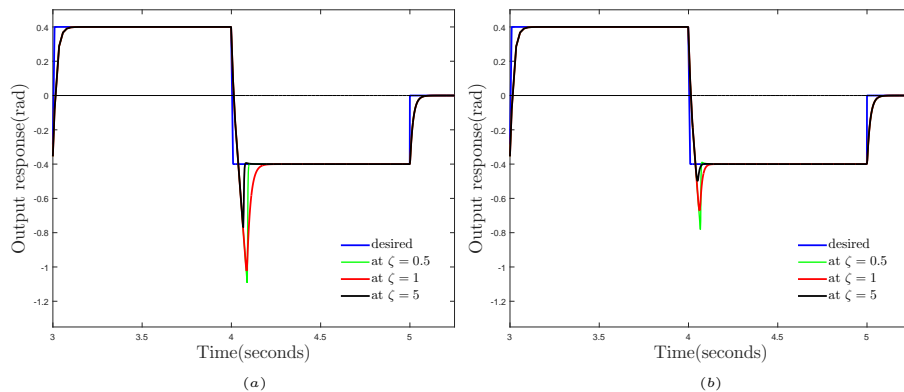


FIGURE 5.11: Output response:(a) Saturation, $\omega_n = 500 \text{ rad/s}$ with AW at different ζ ; (b) Saturation, $\omega_n = 800 \text{ rad/s}$ with AW at different ζ

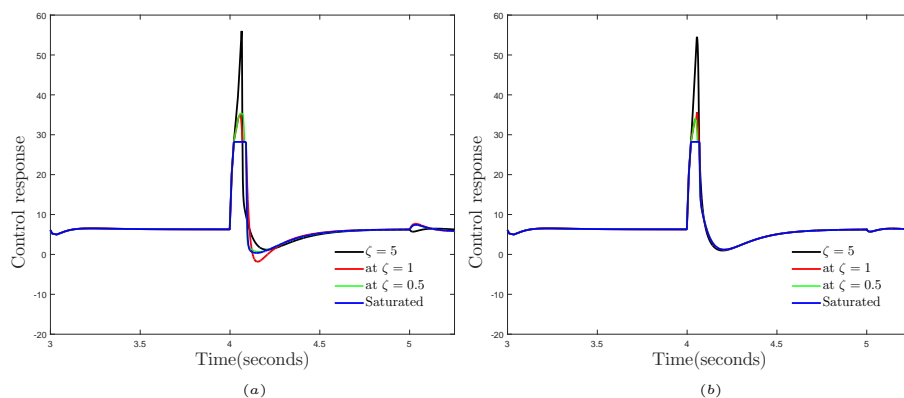


FIGURE 5.12: Control response: [(a), (b)] Saturation, $\omega_n = 500 \text{ rad/s}$ and $\omega_n = 800 \text{ rad/s}$ with AW at different ζ

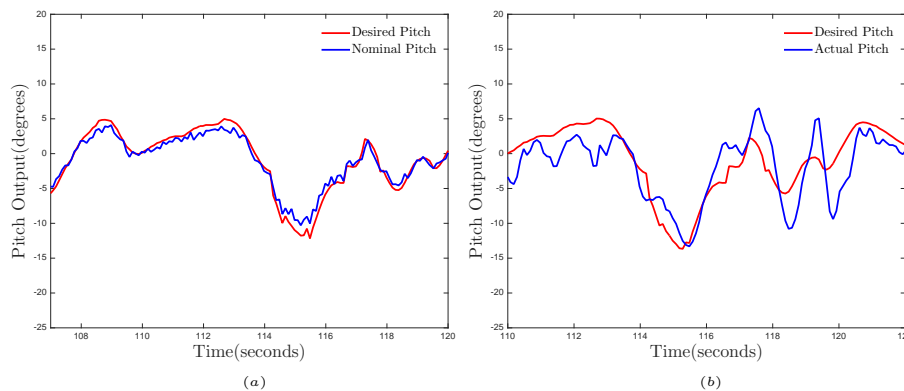


FIGURE 5.13: Pitch angle response-Artificial limit flight section: (a) [from left] Typical Nominal response ; (b) Saturated response no AW

tracking. Figures 5.15a and Figure 5.15b show improved responses when the artificial limits are applied and the AW compensators corresponding to $\omega_n = 840 \text{ rad/s}$ at $\zeta = 0.5$ and $\zeta = 2$ are engaged. Note the good performance of the compensators with the signals in phase with the desired reference. When comparing the results of both values of ω_n , it can be seen that the AW compensators for $\zeta = 2$ produce better responses than the compensators for $\zeta = 0.5$. Since all experiments were carried out outdoors, there are some differences between all flights recorded due to weather conditions such as gust, wind speed etc.

Remark 5.2: Both the simulation tests and the experimental tests confirm that the higher the value of ω_n chosen, the better the performance of the AW compensator at different ζ . However, it

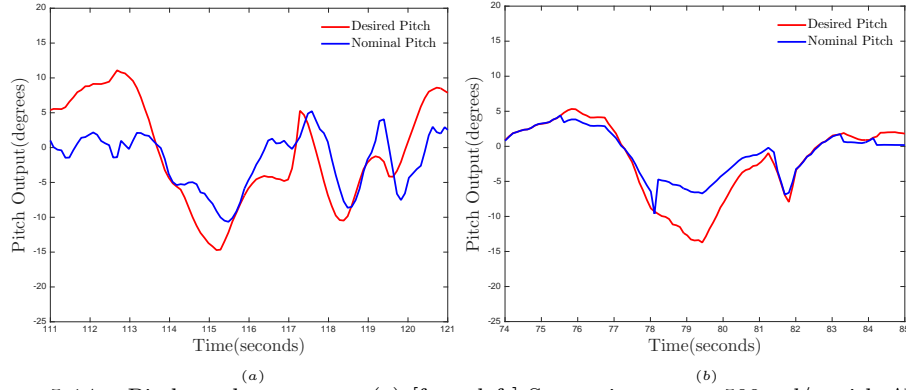


FIGURE 5.14: Pitch angle response: (a) [from left] Saturation, $\omega_n = 500\text{rad/s}$ with AW at $\zeta = 0.5$; (b) Saturation, $\omega_n = 500\text{rad/s}$ with AW at $\zeta = 2$.

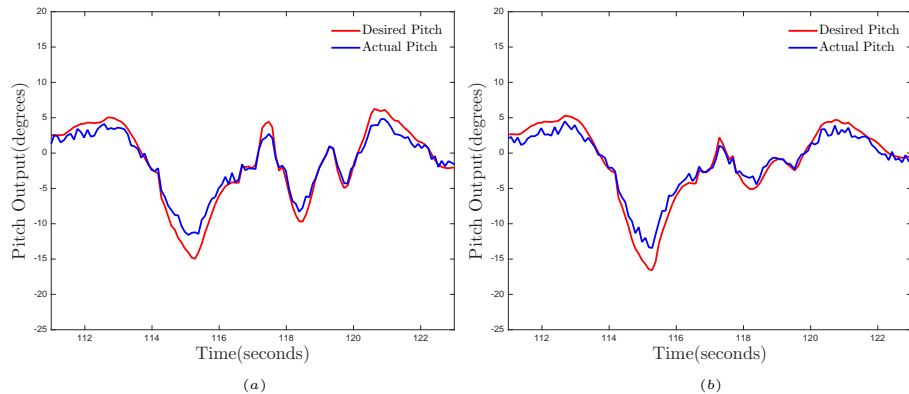


FIGURE 5.15: Pitch angle response: (a) [from left] Saturation, $\omega_n = 840\text{rad/s}$ with AW at $\zeta = 0.5$; (b) Saturation, $\omega_n = 840\text{rad/s}$ with AW at $\zeta = 2$.

is important to note that the choice of ω_n should be such that the AW compensator is sufficiently fast enough to give good performance but within the limit of the quadrotor's processor power: $\omega_n =$ cannot be increased arbitrarily without computational problems.

Remark 5.3: Note also that the responses of other channels apart from the pitch channel were not directly measured during the flight tests but by visual inspection seemed to give acceptable responses. However, the responses of these “offline” channels need to be further investigated to ensure that they perform as required.

5.7 Summary

This chapter has presented a technique for synthesizing AW compensators for systems containing double integrators like the quadrotor UAVs. This was done by analyzing the stability of the system based on a Popov-like sufficient condition presented in [26] to ensure closed-loop global stability of the system. This solution provides a very large set of stabilising AW compensators for the system but simple linear analysis based on the compensator's natural frequency and damping ratio are used to guide choice of a suitable compensator from this set.

The main results show that by selecting a suitable F using a simple, transparent formulae, derived from the compensator's natural frequency and damping ratio, we can obtain good performance for the AW compensator (after stability has been guaranteed). With this approach, there is a

flexible range of values for F for which the system will perform well. Hence within these range of values, F can be chosen based on the designers need and in real time without necessarily having to repeat any stability analysis.

AW compensators synthesized via this approach were applied to the quadrotor system both in simulation and on the experimental platform with good results obtained during periods of saturation. This approach provides a rapid, transparent method for AW design and re-design for the quadrotor and it offers a level of simplicity and flexibility that will be highly appreciated in a practical environment.

Part II

Anti-Windup Design for Fixed Wing UAVs

6 Fixed-Wing UAV Modelling and Control

6.1 Introduction

In the introductory chapter to this thesis, it was disclosed that the study of actuator saturation and AW design solutions will be carried out on two UAV types; a rotary type UAV and a fixed wing type UAV. Part I of this thesis (Chapters 3,4 and 5) focused on tackling actuator saturation in Quadrotor UAVs (a rotary type UAV) with decentralized AW compensator schemes however, Part II of this thesis (Chapters 6 and 7) will focus on tackling actuator saturation in Fixed wing UAVs using AW compensator schemes that can be perceived as decoupled/decentralized.

This chapter will first give a brief description on the development of the basic 6 DOF model of fixed wing UAVs and introduce the **Aerosonde** fixed-wing UAV model. It will also provides an overview of the trimming and linearization of the 6 DOF model of the **Aerosonde** UAV which is used to further develop a suitable control scheme. The contents of this chapter will be used for the subsequent development of suitable AW compensators presented in the next chapter.

6.2 Fixed-wing UAV Equations of Motion

The mathematical modelling process for Fixed-wing UAVs has been described extensively by many authors [146–148] using many different methods of modelling but all stemming from the principles of flight based on the equations of classical mechanics. However, this section will briefly present the dynamic equations of motion for fixed-wing UAVs extracted from [146] as considered within two key coordinate reference systems; the Aircraft’s **Body** axes frame and the Earth’s **Inertial** frame. Detailed description of these reference systems and the relationship between them are provided in Appendix A.

Before proceeding, it is necessary to note the following assumptions for the fixed-wing UAVs. These assumptions allow the UAV’s 6 DOF motion to be described by translational and rotational motion about its centre of mass.

Assumption 6.1.

1. The UAV is a rigid body and its dynamics are defined with respect to the fixed body frame
2. The UAV is symmetrical about the XZ plane.
3. The UAV's mass is constant over time (or subject to negligible variation).

The translational motion can be derived from Newton's second law of linear motion which is given by

$$\{F\}_i = m\left\{\frac{dv}{dt}\right\}_i$$

where F is the force acting on the UAV, m is the mass of the vehicle, v is the velocity of the centre of mass of the UAV and $\{.\}_i$ denotes that the parameter therein is taken with respect to the inertial frame. The velocity of the UAV is taken with respect to a rotating body axes hence the conversion of $\frac{dv}{dt}$ from inertial to body frame is given as

$$\left\{\frac{dv}{dt}\right\}_i = \left\{\frac{dv}{dt}\right\}_b + \{\omega\}_b \times \{v\}_b \quad (6.1)$$

where $\{v\}_b$ consist of linear velocities u, v, w acting in the x, y, z directions respectively, $\{\omega\}_b$ consist of angular velocities p, q, r (i.e. roll, pitch and yaw rates) acting in the x, y, z directions respectively and $\{.\}_b$ denotes that the parameter therein is taken with respect to the body frame. Recall the reference frame definitions given by equations (3.1) and (3.2) and applying the appropriate reference frame transformations to equation (6.1), the force acting on the UAV thus becomes

$$\{F\}_i = m\left(\left\{\frac{dv}{dt}\right\}_b + \{\omega\}_b \times \{v\}_b\right) \quad (6.2)$$

$$\begin{bmatrix} F_x \\ F_y \\ F_z \end{bmatrix} = \begin{bmatrix} m(\dot{u} + rv - qw) \\ m(\dot{v} + pw - ru) \\ m(\dot{w} + qu - pv) \end{bmatrix} \quad (6.3)$$

Similarly, the rotational motion can be derived from Newton's second law of angular motion,

$$\{M_m\}_i = \left\{\frac{dH}{dt}\right\}_i = J\left\{\frac{d\omega}{dt}\right\}_i$$

where M_m is the moment acting on the UAV, H is the angular momentum given as $H = J\omega$ and J^1 is the tensor of inertia matrix given as

$$J \triangleq \begin{bmatrix} J_x & -J_{xy} & J_{xz} \\ -J_{yx} & J_y & -J_{yz} \\ -J_{zx} & -J_{zy} & J_z \end{bmatrix}$$

Since the UAV is considered to be symmetrical about the body axes plane xz , the two pairs of the off-diagonal terms of J matrix become zero, i.e. $J_{xy} = J_{yx} = 0$ and $J_{yz} = J_{zy} = 0$. Hence,

¹The terms J_x, J_y, J_z are referred to as the Moments of Inertia.

following the same process used in the derivation of F and bearing in mind the transformations from inertial to body axes, M_m in body axes results in

$$M_m = \begin{bmatrix} L \\ M \\ N \end{bmatrix} = \begin{bmatrix} \dot{p}J_x + qr(J_z - J_y) - (\dot{r} + pq)J_{xz} \\ \dot{q}J_y + pr(J_z - J_x) + (p^2 - r^2)J_{xz} \\ \dot{r}J_z + pq(J_y - J_x) + (qr + \dot{p})J_{xz} \end{bmatrix} \quad (6.4)$$

where, L, M, N are the moments about x, y, z axes respectively, the terms $\dot{p}J_x, \dot{q}J_y, \dot{r}J_z$ denote angular acceleration, the terms $qr(J_z - J_y), pr(J_z - J_x), pq(J_y - J_x)$ denote gyro precession and the final terms $(\dot{r} + pq)J_{xz}, (p^2 - r^2)J_{xz}, (qr + \dot{p})J_{xz}$ are representative coupling terms.

It is important to note that the kinematics and state variable relationship presented in Section 3.2.2 for Quadrotor UAVs are also applicable to Fixed-wing UAVs as well and hence the kinematics featuring the Euler angles $[\phi, \theta, \psi]$ (roll, pitch and yaw angles) and position vectors $[x, y, z]$ are given as

$$\begin{bmatrix} \dot{\phi} \\ \dot{\theta} \\ \dot{\psi} \end{bmatrix} = \begin{bmatrix} 1 & \sin \phi \tan \theta & \cos \phi \tan \theta \\ 0 & \cos \phi & -\sin \phi \\ 0 & \sin \phi \sec \theta & \cos \phi \sec \theta \end{bmatrix} \begin{bmatrix} p \\ q \\ r \end{bmatrix} \quad (6.5)$$

$$\begin{bmatrix} \dot{x} \\ \dot{y} \\ \dot{z} \end{bmatrix} = \begin{bmatrix} \cos \theta \cos \psi & \cos \psi \sin \theta \sin \phi - \cos \phi \sin \psi & \cos \psi \sin \theta \cos \phi - \sin \phi \sin \psi \\ \cos \theta \sin \psi & \sin \psi \sin \theta \sin \phi - \cos \phi \cos \psi & \sin \psi \sin \theta \cos \phi - \sin \phi \cos \psi \\ -\sin \theta & \cos \theta \sin \phi & \cos \phi \cos \theta \end{bmatrix} \begin{bmatrix} u \\ v \\ w \end{bmatrix} \quad (6.6)$$

Thus, equations (6.3) and (6.4) as well as the kinematic equations (6.5) and (6.6) all represent the complete nonlinear dynamics of a typical fixed-wing UAV modeled as a rigid body with

$$\text{Forces and moments } \kappa = [F_x, F_y, F_z, L, M, N] \quad (6.7)$$

6.2.1 Forces and Moments acting on a Fixed-wing UAV

The forces and moments defined by equations (6.3) and (6.4) can be expressed as the summation of their individual components. These individual components include but are not limited to; (a) Gravitational ($_g$), (b) Propulsion ($_{th}$), (c) Aerodynamic ($_a$) such that a typical force F_* comprises of:

$$F_* = F_{*g} + F_{*th} + F_{*a} \quad \{*\} \text{ represents } x, y, z \text{ directions.}$$

6.2.1.1 Gravitational F_{*g}

The gravitational force also called the weight of the UAV is applied to the centre of gravity of the UAV and is commonly represented in inertial frame as $F_{*g} = [0 \ 0 \ mg]^2$ but resolved in the body frame as

$$F_{*g} = \begin{bmatrix} -mg \sin \theta \\ mg \sin \phi \cos \theta \\ mg \cos \phi \cos \theta \end{bmatrix}$$

Since the UAV's centre of gravity defines the origin of the body axes, there are no moments due to gravity i.e. $L_g, M_g, N_g = 0$.

6.2.1.2 Propulsion F_{*th}, Mo_{*th}

The propulsive forces (also known as **thrust**) and moments are solely generated by the propulsion system or engines of the UAV and is generally considered fixed with respect to the body frame. The propulsive vectors (i.e. thrust vector (F_{*th}) and moment vector (Mo_{*th})) are essentially functions of the airspeed (V_a) and the thrust control command (i.e the throttle (d_τ))

$$F_{*th} = \begin{bmatrix} F_{xth}(V_a, d_\tau) \\ F_{yth}(V_a, d_\tau) \\ F_{zth}(V_a, d_\tau) \end{bmatrix} \quad Mo_{*th} = \begin{bmatrix} L_{th}(V_a, d_\tau) \\ M_{th}(V_a, d_\tau) \\ N_{th}(V_a, d_\tau) \end{bmatrix}$$

however, this depends on the type of propulsion system used and how the engines/ propulsion systems are attached to the aircraft. Most propeller driven propulsion systems in UAVs are commonly arranged such that the thrust vector passes through the centre of gravity of the UAV and the only moment formed is the torque generated by the rotating propeller however, there are many other propulsion system arrangements some of which are described in detail in [149].

6.2.1.3 Aerodynamic F_{*a}, Mo_{*a}

The aerodynamic forces and moments are consequences of the interaction between the surface of the UAV and airflow. They are usually described as functions of the variation in state variables and the deflections of the control surfaces (elevator, aileron, and rudder). Most control surfaces are configured such that

- the deflection of the ailerons d_a control the roll ϕ angle
- the deflection of the elevators d_e control the pitch θ angle
- the deflection of the rudders d_r control the yaw ψ angle

The deflections of the control surfaces act as control inputs that modify the airflow and the pressure distribution around the body of the UAV thus producing corresponding forces. These forces, acting with respect to the centre of gravity of the body, result in aerodynamic moments.

² g is the gravitational constant

Therefore, these aerodynamic forces and moments F_{*a}, Mo_{*a} can be considered to be functions of the control surface deflections d_e, d_a and d_r i.e $F_{*a}(d_e, d_a, d_r), Mo_{*a}(d_e, d_a, d_r)$.

For ease of understanding, the aerodynamic forces and moments F_{*a}, Mo_{*a} are usually analysed in slightly modified versions of the body frame reference called the **Stability** and **Wind**³ axes where the UAV's axis is defined along the projection of the total velocity vector of the moving air (wind) using the airspeed (V_a), angle of attack (AoA, α) and sideslip angle (β).

The aerodynamic forces are assumed to consist of the Lift force (F_{lift}), Drag force (F_{drag}) and Side Force (F_{side}) while the aerodynamic moments are classified as rolling L_A , pitching M_A and yawing N_A moments. They can be expressed in the form

Aerodynamic Forces	Aerodynamic Moments
$F_{lift} = \frac{1}{2}\rho V_a^2 S C_L$	$L_A = \frac{1}{2}\rho V_a^2 S b C_l$
$F_{drag} = \frac{1}{2}\rho V_a^2 S C_d$	$M_A = \frac{1}{2}\rho V_a^2 S c C_m$
$F_{side} = \frac{1}{2}\rho V_a^2 S C_S$	$N_A = \frac{1}{2}\rho V_a^2 S b C_m$

where $C_L, C_D, C_S, C_l, C_m, C_n$ are the nondimensional aerodynamic coefficients⁴ (to be parameterized) that depend on the airfoil, the AoA and the Reynolds number⁵. S is the wing surface area, ρ is the air density, b is the wing span and c is the mean aerodynamic chord. Using the parallel axis theorem [151], the elementary forces and moments from all surfaces can be resolved into body axes and transferred to the centre of gravity of the UAV. This allows for the resultant forces and moments to be easily projected onto the longitudinal and lateral planes of the UAV thus providing a natural ground for the decomposition of the nonlinear model of the UAV. The longitudinal forces and moments consist of F_{lift} , F_{drag} , and M_A acting in the vertical plane of symmetry while the lateral force and moments consist of F_{side} , L_A , and N_A caused by the asymmetric airflow⁶ around the UAV and control surfaces deflection. This natural decomposition into longitudinal and lateral planes is especially useful in the trimming, linearization and control system design.

6.2.1.4 Nonlinear Equations of Motion

In summary, according to this subsection (subsection 6.2.1), the equations of motion can be presented in the form:

$$\begin{bmatrix} F_x \\ F_y \\ F_z \\ L \\ M \\ N \end{bmatrix} \triangleq \begin{bmatrix} F_{xth} + F_{xa} \\ F_{yth} + F_{ya} \\ F_{zth} + F_{za} \\ L_{th} + L_a \\ M_{th} + M_a \\ N_{th} + N_a \end{bmatrix} = \begin{bmatrix} m(\dot{u} + rv - qw) - F_{xg} \\ m(\dot{v} + pw - ru) - F_{yg} \\ m(\dot{w} + qu - pv) - F_{zg} \\ \dot{p}J_x + qr(J_z - J_y) - (\dot{r} + pq)J_{xz} \\ \dot{q}J_y + pr(J_z - J_x) + (p^2 - r^2)J_{xz} \\ \dot{r}J_z + pq(J_y - J_x) + (qr + \dot{p})J_{xz} \end{bmatrix} = \begin{bmatrix} m(\dot{u} + rv - qw) + mg \sin \theta \\ m(\dot{v} + pw - ru) - mg \sin \phi \cos \theta \\ m(\dot{w} + qu - pv) - mg \cos \phi \cos \theta \\ \dot{p}J_x + qr(J_z - J_y) - (\dot{r} + pq)J_{xz} \\ \dot{q}J_y + pr(J_z - J_x) + (p^2 - r^2)J_{xz} \\ \dot{r}J_z + pq(J_y - J_x) + (qr + \dot{p})J_{xz} \end{bmatrix} \quad (6.8)$$

³see Appendix A for more details on the orientation of the body reference frame in the stability and wind reference frame

⁴Reader is referred to [146] for detailed discussion on the parametrization of these coefficients

⁵It is representative of the viscosity of air. See [150] for more details

⁶ The asymmetry can be caused by the side wind or deflection of the rudder

where $F_{xth}, F_{yth}, F_{zth}$ and F_{xa}, F_{ya}, F_{za} are the thrust vector forces and aerodynamic forces respectively while L_{th}, M_{th}, N_{th} and L_a, M_a, N_a are the propulsive moments and aerodynamic moments respectively.

6.2.2 Linearized Equations of Motion

Note that equations of motion (6.8) and kinematic equations (6.5) and (6.6) can be compactly represented as

$$\dot{s} = f(s, \mu) \quad (6.9)$$

where s is a 12 state vector consisting of $s' = [s_d, s_k]$ such that

$$\text{Linear and angular velocities } s_d = [u, v, w, p, q, r]$$

$$\text{Linear and angular positions } s_k = [x, y, z, \phi, \theta, \psi]$$

and μ is the control input vector consisting of elevator, aileron and rudder deflections, together with the throttle control setting $\mu' = [d_e, d_a, d_r, d_\tau]$. Knowledge of the state vector s at any initial time and the applied control inputs from that time forward, completely defines the UAV's motion, which is expressed as the time varying state vector $s(t)$.

The equations of motion specified in equation (6.8) and equivalently equation (6.9) are nonlinear and coupled, however, in order to facilitate the control system design and gain more insight into the stability status of the UAV, linear approximations of these equations are obtained. The small perturbation theory is an approach commonly used to linearize the equations of motion for a trimmed flight condition. A trimmed flight condition is a suitable local equilibrium where a UAV is in a stable non-accelerating flight. Assuming that deviations from this local equilibrium are small, a linearized model is expected to provide useful and fairly accurate representation of the entire nonlinear system.

6.2.2.1 Small perturbation theory & Trimmed flight

In the small perturbation theory, it is possible to express the forces and moments κ (see equation (6.7)), the control input μ and the state vector s as the sum of a nominal or equilibrium value and a perturbation (deviation from the nominal value) where $\kappa = \kappa_0 + \delta\kappa$ $s = s_0 + \delta s$ $\mu = \mu_0 + \delta\mu$. For example, the force F_x can be expressed as $F_x = F_{x0} + \delta F_x$. With this expression for equilibrium and perturbation values, a trimmed flight condition can be given for the system in equation (6.9) such that

$$\dot{s}_0 = f(s_0, \mu_0) = 0 \quad (6.10)$$

According to equation (6.10), the *ideal* equilibrium requires all the derivatives of the s_d and s_k state vectors to be zero however using this for the UAV motion, may not always result in a linear system that is a useful representation of the nonlinear system. For example, equating the derivative of the component x of the s_k state vector to zero implies that the UAV is on the

ground and at rest, also equating the derivative of the component y of the s_k state vector to zero implies that the UAV is flying along a vertical trajectory. Thus as earlier mentioned, suitable trimmed flight conditions are taken for the UAV in a stable non-accelerating flight i.e

$$\dot{s}_{d0} = 0 \quad (6.11)$$

for which individual components of \dot{s}_{k0} may or may not be equal to zero but must remain constant at whatever chosen value.

At this point, the following assumptions can be made;

Assumption 6.2.

1. The UAV's equilibrium point is assumed to be where the resultant of the applied forces and moments is zero (i.e. $\kappa_0 = 0$).
2. Since the perturbation values are small by definition, it is assumed that the products of the perturbed variables are negligible (i.e. assumed to be zero).

Using condition (6.11) and Assumption 6.2, the equations of motion given in equation (6.8), expressed in its equilibrium and perturbation values form can be given as

$$\begin{bmatrix} \delta F_x \\ \delta F_y \\ \delta F_z \\ \delta L \\ \delta M \\ \delta N \end{bmatrix} = \begin{bmatrix} m[\dot{\delta u} - r_0 \delta v - v_0 \delta r + q_0 \delta w + w_0 \delta q + g \sin(\theta_0 + \delta\theta)] \\ m[\dot{\delta v} - p_0 \delta w - w_0 \delta p + r_0 \delta u + u_0 \delta r + g(\sin(\phi_0 + \delta\phi) \cos(\theta_0 + \delta\theta))] \\ m[\dot{\delta w} - q_0 \delta u - u_0 \delta q + p_0 \delta v + v_0 \delta p + g(\cos(\phi_0 + \delta\phi) \cos(\theta_0 + \delta\theta))] \\ \dot{\delta p} J_x + (r_0 \delta q + q_0 \delta r)(J_z - J_y) - (\dot{\delta r} + p_0 \delta q + q_0 \delta p) J_{xz} \\ \dot{\delta q} J_y + (r_0 \delta p + p_0 \delta r)(J_z - J_x) + 2(p_0 \delta r + r_0 \delta p) J_{xz} \\ \dot{\delta r} J_z + (p_0 \delta q + q_0 \delta p)(J_y - J_x) + (r_0 \delta q + q_0 \delta r + \dot{\delta p}) J_{xz} \end{bmatrix} \quad (6.12)$$

Since the equations of motion are a function of not only the system states, but also the control input (equation (6.9)), different control input settings as well as different component choices of the \dot{s}_{k0} state vector can produce different trimmed flight conditions, some of which include trimmed climbing-turning, steady-state turn, straight flight and level symmetric flight. While the basic condition in equation (6.11) is necessary for all trimmed flight conditions, the linearization to be done in this chapter makes use of the commonly used **Straight and Level Symmetric** trimmed flight condition whose additional requirements on the state vector are given as

$$\phi_0 = v_0 = \dot{\phi}_0 = \dot{\theta}_0 = \dot{\psi}_0 = p_0 = q_0 = r_0 = 0 \quad (6.13)$$

Using the additional conditions in equation (6.13), equation (6.12) can be rewritten and simplified with the following approximations

$$\begin{aligned} \sin(\theta_0 + \delta\theta) &\triangleq \sin \theta_0 + \delta\theta \cos \theta_0, & \cos(\theta_0 + \delta\theta) &\triangleq \cos \theta_0 - \delta\theta \sin \theta_0 \\ \sin \delta\phi &\triangleq \delta\phi, & \sin \theta_0 &\triangleq 0, & \cos \delta\phi &\triangleq 1 \end{aligned}$$

such that

$$\begin{bmatrix} \delta F_x \\ \delta F_y \\ \delta F_z \\ \delta L \\ \delta M \\ \delta N \end{bmatrix} = \begin{bmatrix} m[\dot{\delta u} + w_0 \delta q + g \delta \theta \cos \theta_0] \\ m[\dot{\delta v} - w_0 \delta p + u_0 \delta r - g \delta \phi \cos \theta_0] \\ m[\dot{\delta w} - u_0 \delta q + g \delta \theta \sin \theta_0] \\ \dot{\delta p} J_x - \dot{\delta r} J_{xz} \\ \dot{\delta q} J_y \\ \dot{\delta r} J_z + \dot{\delta p} J_{xz} \end{bmatrix} \quad (6.14)$$

For the rest of this section, the perturbed variables $[\delta u, \delta v, \delta w, \delta p, \delta q, \delta r, \delta \theta, \delta \phi]$ and $[\delta F_x, \delta F_z, \delta M, \delta F_y, \delta L, \delta N]$ are replaced with $[u, v, w, p, q, r, \theta, \phi]$ and $[F_x, F_z, M, F_y, L, N]$, for clarity and conciseness, so that equation (6.14) becomes;

$$\begin{bmatrix} F_x \\ F_y \\ F_z \\ L \\ M \\ N \end{bmatrix} = \begin{bmatrix} m[\dot{u} + w_0 q + g \theta \cos \theta_0] \\ m[\dot{v} - w_0 p + u_0 r - g \phi \cos \theta_0] \\ m[\dot{w} - u_0 q + g \theta \sin \theta_0] \\ \dot{p} J_x - \dot{r} J_{xz} \\ \dot{q} J_y \\ \dot{r} J_z + \dot{p} J_{xz} \end{bmatrix} \quad (6.15)$$

From equation (6.15), it can be observed that F_x, F_z, M representing the longitudinal equations are completely decoupled from F_y, L, N representing the lateral equations. These linearized equations can also be rearranged such that;

$$\begin{bmatrix} \dot{u} \\ \dot{v} \\ \dot{w} \\ \dot{p} \\ \dot{q} \\ \dot{r} \end{bmatrix} = \begin{bmatrix} \frac{F_x}{m} + w_0 q + g \theta \cos \theta_0 \\ \frac{F_y}{m} - w_0 p + u_0 r - g \phi \cos \theta_0 \\ \frac{F_z}{m} - u_0 q + g \theta \sin \theta_0 \\ \frac{L J_z + N J_{xz}}{J_x J_z - J_{xz}^2} \\ \frac{M}{J_y} \\ \frac{N J_y + L J_{xz}}{J_x J_z - J_{xz}^2} \end{bmatrix} \quad (6.16)$$

6.2.2.2 Aerodynamic derivatives from Taylor series expansion

In general, the complete linearized equations of motion can be obtained from equation (6.9) for the defined trimmed flight condition ($\dot{s}_0 = f(s_0, \mu_0)$) when the equations are expressed through a first order Taylor series expansion such that

$$\dot{s} - \dot{s}_0 = \frac{\partial f}{\partial s}(s - s_0) + \frac{\partial f}{\partial \mu}(\mu - \mu_0) \quad (6.17)$$

This can be simplified to take the standard state space form

$$\dot{\tilde{s}} = A\tilde{s} + B\tilde{\mu} \quad (6.18)$$

where $\tilde{s} = \dot{s} - \dot{s}_0$, $\tilde{s} = s - s_0$, $\tilde{\mu} = \mu - \mu_0$, $A = \frac{\partial f}{\partial s}$ and $B = \frac{\partial f}{\partial \mu}$.

Specifically, continued development of the linear equations of motion from equation (6.15) involves considering the forces and moments as continuous functions of the variables in the state vector s and their derivatives \dot{s} as well as the control inputs μ such that

$$\kappa = f(\dot{s}, s, \mu). \quad (6.19)$$

These forces and moments are expressed in terms of the changes resulting from the perturbations at the trimmed condition through a first order Taylor series expansion given as

$$f(\dot{s}, s, \mu) = \left. \frac{\partial f}{\partial \dot{s}} \right|_{\substack{s=s_0 \\ \mu=\mu_0}} \delta \dot{s} + \left. \frac{\partial f}{\partial s} \right|_{\substack{s=s_0 \\ \mu=\mu_0}} \delta s + \left. \frac{\partial f}{\partial \mu} \right|_{\substack{s=s_0 \\ \mu=\mu_0}} \delta \mu$$

where $\delta \dot{s}, \delta s, \delta \mu$ are the perturbed variables of the state vector and the control input. As an example, consider the F_x member of the longitudinal equations as given in equation (6.15) and assuming we neglect the quadratic terms in the small perturbations,

$$F_x = m[\dot{u} + g\theta \cos \theta_0] \quad (6.20)$$

The following procedure describes the steps that can be taken to apply a first order Taylor series expansion to F_x and continue the linearization process.

1. If F_x is dependent on the state perturbed variables \dot{u}, w, q and the control input changes d_e, d_τ , It is possible to express F_x using the Taylor series,

$$F_x = \frac{\partial F_x}{\partial u} u + \frac{\partial F_x}{\partial \dot{u}} \dot{u} + \frac{\partial F_x}{\partial w} w + \frac{\partial F_x}{\partial \dot{w}} \dot{w} + \frac{\partial F_x}{\partial q} q + \frac{\partial F_x}{\partial \dot{q}} \dot{q} + \frac{\partial F_x}{\partial d_e} d_e + \frac{\partial F_x}{\partial \dot{d_e}} \dot{d_e} + \frac{\partial F_x}{\partial d_\tau} d_\tau + \frac{\partial F_x}{\partial \dot{d_\tau}} \dot{d_\tau} \quad (6.21)$$

2. The partial derivatives $\frac{\partial F_x}{\partial \dot{u}} \dot{u}, \frac{\partial F_x}{\partial \dot{w}} \dot{w}, \frac{\partial F_x}{\partial \dot{q}} \dot{q}, \frac{\partial F_x}{\partial \dot{d_e}} \dot{d_e}, \frac{\partial F_x}{\partial \dot{d_\tau}} \dot{d_\tau}$ are generally considered to be dimunitive and are thus negligible, hence equation (6.21) can be reduced to

$$F_x = \frac{\partial F_x}{\partial u} u + \frac{\partial F_x}{\partial w} w + \frac{\partial F_x}{\partial d_e} d_e + \frac{\partial F_x}{\partial d_\tau} d_\tau \quad (6.22)$$

3. Now substituting equation (6.22) in equation (6.20) results in

$$\frac{1}{m} \left[\frac{\partial F_x}{\partial u} u + \frac{\partial F_x}{\partial w} w + \frac{\partial F_x}{\partial d_e} d_e + \frac{\partial F_x}{\partial d_\tau} d_\tau \right] = \dot{u} + g\theta \cos \theta_0 \quad (6.23)$$

4. Replacing the significant partial derivatives $\frac{\partial F_x}{m \partial u}, \frac{\partial F_x}{m \partial w}, \frac{\partial F_x}{m \partial d_e}, \frac{\partial F_x}{m \partial d_\tau}$ (also known as the aerodynamic derivatives) with $F_{xu}, F_{xw}, F_{xd_e}, F_{xd_\tau}$ and slightly rearranging equation (6.23) results in

$$\dot{u} = F_{xu} u + F_{xw} w + g\theta \cos \theta_0 + F_{xd_e} d_e + F_{xd_\tau} d_\tau$$

5. Assuming that the equilibrium $\theta_0 = 0$ then the above equation can be simplified to become

$$\dot{u} = F_{xu}u + F_{xw}w + g\theta + F_{xd_e}d_e + F_{xd_\tau}d_\tau \quad (6.24)$$

This procedure can be repeated for the other force and moment members of equation (6.15). Detailed developments of these can be found in [146, 152]. When the Taylor expansions of each of these forces and torques are substituted into equation (6.15), the decoupled linear equations can be expressed in terms of the aerodynamic (stability and control) derivatives. Thus the linearized equations of motion in state space form are given as;

$$\begin{bmatrix} \dot{u} \\ \dot{w} \\ \dot{q} \\ \dot{\theta} \end{bmatrix} = \begin{bmatrix} F_{xu} & F_{xw} & 0 & g \\ F_{zu} & F_{zw} & F_{zq} & 0 \\ M_u & M_w & M_q & 0 \\ 0 & 0 & 1 & 0 \end{bmatrix} \begin{bmatrix} u \\ w \\ q \\ \theta \end{bmatrix} + \begin{bmatrix} F_{xd_e} & F_{xd_\tau} \\ F_{zd_e} & F_{zd_\tau} \\ M_{d_e} & M_{d_\tau} \\ 0 & 0 \end{bmatrix} \begin{bmatrix} d_e \\ d_\tau \end{bmatrix} \quad \text{Longitudinal} \quad (6.25)$$

$$\begin{bmatrix} \dot{v} \\ \dot{p} \\ \dot{r} \\ \dot{\phi} \end{bmatrix} = \begin{bmatrix} F_{yv} & 0 & F_{yr} & g \\ L_v & L_p & L_r & 0 \\ N_v & N_p & N_r & 0 \\ 0 & 1 & 0 & 0 \end{bmatrix} \begin{bmatrix} v \\ p \\ r \\ \phi \end{bmatrix} + \begin{bmatrix} F_{yd_a} & F_{yd_r} \\ L_{d_a} & L_{d_r} \\ N_{d_a} & N_{d_r} \\ 0 & 0 \end{bmatrix} \begin{bmatrix} d_a \\ d_r \end{bmatrix} \quad \text{Lateral} \quad (6.26)$$

where d_a, d_e, d_r, d_τ are the control input changes for the aileron, elevator, rudder and throttle. The variables represented as $*_u, *_v, *_w, *_p, *_q, *_r$ are the stability derivatives and $*_{d_e}, *_{d_\tau}, *_{d_a}, *_{d_r}$ are the control derivatives.

Remark 6.1: It is important to note that when dealing with modern UAVs in a practical situation, it may be much more relevant to use the AoA α instead of w in the longitudinal plane and the sideslip angle β instead of v in the lateral plane based on the relationship;

$$\dot{\alpha} = \frac{\dot{w}}{V_a} \quad \dot{\beta} = \frac{\dot{v}}{V_a}$$

where V_a is the airspeed. This is because in recent times, most UAV critical performance parameters are based on the AoA & β values and many modern avionics instruments are AoA based instruments.

6.2.3 The Aerosonde UAV

The Aerosonde UAV, shown in Figure 6.1 [3], is a small UAV developed for weather-reconnaissance and remote-sensing mission. Its basic structure is common to many UAVs but it has an inverted V-tail system. With this unconventional shape, its control surfaces comprise of right and left ailerons, right and left flaps and the right and left inverted V tail control surfaces referred to as ruddervators because they combine the tasks of the elevators and rudders such that the same directional deflection of the control surfaces generates an elevator response and opposing deflection of the control surfaces generates a rudder response. In this study, the ruddervator control



FIGURE 6.1: The Aerosonde™ UAV [3]

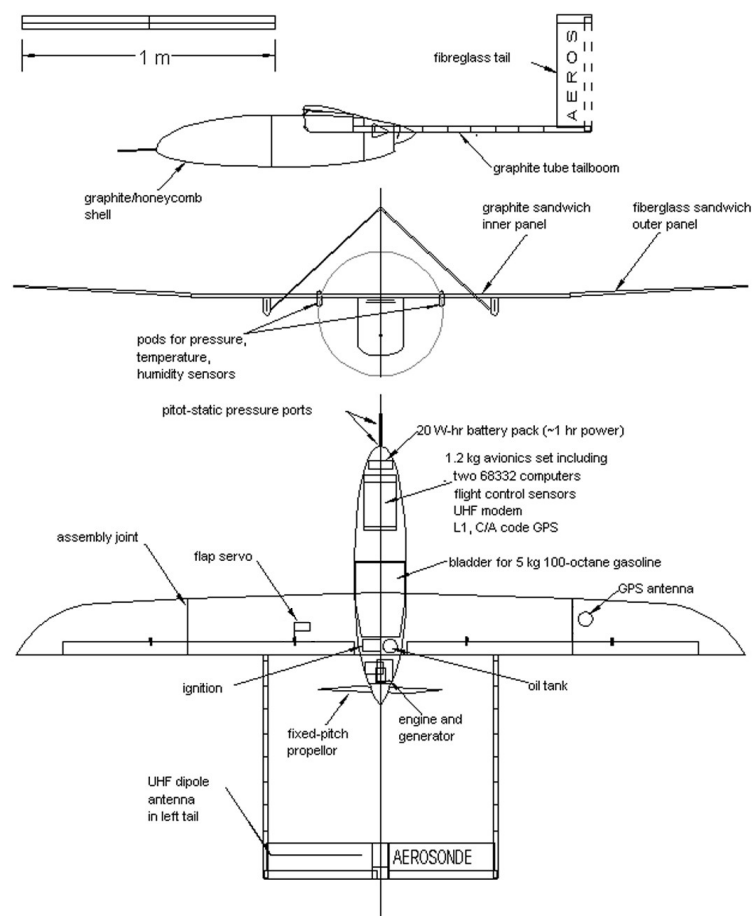


FIGURE 6.2: Aerosonde UAV Layout [3]

surfaces are considered as rudders and elevators (i.e separate control surfaces); however in reality, they actuate the same physical control surface. This is so chosen so that the saturation limits (needed for tasks in the next chapter) on the control surfaces can be easily and clearly represented. This chapter makes use of a sample model of the Aerosonde UAV developed by

Unmanned Dynamics LLC ⁷ whose parameter configurations, aerodynamic derivatives and general specifications can be found in [153, 154]. A summary of the UAV's specifications are listed in Table 6.1 [3].

The physical UAV's flight envelope is such that $-45^\circ \leq \phi \leq 45^\circ$, $-15^\circ \leq \theta \leq 15^\circ$, $15ms^{-1} \leq Va \approx u \leq 50ms^{-1}$ and $0m \leq h \approx -z \leq 3000m$ [155]. A linearized model of the UAV is obtained at a representative trim condition for straight wings level flight with altitude h at $1000m$ and velocity Va at $25m/s$. At this trim condition⁸, the linearized model operates at the equilibrium point listed in Table 6.2

The dynamic stability properties of the open loop dynamics were analysed for the longitudinal and lateral modes to ensure that it satisfies the MIL-F-8785C flying qualities requirements [156] and these are shown in Table 6.3. Note that the Aerosonde UAV is a Class "1" UAV assumed to observe flight phase categories "A", "B" and "C" (See MIL-F-8785C Handbook [156] for details on the flight phase categories). The longitudinal dynamics can be broken down into two dynamic modes: the phugoid (PH) mode and the short-period pitch oscillation (SPPO) mode. The phugoid mode dominates the response in states u and θ and the short-period mode dominates the response in states w and q . The eigenvalues of the longitudinal modes for the Aerosonde UAV model are complex and have negative real parts meaning that it is dynamically stable thus if there is an initial disturbance, the response will decay sinusoidally with time. However it can be observed that the damping of the short period mode is too low compared to the requirements stated in Table 6.3 while the phugoid mode properties are within the range requirements. The lateral dynamics are overseen by the spiral mode, the Dutch roll mode and the roll subsidence mode. The lateral modes characteristics all fall within the specified requirements (including time constants) except from Table 6.3, it shows that the spiral motion contained a positive real eigenvalue indicating an unstable divergent spiral whereas the dutch roll and roll subsidence are stable. This unstable divergent spiral may be caused in part due to the unusual V-tail configuration of the tail plane. In piloted aircrafts, managing its effect will depend on how quickly the spiral mode will diverge⁹; this is described by the Time to Double Amplitude (TTD) equation (6.27). If the TTD is too small, it will require that a pilot will have to dedicate time and effort to continuously maintain heading and level flight.

$$TTD = \frac{\ln 2}{Freq_{spiral}} = 2\pi \times \frac{\ln 2}{0.0764rad/s} = 57.003s \quad (6.27)$$

⁷Note that the specific version used is that amended by James F Whidborne to work with MATLAB/Simulink Aerospace block library

⁸Note also that the flaps are level (ie not used in simulation)

⁹or more practically how quickly the roll angle will double in amplitude

TABLE 6.1: Aerosonde UAV specifications

Mass (Gross)	13.5 kg
Wing Span	2.90 m
Endurance	10 hrs
Speed	150 km/hr
Inertia (J_x, J_y, J_z)	0.824,1.76,0.120 kgm ²
Payload capacity	up to 2 kg

TABLE 6.2: Aerosonde equilibrium point

State x_0		Output y_0		Input u_0	
u	24.92m/s	x	0m	d_τ	0.512
v	0.0125m/s	y	0m	d_a	-0.0080rad
w	1.389m/s	z	-1000m	d_e	-0.0468rad
ϕ	0rad	V_a	25m/s	d_r	-0.0007rad
θ	0.0497rad	α	0.0497rad		
ψ	0.0002rad	β	0.00011rad		
p	0rad/s	ϕ	0rad		
q	0rad/s	θ	0.0497rad		
r	0rad/s	ψ	0.0002rad		
x	0m	p	0rad/s		
y	0m	q	0rad/s		
z	-1000m	r	0rad/s		

In the case of the Aerosonde, the TTD value meets the requirements in all flight phases including

TABLE 6.3: Stability properties of open loop dynamics

Longitudinal Modes	Eigen-values	Damping	Frequency (rad/s)	Requirements
Phugoid	-0.015 $\pm 0.071i$	0.212	0.0733	All* $damp \geq 0.04$
SPPO	-4.28 $\pm 0.531i$	0.255	16.8	Cat. A&C: $0.35 \geq damp \geq 1.3$ Cat. B: $0.3 \geq damp \geq 2$
Lateral Modes	Eigen-values	Damping, Time constant (τ_c)	Frequency (rad/s)	Requirements
Dutch roll	-7.93 $\pm 5.30i$	0.198, 1.26	5.36	Cat. A: $damp > 0.19$ Cat. B&C: $damp > 0.08$
Roll subsidence	-14.7	1, 0.0679	14.7	Cat. A&C: $\tau_c < 1$ Cat. B: $\tau_c < 1.4$
Spiral	0.0764	-1, 13.1	0.0764	Cat. A&C: $TTD > 12s$ Cat. B: $TTD > 20s$

All* refers to All flight phase Categories A,B & C

Cat. refers to the specific flight phase Category/Categories

the takeoff and landing (T&L) (i.e, flight phase Category "C") and will require little pilot monitoring and control. In summary, some form of stability augmentation is required to improve the short period damping and general stability of the open loop model.

6.3 Controller Design

Before the closed loop controller can be designed, the model's stability is improved using the stability augmentation system (SAS) shown in Figure 6.3 in order to compensate for the inadequacies of the longitudinal and lateral modes mentioned earlier. The SAS consists of;

1. **Pitch damper:** The objective of the pitch damper is to compensate for the short period low damping. It contains q and θ (or AoA) proportional feedback gains (K_{q-e} and $K_{\theta-e}$)

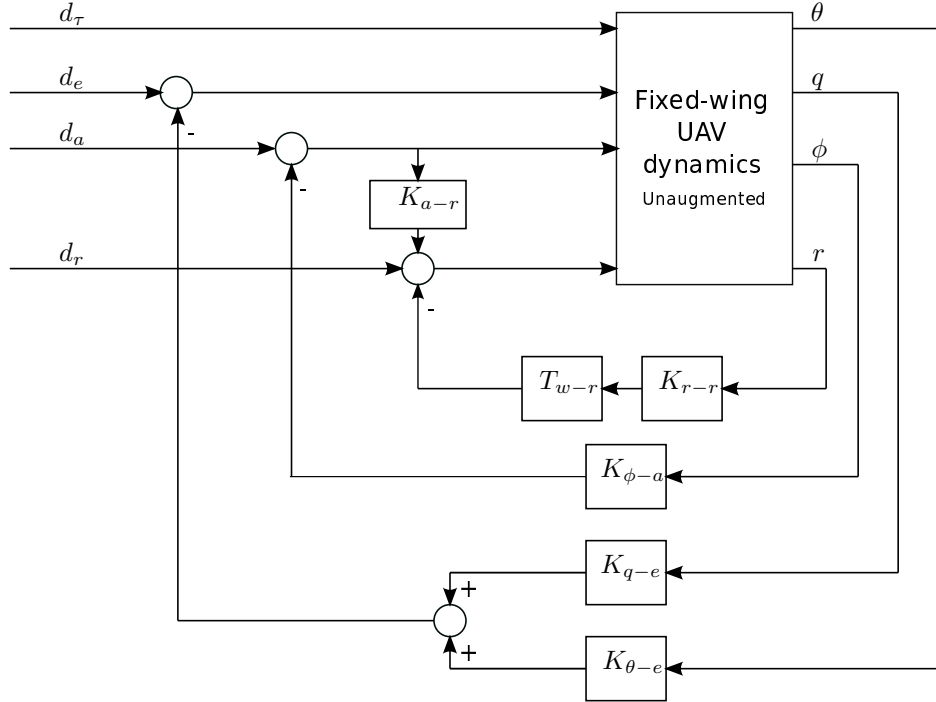


FIGURE 6.3: Stability Augmentation System

2. **Yaw damper:** This is setup in a similar way to the pitch damper except in this case the yaw rate gain (K_{r-r}) is chosen to further improve the dutch roll damping ratio and an aileron-rudder gain (K_{a-r}) is chosen to improve the roll-yaw coordination (i.e prevent sideslip) in a turn. A washout filter (Time constant T_{w-r}) is also included to prevent the yaw rate feedback loop from opposing the roll in a horizontal steady turn.
3. **Spiral mode stabilizer:** This consist of a ϕ feedback gain ($K_{\phi-a}$) used to compensate the destabilizing effect of the washout filter on the spiral mode.

The SAS described above has been used for a variety of fixed wing UAVs [157, 158] and the values of the SAS gains and constants found to give improved and suitable responses are shown in Table 6.4. According to Figure 6.3, it is important to note that $[d_\tau, d_a, d_e, d_r]$ represents the control surface inputs before the SAS is applied while $[d_{\tau*}, d_{a*}, d_{e*}, d_{r*}]$ are the control inputs after the SAS is applied. $d_{\tau*}, d_{a*}, d_{e*}$ and d_{r*} will become important in the next chapter when considering rate saturation limits because they are the actual control inputs to which the rate saturation limits are applied. However for the remainder of this chapter, d_τ, d_a, d_e and d_r will be used in the controller design process as the control inputs.

TABLE 6.4: SAS gains and constants

K_{q-e}	-0.29	K_{r-r}	-0.25
$K_{\theta-e}$	-0.9	K_{a-r}	0.6
$K_{\phi-a}$	-0.22	T_{w-r}	1

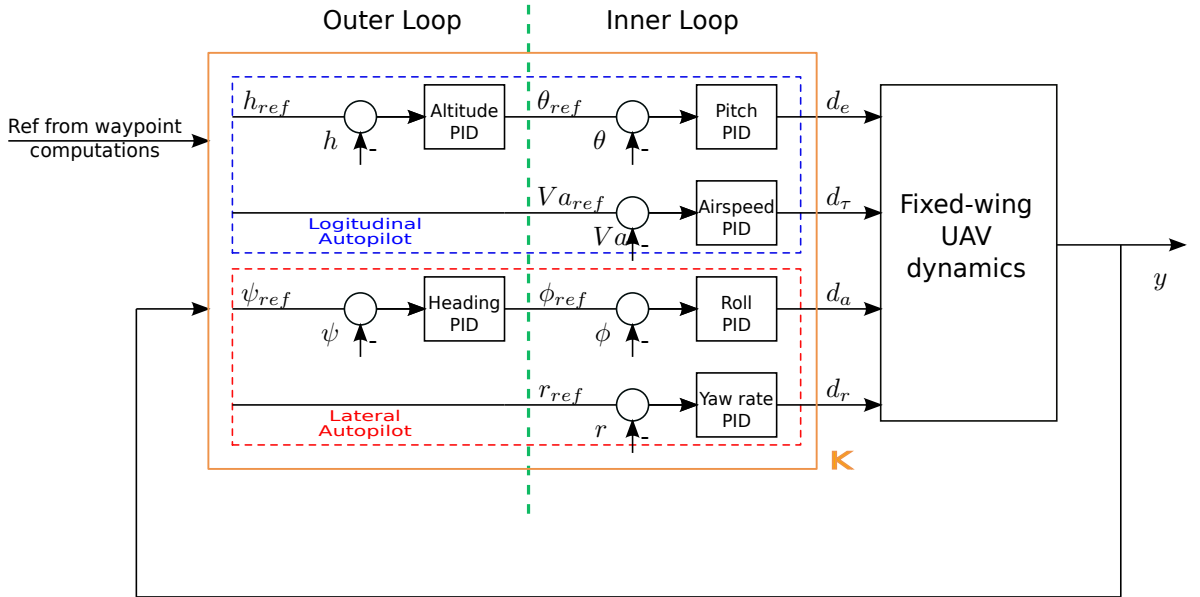


FIGURE 6.4: Full Controller Architecture

Autonomous flight for this UAV is achieved using an approach that involves a low level inner loop control system that keeps the UAV flying through attitude control enclosed within a high level outer loop control system on altitude and heading control for trajectory tracking as shown in Figure 6.4. However the controller design presented in this section is restricted to the inner loop control system.

The main control objective is to achieve basic attitude control in the inner loop using the architecture shown in Figure 6.5. The attractive decoupling along the longitudinal and lateral planes in the augmented linear model is taken advantage of, to design the attitude controller such that the pitch, roll, yaw and airspeed controllers can be designed independently with each control loop employing simple PID controllers. This controller scheme can be considered to be adequate for the nonlinear UAV model, since it is assumed that the UAV makes small angular deflections with limited set of maneuvers and the angular rates are kept as small as possible so that the error arising from coupling effects in roll-yaw is very much minimized.

6.3.1 Longitudinal Control K_{long}

In the longitudinal axis, the pitch θ is controlled by the elevator response d_e of the ruddervators. The pitch error is generated from the difference between the commanded pitch angle, θ_{ref} and the plant output being the actual pitch angle θ . This is fed to the Pitch PID block which is used to drive the pitch error to zero. From Figure 6.4, the commanded pitch angle is generated from the altitude error in the outer loop and is ideal for controlling the UAV's altitude when the altitude error is small.

Similarly, the airspeed Va is controlled by the throttle and the airspeed error is generated from the difference between the commanded Va_{ref} and the sensor measured Va . This error is fed

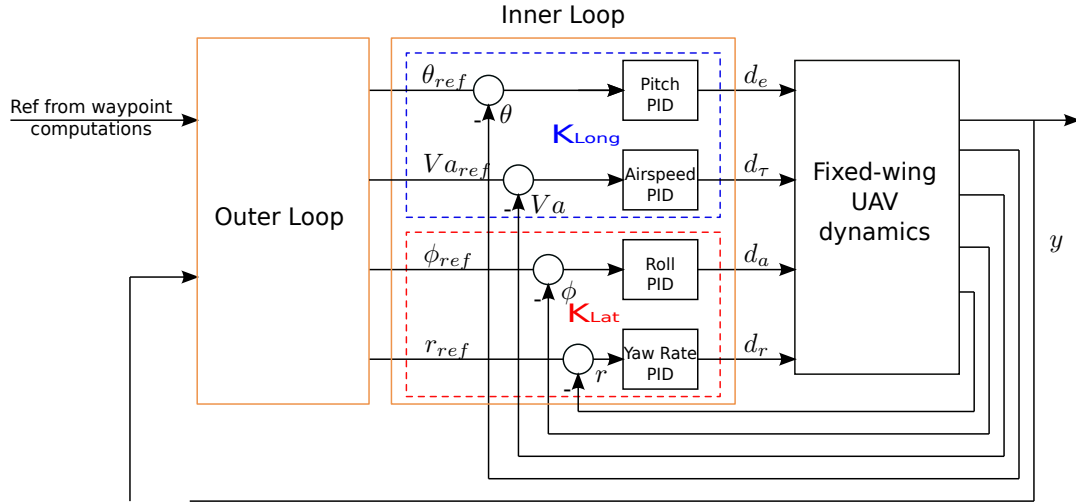


FIGURE 6.5: Inner Loop representation of controller architecture

into the Airspeed PID block which is used to produce the desired control command d_τ for the throttle.

The following control law is used for the longitudinal control.

$$\frac{d_e(s)}{[\theta_{ref} - \theta](s)} = K_{\theta,P} + \frac{K_{\theta,I}}{s} + sK_{\theta,D} \quad (6.28)$$

$$\frac{d_\tau(s)}{[Va_{ref} - Va](s)} = K_{Va,P} + \frac{K_{Va,I}}{s} + sK_{Va,D} \quad (6.29)$$

6.3.2 Lateral Control K_{lat}

On the lateral axis, the roll ϕ is controlled by the aileron d_a . The roll error is generated from the difference between the commanded roll angle, ϕ_{ref} and the actual roll angle ϕ . This is fed to the Roll PID block which is used to drive the roll error to zero. From Figure 6.4, the commanded roll angle is generated from the heading error in the outer loop.

Similarly, the yaw rate r is controlled by the rudder response of the ruddervators via the yaw rate error ($r_{ref} - r$) which is fed into the Yaw rate PID block that is used to produce the desired control command d_r .

The following control law is used for the lateral control.

$$\frac{d_a(s)}{[\phi_{ref} - \phi](s)} = K_{\phi,P} + \frac{K_{\phi,I}}{s} + sK_{\phi,D} \quad (6.30)$$

$$\frac{d_r(s)}{[r_{ref} - r](s)} = K_{\psi,P} + \frac{K_{\psi,I}}{s} + sK_{\psi,D} \quad (6.31)$$

where

- $K_{\phi,P}, K_{\theta,P}, K_{\psi,P}, K_{Va,P}$ are the proportional gains,
- $K_{\phi,I}, K_{\theta,I}, K_{\psi,I}, K_{Va,I}$ are the integral gains,

TABLE 6.5: Approximate values of Aerosonde controller PID Gains

$K_{\phi,P}$	0.4	$K_{\phi,I}$	0.2	$K_{\phi,D}$	0.004
$K_{\theta,P}$	1	$K_{\theta,I}$	0.09	$K_{\theta,D}$	0.04

- $K_{\phi,D}, K_{\theta,D}, K_{\psi,D}, K_{Va,D}$ are the derivative gains,
- d_a, d_e, d_r, d_τ are the control inputs,
- $\phi_{ref}, \theta_{ref}, r_{ref}, Va_{ref}$ are the desired reference and
- ϕ, θ, r, Va are the system outputs.

Remark 6.2: While it is acknowledged that there are many other controller types that can be used and may perhaps perform better than the adopted control scheme, the chosen controller design approach is preferred because it is commonly used in practical UAV control systems and simple to implement. Also the performance of the controller decreases for flight conditions far from the design trim point, however appropriate gain scheduling can be used to maintain desired performance across the whole flight envelope. A summary of the feedback gains for pitch and roll controllers are shown in Table 6.5 and Figure 6.6 shows responses of the nonlinear model when a step reference signal of 0.4 rad was commanded on the pitch and roll during nominal operation while a pulse response of 0.01 rad/s was commanded on the yaw rate to give an approximate 0.55 rad of yaw.

6.4 Summary

This chapter described the general nonlinear fixed wing UAV dynamics along with its kinematics and the flight controller design structure used for the chosen UAV platform - The **Aerosonde** UAV. An outline of the trimming and linearization of the UAV model is also presented showing the natural decoupling along the longitudinal and lateral degrees of freedom of the UAV.

An analysis of the longitudinal and lateral dynamic modes of the open loop Aerosonde UAV was performed and some unstable modes were observed. These open loop instabilities were corrected using a stability augmentation system (SAS) consisting of a pitch damper, a yaw damper and a spiral mode stabilizer. The augmented UAV model was then used to construct the autopilot controller focusing on the attitude controller of the inner loop. The controller was designed using PID controllers to adequately control the pitch, roll, yaw and airspeed of the UAV. The chapter was concluded by simulating the closed loop performance of the controller and the UAV by applying desired pitch and roll step inputs.

In the next chapter, the design of AW compensators that can be perceived as decoupled are presented and applied to the fixed wing UAV plant and controller structure described in this chapter.

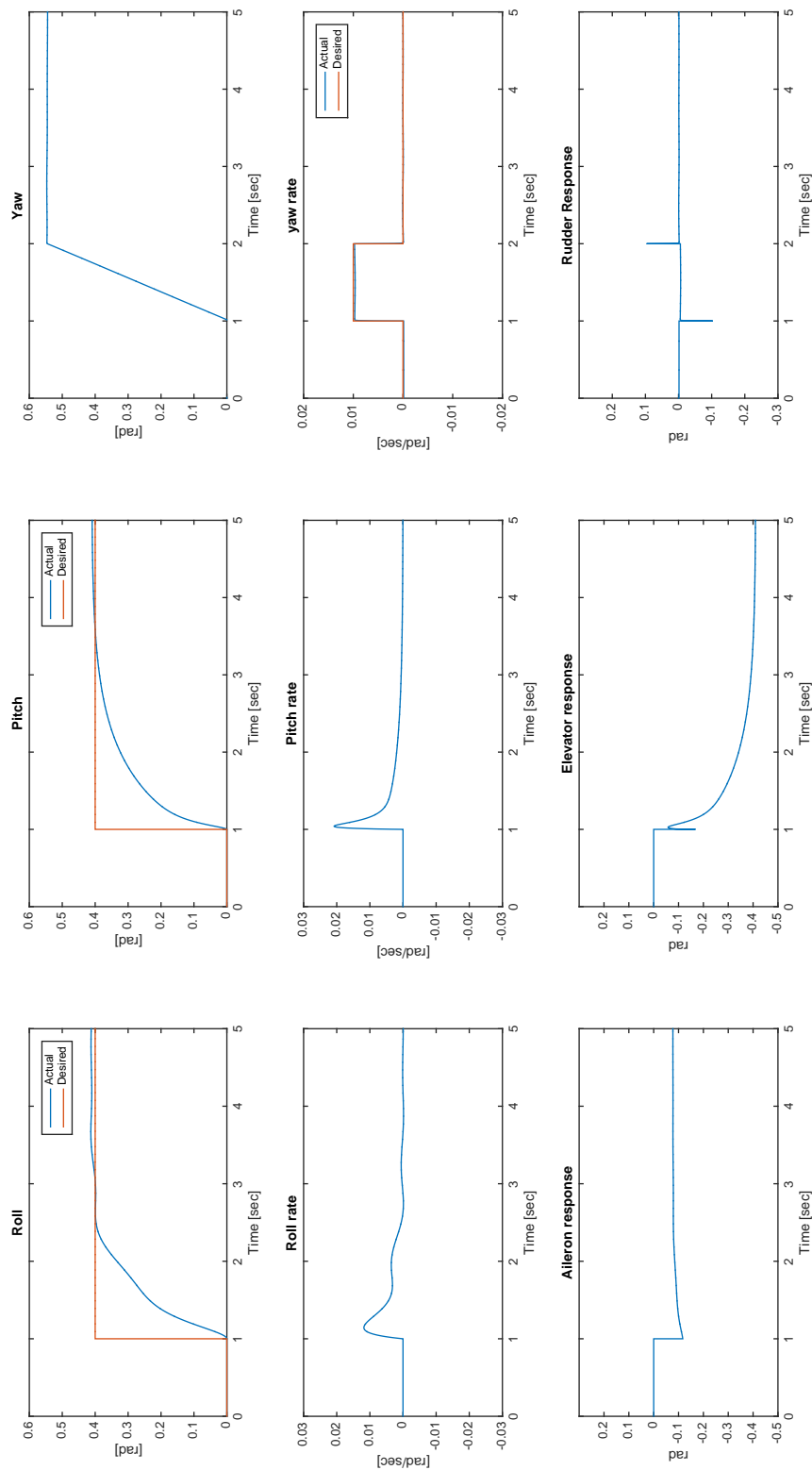


FIGURE 6.6: Nominal closed-loop simulation results

7 Decoupled AW design with application to fixed-wing UAV

7.1 Introduction

In Part 1 of this thesis, the focus was on magnitude saturation since saturation of the electric motor speed caused detrimental effects on quadrotor UAVs in some circumstances. However, in fixed wing UAVs which are actuated by aerodynamic control surfaces, the typical and more precarious saturation phenomena experienced is that of rate saturation, i.e the rate at which the actuator motion is limited. The presence of the rate saturation is well known to lead to poor performance in many fixed wing aircrafts both manned and unmanned [159–162].

A common method for dealing with the problem of actuator rate saturation in fixed wing UAVs is the use of hardware and/or software rate limiters which work by ensuring that no rate commands beyond the actuator’s capabilities are sent to the actuators, however, this may limit the performance of the UAV during periods of nominal operation (i.e, when there is no saturation) [9, 22]. In recent times, research into the application of modern AW schemes to solve this problem in piloted aircrafts can be found [7, 19, 22, 30, 163], but very few attempts have been made to apply modern AW schemes to solve the problem of rate saturation in fixed wing UAVs [29, 164].

By exploiting the structure of the fixed wing UAV’s system dynamics, this chapter proposes the design of AW compensators that can be perceived as decoupled to tackle the problem of actuator rate saturation. The AW compensator design technique used in this chapter follows the principles and structure presented by [23]. This chapter describes result obtained from nonlinear simulations with various AW compensators engaged. In particular, results from MIMO and decoupled AW compensators are described and compared.

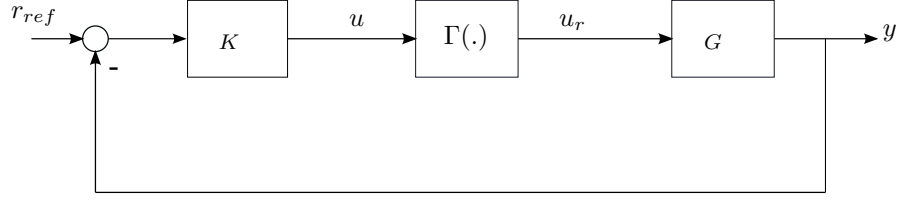


FIGURE 7.1: Rate saturated system

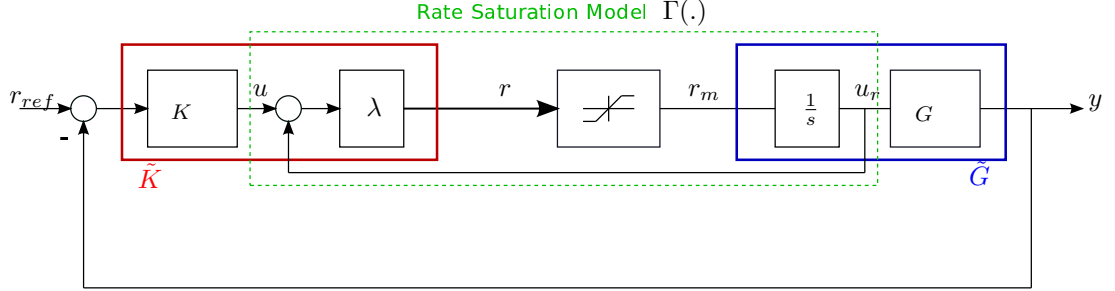


FIGURE 7.2: Rate saturated system fitted with rate saturation model

7.2 Decoupled Anti-windup design for the fixed-wing UAV structure

7.2.1 Typical AW design structure with rate saturation

Consider Figure 7.1 which shows the interconnection of a typical MIMO plant $G(s)$ and MIMO controller $K(s)$ where $r_{ref} \in \mathbb{R}^{n_r}$ is the reference, $y \in \mathbb{R}^p$ is the plant output and the operator $\Gamma(\cdot) : \mathbb{R}^m \mapsto \mathbb{R}^m$ represents the rate saturation problem mapping the desired control input $u \in \mathbb{R}^m$ to the plant input (rate saturated input) $u_r \in \mathbb{R}^m$. The closed loop system in Figure 7.2 is fitted with the rate saturation model proposed in Section 2.2 as depicted in Figure 2.2. The dynamics of the rate saturation model have been partitioned in such a way that the magnitude saturation defined by $r_m = sat(r)$ is separated from the additional dynamics consisting of the integrator and the gain λ . The additional dynamics are absorbed into the nominal UAV plant and controller such that the integrator is merged with the nominal plant to form an extended model of the plant $\tilde{G}(s)$ and the gain λ is also merged with the linear controller to form an extended model of the controller $\tilde{K}(s)$. If the state-space realisation of the plant $G(s)$ is given as

$$G(s) \sim \left[\begin{array}{c|c} A_p & B_p \\ \hline C_p & D_p \end{array} \right]$$

then the state space realization of the extended plant model \tilde{G} becomes

$$\tilde{G}(s) = \left[\begin{array}{c} G(s) \frac{1}{s} \\ I \frac{1}{s} \end{array} \right] \sim \left[\begin{array}{cc|c} A_p & B_p & 0 \\ 0 & 0 & I \\ \hline C_p & D_p & 0 \\ 0 & I & 0 \end{array} \right] = \left[\begin{array}{c|c} \tilde{A}_p & \tilde{B}_p \\ \hline \tilde{C}_p & 0 \end{array} \right] \quad \text{where } \tilde{D}_p \triangleq 0 \quad (7.1)$$

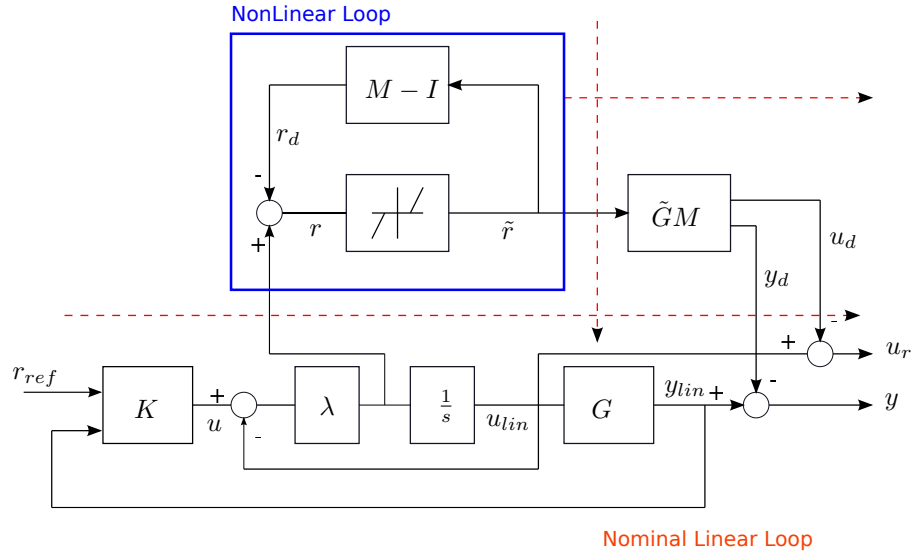


FIGURE 7.4: Equivalent representation of AW system in Figure 7.3

form;

$$\Theta(s) = \begin{bmatrix} M(s) - I \\ \tilde{G}(s)M(s) \end{bmatrix} \sim \begin{bmatrix} \tilde{A}_p + \tilde{B}_p F & \tilde{B}_p \\ F & 0 \\ \tilde{C}_p & 0 \end{bmatrix} \quad (7.4)$$

where F is a free parameter to be chosen such that $\tilde{A}_p + \tilde{B}_p F$ is Hurwitz.

Ordinarily, F can be obtained once a solution to the LMI (4.19) in Theorem 4.5 [58] exists, provided that it is under the logical assumption that during normal operation (i.e no saturation), the controller $\tilde{K}(s)$ has been designed to stabilise the plant $\tilde{G}(s)$ and $\tilde{G}(s)$ is asymptotically stable (i.e $\tilde{G}(s) \in \mathcal{RH}_\infty$). However it is important to note that the properties of $\tilde{G}(s)$ now pose a new problem. Due to the presence of the integrator in $\tilde{G}(s)$, the system now has a pole located at zero, thus even if the poles of the original plant $G(s)$ have negative real parts i.e $G(s) \in \mathcal{RH}_\infty$, $\tilde{G}(s) \notin \mathcal{RH}_\infty$ but is inevitably neutrally stable.

The implication is that achieving global asymptotic stability and global finite \mathcal{L}_2 gain minimization for the entire system with AW compensation is infeasible, therefore attention is focused on finding local solutions instead. Having said this, if the linear loop consisting of $\tilde{K}(s)$ and $\tilde{G}(s)$ (ie linear $G(s)$ and $K(s)$ with its rate saturation dynamics) is internally stable and well-posed, then the AW problem can be reduced to that of finding a transfer function $M(s) \in \mathcal{RH}_\infty$ such that the nonlinear loop in Figure 7.4 is zero-input locally asymptotically stable if $G(s) \in \mathcal{RH}_\infty$ and the mapping $\mathcal{T}_p : r_{lin} \mapsto \tilde{y}_d$ is minimized such that $\|\mathcal{T}_p\|_{\mathcal{L}_2} < \gamma$ for some $\gamma > 0$ where $\tilde{y}_d = [y'_d, u'_d]$.

The solution involving the alternative LMI (4.21) in Remark 4.2 and [165] shows the synthesis of a locally performing AW compensator addressing the AW problem described above where an additional parameter ϵ which defines the size of the sector of operation (i.e where our results are valid) is used to restrict the region for which asymptotic stability is guaranteed and performance degradation is minimized (a small \mathcal{L}_2 gain is obtainable). This implies that the standard deadzone $Dz(r) = r - sat(r)$ no longer occupies the full Sector $[0, I]$, but is restricted to some narrower

sector, $\text{Sector}[0, \epsilon I]$ where $0 < \epsilon < 1$. Note that as ϵ approaches one, stability and performance consideration draws closer towards global results.

7.2.2 Decoupled UAV plant-controller representation

The full MIMO AW compensator AW compensator synthesized using the structure described above and the LMI (4.21) is sufficient to tackle the rate saturation problem in a fixed wing UAV, However, this section tries to simplify the AW tuning and operation by attempting to decentralize the AW compensator design for the Aerosonde fixed wing UAV ¹, using the decoupled dynamics of the UAV described in the previous chapter.

Given that the plant $G(s)$ represents the nominal fixed wing UAV dynamics with state space realization

$$G(s) \sim \left[\begin{array}{c|c} A & B \\ \hline C & D \end{array} \right]$$

and the controller $K(s)$ represents the nominal linear flight controller with SAS, it is assumed that they have the structures

$$G(s) = \text{diag}(G_{lon}(s), G_{lat}(s)) \quad (7.5)$$

$$K(s) = \text{diag}(K_{lon}(s), K_{lat}(s)) \quad (7.6)$$

where $G_{lon}(s), G_{lat}(s)$ are the decoupled longitudinal and lateral dynamics of the linear fixed wing UAV. Both components of the decoupled plant dynamics are still MIMO systems but this simplifies the controller design process allowing decoupled linear controllers $K_{lon}(s), K_{lat}(s)$ to be designed separately for $G_{lon}(s)$ and $G_{lat}(s)$ respectively. According to the system in Figure 7.2, parts of the rate saturation dynamics are merged with the UAV plant $G(s)$ and controller $K(s)$ as discussed in the previous section such that an extended model of the plant and controller emerges ($\tilde{G}(s)$ is the extended plant and $\tilde{K}(s)$ is the extended controller). It is important to note that the unconstrained closed loop system behaves as a truly decoupled system such that each element of $K(s)$ controls its corresponding element in $G(s)$. According to the rate saturation model used (see Section 2.2), the rate saturation $\Gamma(u)$ and consequently the resulting magnitude saturation $\text{sat}(r)$ are considered to be decentralized. The rate saturated system also tends to preserve this attractive decoupling of the longitudinal and lateral dynamics during periods of saturation, such that each component of $\tilde{K}(s)$ controls its corresponding component in $\tilde{G}(s)$ where

$$\tilde{G}(s) = \text{diag}(\tilde{G}_{lon}(s), \tilde{G}_{lat}(s)) \quad (7.7)$$

$$\tilde{K}(s) = \text{diag}(\tilde{K}_{lon}(s), \tilde{K}_{lat}(s)) \quad (7.8)$$

An alternative to the generic MIMO AW compensator is proposed for the system in Figure 7.3 such that the new AW compensator structure contains two AW compensators allowing the

¹Recall that the Aerosonde UAV control inputs for the elevator d_{e*} and rudder d_{r*} actuate the same physical control surfaces (the ruddervator control surfaces). However, for the work done in this chapter, it is assumed that the control inputs for the elevator d_{e*} and rudder d_{r*} actuate separate control surfaces.

MIMO AW compensator is broken into $\Theta(s) = \text{diag}[\Theta_{lon}(s)\Theta_{lat}(s)]$. The following assumptions are made before this approach is presented.

- Assumption 7.1.*
1. The extended plant and controller have the structures (7.7)-(7.8)
 2. The unconstrained closed-loop interconnection of the extended plant $\tilde{G}(s)$ and extended controller $\tilde{K}(s)$ (including the rate saturation dynamics) is well-posed and internally stable
 3. $G(s) \in \mathcal{RH}_\infty$ (7.5) (and by extension $G_{lon}(s), G_{lat}(s)$ is stable)

Now if each component of $\tilde{G}(s)$ has the right co-prime factorization of

$$\begin{aligned}\tilde{G}_{long}(s) &= M_{lon}(s)^{-1}N_{long}(s) \\ \tilde{K}_{lat}(s) &= M_{lat}(s)^{-1}N_{lat}(s)\end{aligned}$$

where $M_{lon}(s) \in \mathcal{RH}_\infty$ and $M_{lat}(s) \in \mathcal{RH}_\infty$, the AW compensator structure can be chosen to have the form

$$\Theta(s) = \begin{bmatrix} M(s) - I \\ \tilde{G}(s)M(s) \end{bmatrix}, \quad (7.9)$$

such that for $M(s) = \text{diag}(M_{lon}(s), M_{lat}(s))$ and $\tilde{G}(s) = \text{diag}(\tilde{G}_{lon}(s), \tilde{G}_{lat}(s))$,

$$\Theta_{lon}(s) = \begin{bmatrix} M_{lon}(s) - I \\ \tilde{G}_{lon}(s)M_{lon}(s) \end{bmatrix} \quad \text{and} \quad \Theta_{lat}(s) = \begin{bmatrix} M_{lat}(s) - I \\ \tilde{G}_{lat}(s)M_{lat}(s) \end{bmatrix} \quad (7.10)$$

$$\Theta(s) = \text{diag}(\Theta_{lon}(s), \Theta_{lat}(s)) \quad (7.11)$$

This implies that the MIMO AW compensator can be considered decentralized from the point of view of the signals r and r_m such that $\Theta(s) = \text{diag}(\Theta_{lon}(s), \Theta_{lat}(s))$, allowing the independent design of AW compensators for each decoupled UAV MIMO loop (i.e Longitudinal and Lateral).

Given that the state space realization of the extended plant is

$$\tilde{G}(s) = \left[\begin{array}{cc|c} A & B & 0 \\ 0 & 0 & I \\ \hline C & D & 0 \\ 0 & I & 0 \end{array} \right] = \left[\begin{array}{c|c} \tilde{A} & \tilde{B} \\ \hline \tilde{C} & 0 \end{array} \right] \quad \text{where } \tilde{D} \triangleq 0 \quad (7.12)$$

The AW compensator $\Theta(s)$ will have the structure

$$\Theta(s) = \text{diag}(\Theta_{lon}(s), \Theta_{lat}(s)) \sim \left[\begin{array}{c|c} \tilde{A} + \tilde{B}F & \tilde{B} \\ \hline F & 0 \\ \tilde{C} & 0 \end{array} \right] \quad (7.13)$$

where

$$\begin{aligned}\tilde{A} &= \text{diag}(\tilde{A}_{lon}, \tilde{A}_{lat}) & \tilde{B} &= \text{diag}(\tilde{B}_{lon}, \tilde{B}_{lat}) \\ \tilde{C} &= \text{diag}(\tilde{C}_{lon}, \tilde{C}_{lat}) & F &= \text{diag}(F_{lon}, F_{lat}),\end{aligned}$$

As shown in previous AW synthesis and according to Figure 7.4, the AW problem can be reduced to that of ensuring the stability of the nonlinear loop while minimizing the mapping $\|\mathcal{T}_p\|_{\mathcal{L}_2} < \gamma$. Thus, the following theorem sets up necessary and sufficient conditions to guarantee marginal asymptotic stability of the nonlinear loop in Figure 7.4 and subsequently the entire closed-loop system in Figure 7.3, while ensuring that the mapping $\mathcal{T}_p : r_{lin} \mapsto \tilde{y}_d$ which determines the deviation of the nonlinear system performance from the nominal is minimized such that $\|\mathcal{T}_p\|_{\mathcal{L}_2} < \gamma$ for some $\gamma > 0$

Theorem 7.1. If Assumption 7.1 is satisfied and there exist matrices $Q = \text{diag}(Q_{lon}, Q_{lat}) > 0$, diagonal $Q = \text{diag}(Q_{lon}, Q_{lat}) > 0$ and $L = \text{diag}(L_{lon}, L_{lat})$, and scalars $\gamma = \text{diag}(\gamma_{lon}, \gamma_{lat}) > 0$ and $0 < \epsilon < 1$ such that the following LMI

$$\text{He} \left\{ \begin{bmatrix} \tilde{A}Q + \tilde{B}L & \tilde{B}U & 0 & 0 \\ -\epsilon L & -U & \epsilon I & 0 \\ 0 & 0 & -\frac{\gamma}{2}I & 0 \\ \tilde{C}Q & 0 & 0 & -\frac{\gamma}{2}I \end{bmatrix} \right\} < 0 \quad (7.14)$$

hold, then the AW compensator (7.11) with $F = LQ^{-1}$ ensures that the system in Figure 7.3 is locally asymptotically stable, well posed and such that $\|\mathcal{T}\|_{\mathcal{L}_2} < \gamma$.

Proof: The LMI (7.14) is a copy of the alternative LMI (4.21) in Remark 4.2. The proof is exactly the same as that provided in [165] for the LMI (4.21) except in this case, the state space realization of the nonlinear loop of $\Theta(s)$ in (7.13) is

$$\begin{aligned}\dot{\tilde{x}} &= (\tilde{A} + \tilde{B}F)\tilde{x} + \tilde{B}\tilde{r} \\ r_d &= F\tilde{x} \\ \tilde{y} &= \tilde{C}\tilde{x}\end{aligned} \quad (7.15)$$

where $\tilde{A} = \text{diag}(\tilde{A}_{lon}, \tilde{A}_{lat})$, $\tilde{B} = \text{diag}(\tilde{B}_{lon}, \tilde{B}_{lat})$, $\tilde{C} = \text{diag}(\tilde{C}_{lon}, \tilde{C}_{lat})$, $F = \text{diag}(F_{lon}, F_{lat})$, $\tilde{r} = Dz(r) = Dz(r_{lin} - r_d)$, $\tilde{x} = [x', u'_r]$, $\tilde{y} = [y', u'_r]$ and $\tilde{y}_d = [y'_d, u'_d]$.

Thus, to guarantee stability and ensure that $\|\mathcal{T}\|_{\mathcal{L}_2} < \gamma$, the following inequality should hold for some Lyapunov function $V(\tilde{x}) = \tilde{x}'P\tilde{x} > 0$ where $P = \text{diag}(P_{lon}, P_{lat})$, and some scalar $\gamma = \text{diag}(\gamma_{lon}, \gamma_{lat}) > 0$, provided the deadzone $Dz(r)$ belongs to the Sector $[0, \epsilon I]$.

$$\dot{V}(\tilde{x}) - \gamma \|r_{lin}\|^2 + \frac{1}{\gamma} \|\tilde{y}_d\|^2 + \Lambda(r) < 0. \quad (7.16)$$

where $\Lambda(r)$ represents the Sector $[0, \epsilon I]$ inequality [125] for which the deadzone sector is defined and is given as

$$\Lambda(r) = Dz(r)'W(\epsilon r - Dz(r)) \geq 0 \quad \text{for some diagonal matrix } W > 0 \quad (7.17)$$

The LMI (7.14) is obtained after substituting for \tilde{x} , r_d and \tilde{y}_d from Equation (7.15) and applying Schur complement and the congruence transformation

$$\text{diag}(P^{-1}, W^{-1}, I, I) = \text{diag}(Q, U, I, I)$$

to the inequality (7.16). \square

Remark 7.1: Theorem 7.1 provides conditions which enable two AW compensators having the form (7.11) to be synthesized for the UAV plant decoupled into its longitudinal and lateral dynamics. However, it is emphasized that the two AW compensators are multivariable AW compensators but in some way is a decentralized AW structure that allows each AW compensator cater for its corresponding decoupled MIMO loop thus simplifying the AW design process and providing ease of operation of the compensators in practical UAV systems.

7.3 Simulation Results

A full MIMO AW compensators and two AW compensators corresponding to the structure (7.11) were designed for the Aerosonde UAV model and controller described in the previous chapter. The interest in comparing the two structured AW compensators with the full MIMO compensator lies in the behaviour of the system in nonlinear simulation. The linear model exhibits a clear decoupling between longitudinal and lateral behaviour, but some coupling is present in the nonlinear model. It is therefore important to uncover how useful the decoupled structure is in more realistic circumstances

7.3.1 Longitudinal Simulation Results

For the longitudinal dynamics simulations, the effects of saturation and the AW compensation will be observed on the pitch θ angle with a pulse reference of 8° commanded on the pitch.

Figures 7.5a/7.6a show a nominal pitch response of the system and its corresponding control response. Figures 7.5b/7.6b shows the saturated pitch response of the system with an elevator rate saturated command when no AW compensation is used; the rate saturation has resulted in loss of tracking behaviour and is becoming unstable with time. Tracking of the desired pitch is recovered and better responses are observed when the full MIMO AW and Longitudinal AW compensators are engaged for different operating points as can be seen in Figures 7.7c/7.8c and Figures 7.7d/7.8d respectively. The elevator control responses when the full MIMO AW and Longitudinal AW compensators are engaged are shown in Figures 7.9c/7.9d respectively.

7.3.2 Lateral Simulation Results

For the lateral dynamics simulations, the effects of saturation and the AW compensation will be observed on the roll ϕ angle with a pulse reference of 8° commanded on the roll.

Figures 7.10a/7.11a show a nominal roll response of the system and its corresponding control response. Figures 7.10b/7.11b shows the saturated roll response of the system with an aileron rate

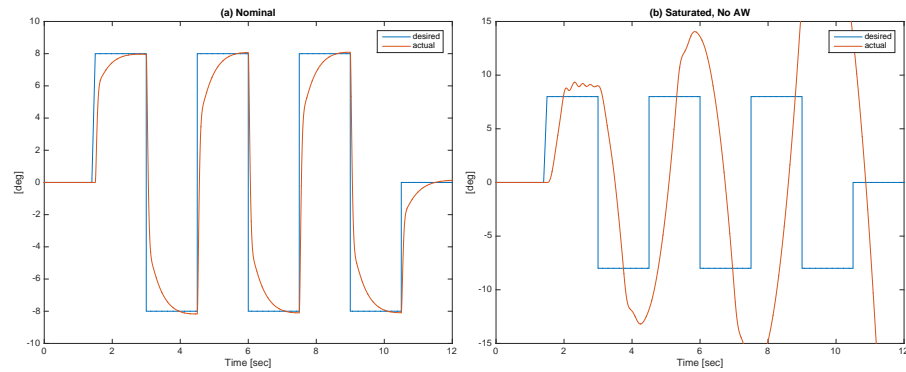


FIGURE 7.5: Pitch angle response: (a) [from left] Nominal and (b) Saturation, no AW

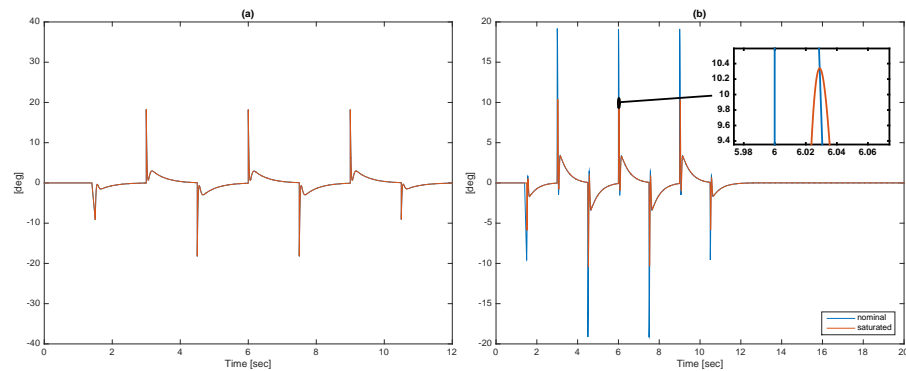
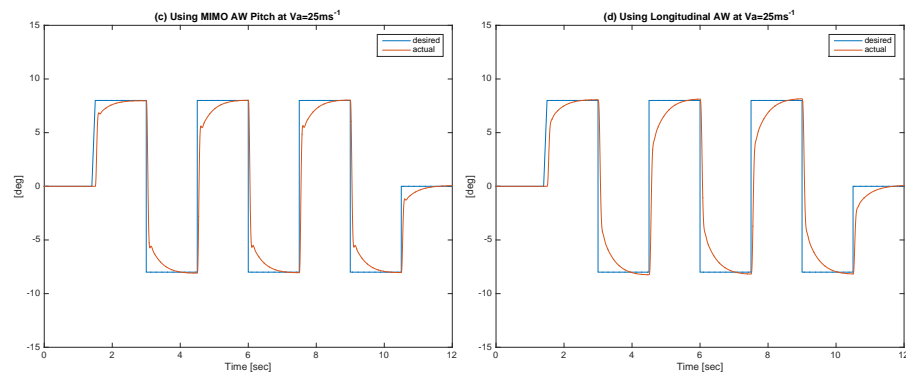


FIGURE 7.6: Elevator command with rate saturation: (a) [from left] Nominal and (b) Saturation, no AW

FIGURE 7.7: Pitch angle response at $V_a=25\text{ms}^{-1}$: (c) [from left] Saturation, full MIMO AW and (d) Saturation, Longitudinal AW

saturated command when no AW compensation is used; the rate saturation causes the performance to deteriorate and exhibits classic windup effects such as large overshoots, loss of tracking behaviour etc. Significant improvements over the uncompensated responses are observed when the full MIMO AW and Lateral AW compensators are used as can be seen in Figures 7.12c/7.13c and Figures 7.12d/7.13d respectively. The aileron control responses when the full MIMO AW and Lateral AW compensators are engaged are shown in Figures 7.14c/7.14d respectively.

Remark 7.2: According to Figures 7.7 and 7.8, the longitudinal decoupled AW compensators performed slightly better than the full MIMO AW compensators in general while according to Figures 7.12 and 7.13, the full MIMO AW compensator slightly performed better than the

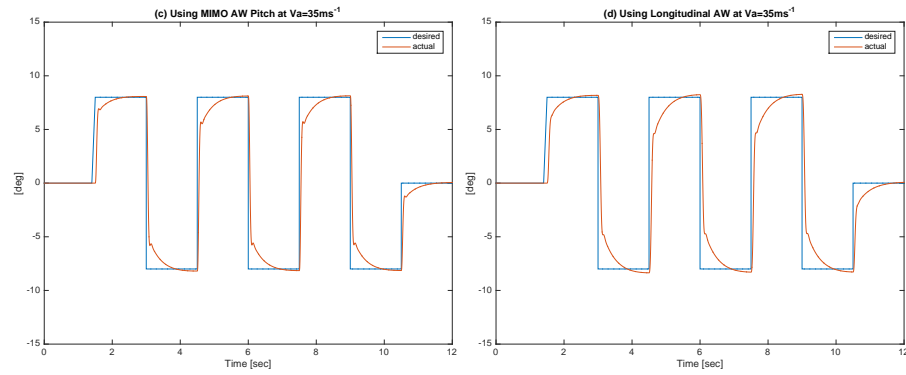


FIGURE 7.8: Pitch angle response at $V_a=35\text{ms}^{-1}$: (c) [from left] Saturation, full MIMO AW and (d) Saturation, Longitudinal AW

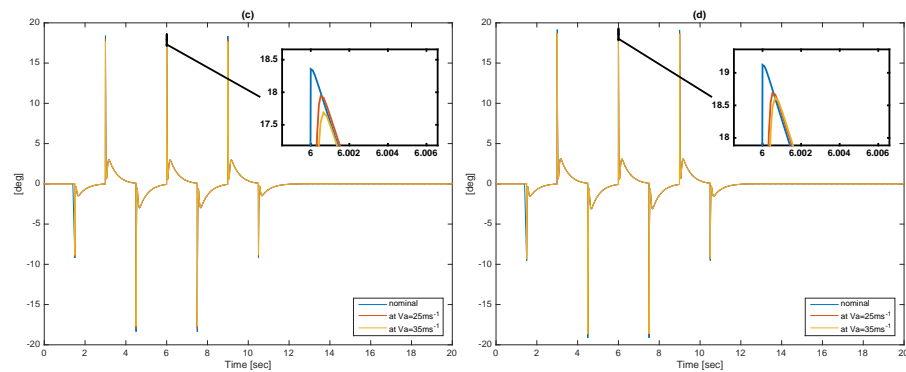


FIGURE 7.9: Elevator command with rate saturation: (c) [from left] Saturation, full MIMO AW and (d) Saturation, Longitudinal AW

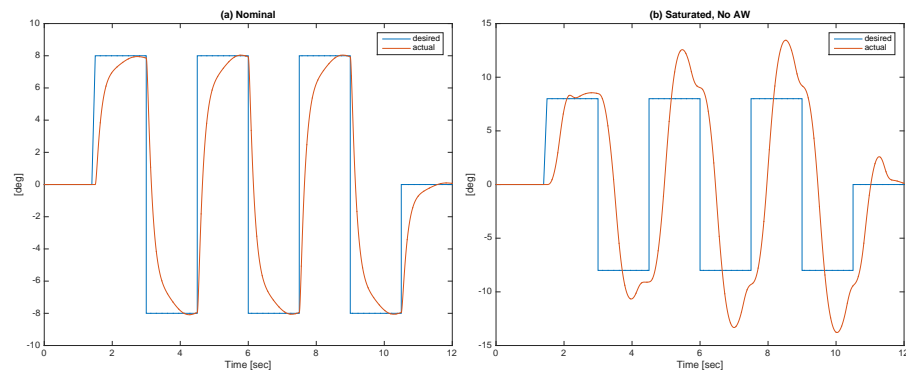


FIGURE 7.10: Roll angle response: (a) [from left] Nominal and (b) Saturation, no AW

lateral decoupled AW compensator in general. The designed AW compensators (Full MIMO, longitudinal and lateral) were constructed using the linearized decoupled dynamics and applied to the nonlinear model of the UAV. Thus it is important to note that slight coupling effects between the longitudinal and lateral axis that exist in the nonlinear model will contribute to the degradation in stability and performance even with AW compensation. However this may depend on how close the operating point on the flight envelope is to the trim points used for the linearization of the nonlinear model. This is evidenced by the subtle differences between the results in Figures 7.12 and 7.13 as well as Figures 7.7 and 7.8 where it can be seen that both the full MIMO and decoupled AW compensators at the operating point characterized by

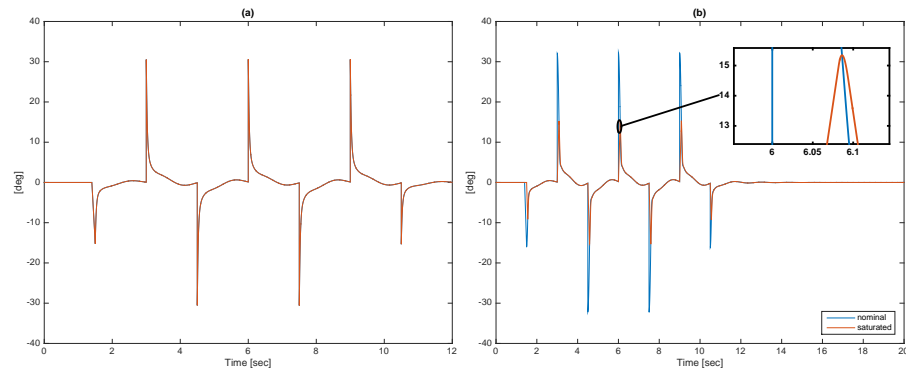


FIGURE 7.11: Aileron command with rate saturation: (a) [from left] Nominal and (b) Saturation, no AW

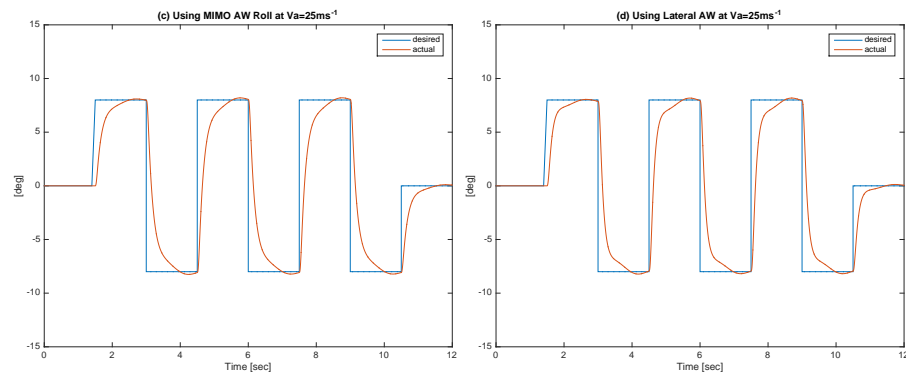


FIGURE 7.12: Roll angle response at $V_a = 25 \text{ ms}^{-1}$: (c) [from left] Saturation, full MIMO AW and (d) Saturation, Lateral AW

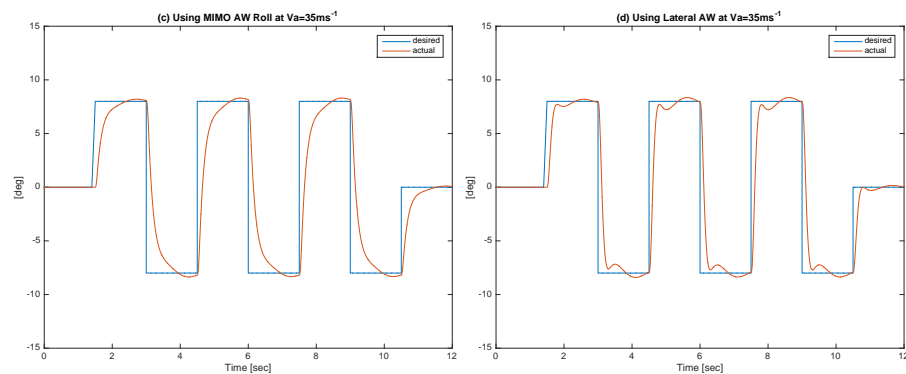


FIGURE 7.13: Roll angle response at $V_a = 35 \text{ ms}^{-1}$: (c) [from left] Saturation, full MIMO AW and (d) Saturation, Lateral AW

an airspeed of 25 ms^{-1} perform slightly better than the AW compensators at the operating point characterized by an airspeed of 35 ms^{-1} . In some cases with certain operating points, the decoupled AW compensator may perform better than the MIMO AW compensator.

7.4 Summary

In summary, this chapter presented a method for designing decoupled AW compensators to tackle the problem of rate saturation in fixed wing UAVs. This was done by using the rate

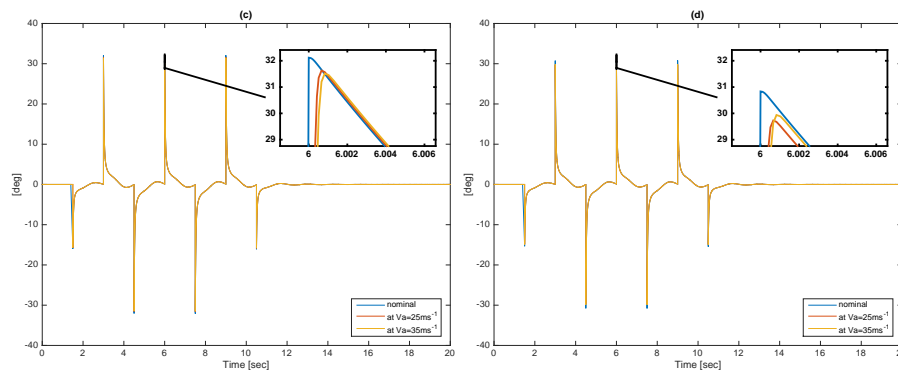


FIGURE 7.14: Aileron command with rate saturation: (c) [from left] Saturation, full MIMO AW and (d) Saturation, Lateral AW

saturation model mentioned in Section 2.2 on the UAV plant-controller system and restructuring the system such that parts of the rate saturation dynamics are fused with the nominal UAV plant and controller to form an extended model of the plant and controller leaving a magnitude saturation as the only nonlinear element in the system. This process further exploited the natural decoupling of the UAV into its longitudinal and lateral dynamics such that the typical AW approach described in Section 4.3.1 and [23] can be applied to form two decoupled (but still MIMO) AW compensators.

The main results show that the decoupled longitudinal and lateral AW compensators performed considerably well when applied to a rate saturated system of the Aerosonde fixed wing UAV model described in the previous chapter. When the performance of the decoupled longitudinal and lateral AW compensators are compared with the performance of the full MIMO AW compensator at different operating points of the flight envelope, it was observed that at some operating points, the full MIMO AW compensator may perform slightly better than the decoupled AW compensators and at other operating points, the decoupled compensators may perform slightly better than the full MIMO AW compensator. This may however depend on how close the operating point on the flight envelope is to the trim points used for the linearization of the nonlinear model to obtain the decoupled linear dynamics.

It is important to note that the control inputs for the elevator d_{e*} and rudder d_{r*} for the Aerosonde UAV, in reality, actuate the same physical control surfaces (the ruddervator control surfaces). However, for the work done in this chapter, it was assumed that the control inputs d_{e*} and d_{r*} actuate separate elevator control surfaces and rudder control surfaces respectively.

8 Conclusion and Future Work

8.1 Summary of Main Contributions

This thesis presented a number of appealing ways to synthesize decentralized AW compensators for Quadrotor UAVs and Fixed-wing UAVs. These AW compensator design approaches were developed to tackle the problem of actuator magnitude saturation in Quadrotor UAVs and the problem of actuator rate saturation in Fixed-wing UAVs. The AW compensation techniques developed in this thesis are founded on the AW configuration first proposed by [85] and the fullorder MIMO AW compensation techniques developed by [23, 58]. This work was motivated by the desire to develop flexible and easy to operate AW compensators that will be used on UAVs in real flight conditions and attempted to decentralize the operation of a typical MIMO AW compensator in such a way that it will have some structure that is appealing to a practical control engineer. The main contributions of the thesis can be summarised as follows;

Channel-by-channel AW design for class of MIMO systems

In Chapter 4, using the AW design technique developed by [23, 58], it was shown that globally stabilizing SISO-like full order AW compensators can be designed for each individual control loop of a certain class of MIMO systems which can be modelled as a series interconnection of a diagonal dynamic part and a non-diagonal, but invertible, static part. This design approach has great practical appeal due to its transparency, flexibility (each channel AW compensator can be designed and re-designed independent of the others) and ease of monitoring; attributes that are very much appreciated by practical control engineers. The quadrotor UAV dynamics can be considered as a series interconnection of a static non-diagonal, but invertible matrix X and a system of double integrators. The Quadrotor UAV is said to belong to the class of MIMO systems described above.

Pseudo-Decentralized AW design for class of MIMO systems

The design of globally stabilizing full order AW compensators that exploit the structure of the earlier mentioned class of MIMO systems in order to impose some form of transparent structure on the AW compensator design. This design is beneficial for systems where the "virtual" inputs

of the plant as described in Section 4.4.2 of Chapter 4 can be easily accessed and measured by the design process. However, it is emphasized that this AW compensator is a MIMO AW compensator but with a decentralized structure hence the reason why it is called “pseudo”-decentralised.

Alternative approach to the use of LMIs in AW synthesis for systems containing double integrators

The AW design technique developed by [23, 58] solved the AW problem by using LMI optimisation techniques to provide stability guarantees and some level of performance (in the form of \mathcal{L}_2 gain minimization). Although LMI-based approaches make AW design systematic and tractable, the use of LMIs, tend to carry a higher computational burden in some systems and would normally generate one “*optimal*” solution which may not necessarily be the only solution yielding a “good” AW compensator. The approach to designing globally stabilising AW compensators for double integrator systems developed in Chapter 5 replaces this LMI optimisation technique with a technique that uses simple conditions to provide nonlinear stability guarantees (based on the results of [26]) and presents linear-based guidelines for choosing AW compensator parameters needed for performance consideration.

The application of developed techniques to a realistic quadrotor UAV

The above mentioned techniques were used to design AW compensators to alleviate the magnitude saturation problem in a realistic experimental quadrotor UAV: A modified 3DR Quadrotor UAV. The experimental quadrotor was assembled, programmed and configured for autonomous flight with the help of third year undergraduate project students Ahmed Hamouda and Declan Lawlor. The first phase of flight tests took place between the period of January 2015 and August 2015. The purpose of the first phase of flight tests were to observe the saturation limits in flight patterns and observe the performance of the pseudo-decentralized AW compensator and the channel by channel AW compensators. The final flight test phase took place between the period of October 2015 and February 2016. The purpose of the final phase of flight tests were to observe the performance of the AW compensators designed using the techniques developed in Chapter 5. All flight tests yielded good results as shown in the results sections of Chapters 4 and 5.

Decoupled AW design for rate saturated fixed wing UAVs

The primary objective of the work described in Chapter 7 was to design AW compensators to tackle the problem of actuator rate saturation in Fixed wing UAVs while exploiting the natural decoupling of Fixed wing UAV dynamics into Longitudinal and Lateral dynamics; thus providing some sort of appealing structure. The rate saturation model used allowed the typical rate saturation to be expressed in terms of a magnitude saturation however this, in some way, complicated the AW problem such that the global stability guarantee condition enforced in previous AW compensator designs had to be relaxed to a local or semi-global stability guarantee.

Therefore two locally stabilizing full order MIMO AW compensators based on the techniques by [23, 25] are designed and implemented for Fixed wing UAV dynamics that has been decomposed into two decoupled subsystems (i.e the Longitudinal and the Lateral dynamics).

8.2 Future Work

Some possible paths for future work include;

- a. **Reduced order AW compensators:** The focus of AW compensator design in this thesis was on full-order AW compensators. Full order AW compensators are attractive because they always exist for any stable plant [166], however they usually require higher computational requirements. Reduced order AW compensators (static and low order) have been shown by a number of researchers [60, 167, 168] to be a less computationally intensive option with reduced complexity and some researchers have demonstrated that good results can be obtained from practical implementation of some of these reduced order AW compensators on real-life systems [137]. These researchers have also shown that reduced order AW compensators may come with a price of sacrificing global stability requirements for local stability requirements and the sacrifice on performance may range from negligible to significant impact but it would be interesting to attempt performing analysis of static and low order AW compensators with application to UAVs in hopes of achieving results closely related to that obtained from full order AW compensators but with less computational overhead and reduced complexity.
- b. **Accounting for Uncertainty:** Model uncertainty is another important problem faced in control systems. A number of researchers have considered the problem of accounting for uncertainty and disturbance in the design of robust flight controllers for UAVs [169–172] with very few considering the combined problem of actuator saturation in systems with uncertainties [173–175]. This combined problem of actuator saturation in the presence of uncertainty has been generally ignored by most researchers, more effort needs to be dedicated to addressing this issue in UAVs especially since it is known that UAVs are generally plagued with uncertainties and constraints [176–178]. The fullorder MIMO AW compensation techniques [23, 58] used in this thesis were developed to account for uncertainty & disturbances however, it will be advantageous to formally investigate this issue when incorporated with the decentralized/decoupled AW techniques developed in this thesis; this is a possible area for future investigation.
- c. **GULMA UAV Model:** In the introduction, it was briefly mentioned that the work conducted on fixed wing UAVs was meant to be implemented on the Nigerian Air Force (NAF) “GULMA” UAV, an experimental indigenous surveillance UAV. However due to problems associated with obtaining the full parameter specifications (including stability and control derivatives) that can be reconciled with the physical UAV on ground and some issues regarding military confidentiality requirements, it was decided that a working model of another UAV of similar build and design to the GULMA UAV will be obtained and used to develop the proposed AW techniques. The replacement UAV model used was the Aerosonde UAV but it mainly differs from the GULMA UAV in that it has a V-tail system whereas the GULMA

UAV has a T-tail system. There are other subtle and minor differences but all these are not likely to affect the AW compensator design technique that will be used. The author intends to carry out further investigations into transferring the AW compensator techniques used in the design of the Aerosonde UAV to the GULMA UAV in order to perform flight tests and evaluate the performance of these compensators on physical fixed wing UAV platforms.

A Coordinate Reference Systems.

A.1 Reference Frame Definitions

To completely understand the motion of a UAV in flight, it is important to clearly define some set of axes frame which will act as a reference from which the equations of motion of the UAV can be derived. There are different types of axes/reference frames defined for typical conventional aircraft systems however four of these reference frames related to the motion of UAVs are discussed as follows;

A.1.1 Inertial Frame e

This reference frame is also called the fixed earth axis frame. This frame system is considered as the frame where Newton's Laws apply and is generally fixed in space with respect to the earth. This frame is a convenient reference whose origin O can be fixed at any point on the earth's surface, but is usually chosen to coincide with the centre of gravity of the UAV at the start of flight.

In this frame, OZ_e axis points downwards, parallel to the local direction of gravity towards the centre of the earth. OX_e and OY_e axes lie in a plane tangential to the earth's surface with OX_e oriented eastwards (or sometimes northwards) and OY_e oriented southwards (or sometimes eastwards).

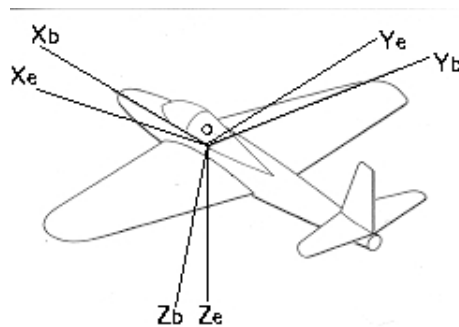


FIGURE A.1: Definition of Inertial and Body Reference Frames

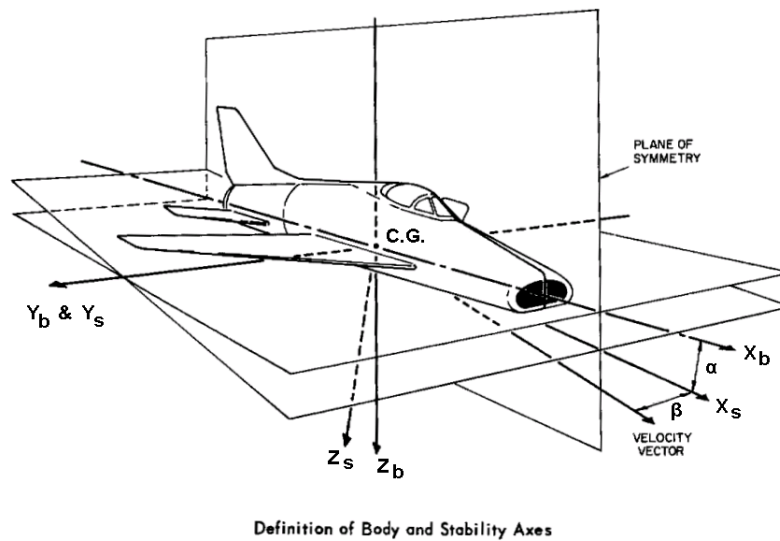


FIGURE A.2: Body and Stability axes Reference Frames [4]

A.1.2 Body Frame b

This reference frame is a right-handed set of mutually perpendicular axes that are generally fixed to the UAV's body and are moving with it. It coincides with the UAV's body plane of symmetry and its origin O is at the centre of gravity of the UAV. In this frame, OZ_b axis is pointing downwards, perpendicular to OX_b and is contained in the plane of symmetry. OX_b axis is contained in the plane of symmetry, and is positive forward (towards nose of the airplane) while OY_b axis lies perpendicular to the plane of symmetry and is directed in such a way that $OX_bY_bZ_b$ is a right handed system.

A.1.3 Stability axes Frame s

This is a peculiar type of the body frame that is used to study small deviations from a nominal flight condition. The body reference frame OY_b plane and the stability reference frame OY_s coincide with each other while OX_s is chosen parallel to the projection of the true airspeed V_a vector on the X_bOZ_b plane and OZ_s is in the plane of symmetry of the UAV. The angle between OX_s plane and the OX_b plane is defined as the angle of attack α . It can be seen from Figure A.2 that it is the body axis when the angle of attack α is zero.

A.1.4 Wind axes Frame w

This is also another peculiar body axes system in which the axis OX_w plane is tangential to the flight path in the forward direction and is aligned with the airspeed V_a vector of the UAV. OZ_w is perpendicular to OX_w and is contained in plane of symmetry for normal flight. OY_w plane lies perpendicular to OX_w and OZ_w and is directed in such a way that $OX_wY_wZ_w$ is a right handed triad. The angle between the OX_w plane and OX_s plane is defined as the side-slip β .

If $\beta = 0$ then the stability axes coincide with the wind axis. The wind axis is also called the flight-path axis and its relationship with the stability axes can be seen in Figure A.3.

A.2 Coordinate Transformation

A.2.1 From Inertial Frame to Body Frame

To translate between inertial frame and body frame and vice versa, intermediate axis sets can be considered in order to simplify the process. These intermediary axis frames will be referred to as **Vehicle frames** and they are based on the rotation of the original axis about an axis plane by a certain displacement angle. The transformation from inertial frame through the vehicle frames to the body frame is outlined as follows

1. Rotate OX_e , OY_e and OZ_e about the OZ_e plane by an angle ψ (yaw angle), this is the first 1st rotation from the **inertial frame** to the **vehicle frame 1**,
2. Rotate the new OX_1 , OY_1 and OZ_1 about the OY_1 plane by an angle θ (pitch angle), this is the second 2nd rotation from **vehicle frame 1** to the **vehicle frame 2**,
3. Rotate the new OX_2 , OY_2 and OZ_2 about the OX_2 plane by an angle ϕ (roll angle), this is the final rotation from **vehicle frame 2** to the **body frame**,

The axes rotations can be presented as

$$\begin{bmatrix} X_e \\ Y_e \\ Z_e \end{bmatrix} \xrightarrow[\psi]{1^{st} \text{ Rotation } (R_v)} \begin{bmatrix} X_1 \\ Y_1 \\ Z_1 = Z_e \end{bmatrix} \xrightarrow[\theta]{2^{nd} \text{ Rotation } (R_{v1})} \begin{bmatrix} X_2 \\ Y_2 = Y_1 \\ Z_2 \end{bmatrix} \xrightarrow[\phi]{\text{final Rotation } (R_{v2})} \begin{bmatrix} X_b = X_2 \\ Y_b \\ Z_b \end{bmatrix}$$

$\underbrace{\hspace{15em}}_R$

where ψ, θ, ϕ are the Euler angles and R_v, R_{v1} and R_{v2} are the first, second and final rotations of the vehicle frames. The resultant transformation matrix R from inertial to body frame is given

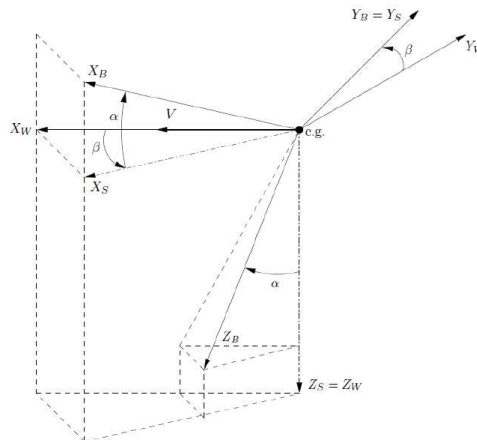


FIGURE A.3: Relationship between Stability axis and Wind axis [5]

as $R = R_v \cdot R_{v1} \cdot R_{v2}$, where R_v , R_{v1} and R_{v2} as derived in [24] is given as

$$R_v = \begin{bmatrix} 1 & 0 & 0 \\ 0 & \cos \phi & -\sin \phi \\ 0 & \sin \phi & \cos \phi \end{bmatrix}, R_{v1} = \begin{bmatrix} \cos \psi & \sin \psi & 0 \\ -\sin \psi & \cos \psi & 0 \\ 0 & 0 & 1 \end{bmatrix}, R_{v2} = \begin{bmatrix} \cos \theta & 0 & \sin \theta \\ 0 & 1 & 0 \\ -\sin \theta & 0 & \cos \theta \end{bmatrix}$$

such that R becomes

$$R = \begin{bmatrix} \cos \psi & \sin \psi & 0 \\ -\sin \psi & \cos \psi & 0 \\ 0 & 0 & 1 \end{bmatrix} \begin{bmatrix} \cos \theta & 0 & \sin \theta \\ 0 & 1 & 0 \\ -\sin \theta & 0 & \cos \theta \end{bmatrix} \begin{bmatrix} 1 & 0 & 0 \\ 0 & \cos \phi & -\sin \phi \\ 0 & \sin \phi & \cos \phi \end{bmatrix}$$

$$R = \begin{bmatrix} \cos \theta \cdot \cos \psi & \cos \psi \cdot \sin \theta \cdot \sin \phi - \cos \phi \cdot \sin \psi & \cos \psi \cdot \sin \theta \cdot \cos \phi - \sin \phi \cdot \sin \psi \\ \cos \theta \cdot \sin \psi & \sin \psi \cdot \sin \theta \cdot \sin \phi - \cos \phi \cdot \cos \psi & \sin \psi \cdot \sin \theta \cdot \cos \phi - \sin \phi \cdot \cos \psi \\ -\sin \theta & \cos \theta \cdot \sin \phi & \cos \phi \cdot \cos \theta \end{bmatrix}$$

A.2.2 From Body Frame to Wind/Stability axes Frame

Similar to the process followed in the previous subsection, the transformation from body frame to the wind/stability axes frame according to Figure A.2 is outlined as follows

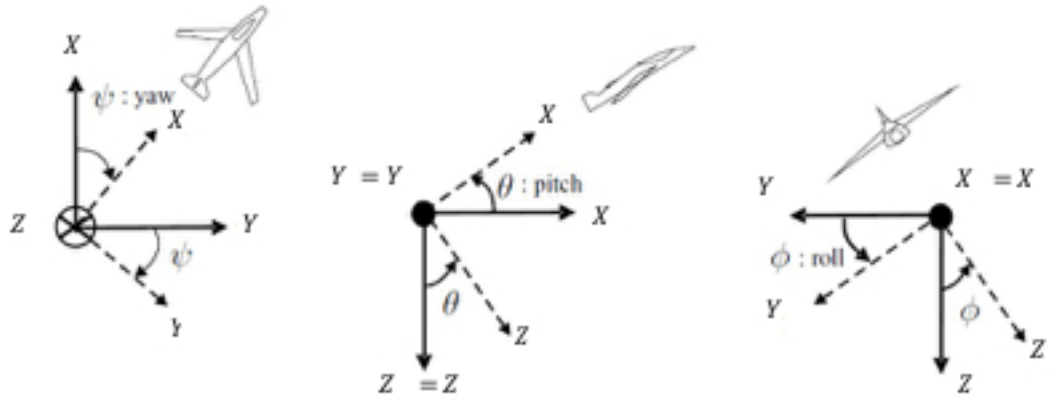


FIGURE A.4: Rotations from inertial frame through vehicle frames to body frame [5]

1. Rotate OX_b , OY_b and OZ_b about the OZ_b plane by an angle α (angle of attack), this is the first 1st rotation from the **body frame** to the **stability axes frame**,
2. Rotate the new OX_s , OY_s and OZ_s about the OY_s plane by an angle β (sideslip angle), this is the final rotation from **stability axes frame** to the **wind axes frame**,

The axes rotations can be presented as

$$\begin{array}{c} \left[\begin{array}{c} X_e \\ Y_e \\ Z_e \end{array} \right] \xrightarrow[\alpha]{1^{st} \text{ Rotation } (T_{s1})} \left[\begin{array}{c} X_s \\ Y_s \\ Z_s = Z_e \end{array} \right] \xrightarrow[\phi]{\text{final Rotation } (T_{s2})} \left[\begin{array}{c} X_w \\ Y_w = Y_s \\ Z_w \end{array} \right] \end{array}$$

$\underbrace{\hspace{15em}}_T$

where α, β are the angle of attack and side-slip angle respectively and T_{s1} and T_{s2} are the first and final rotations of the stability frame. The resultant transformation matrix T from inertial to body frame is given as $T = T_{s2}.T_{s1}$, where T_{s1} and T_{s2} as derived in [24] is given as

$$T_{s2} = \begin{bmatrix} \cos \beta & \sin \beta & 0 \\ -\sin \beta & \cos \beta & 0 \\ 0 & 0 & 1 \end{bmatrix}, T_{s1} = \begin{bmatrix} \cos \alpha & 0 & \sin \alpha \\ 0 & 1 & 0 \\ -\sin \alpha & 0 & \cos \alpha \end{bmatrix}$$

such that T becomes

$$T = \begin{bmatrix} \cos \beta & \sin \beta & 0 \\ -\sin \beta & \cos \beta & 0 \\ 0 & 0 & 1 \end{bmatrix} \begin{bmatrix} \cos \alpha & 0 & \sin \alpha \\ 0 & 1 & 0 \\ -\sin \alpha & 0 & \cos \alpha \end{bmatrix}$$

$$T = \begin{bmatrix} \cos \alpha \cdot \cos \beta & \cos \beta & \sin \alpha \cdot \cos \beta \\ -\sin \beta \cdot \cos \alpha & \sin \beta & -\sin \alpha \cdot \sin \beta \\ -\sin \alpha & 0 & \cos \alpha \end{bmatrix}$$

References

- [1] A. Zheng, M. V. Kothare, and M. Morari, “Anti-windup design for internal model control,” *International Journal of Control*, vol. 60, no. 5, pp. 1015–1024, 1994.
- [2] A. Adegbege and W. Heath, “Two-stage multivariable antiwindup design for internal model control constraints,” in *Proceedings of 9th International Symposium on Dynamics and Control of Process Systems, International Federation of Automatic Control, Leuven, Belgium:[sn]*, 2010, pp. 276–281.
- [3] J. Maurer, “Polar remote sensing using an unpiloted aerial vehicle (UAV),” 2016. [Online]. Available: <http://www2.hawaii.edu/~jmaurer/uav/>
- [4] E. Cruiser. (2016, November) Definition of stability and body axes. [Online]. Available: https://dodlithr.blogspot.com.ng/2011_09_01_archive.html
- [5] Y. Tang, “Fault tolerant control for nonlinear aircraft based on feedback linearization,” Ph.D. dissertation, University of Hull, 2013.
- [6] T. Hu and Z. Lin, *Control systems with actuator saturation: analysis and design*. Springer, 2001.
- [7] J. Sofrony, M. C. Turner, I. Postlethwaite, O. Brieger, and D. Leissing, “Anti-windup synthesis for PIO avoidance in an experimental aircraft,” in *Decision and Control, 2006 45th IEEE Conference on*. IEEE, 2006, pp. 5412–5417.
- [8] D. T. McRuer, *Aviation Safety and Pilot Control: Understanding and Preventing Unfavorable Pilot-Vehicle Interactions*, 1997.
- [9] H. Duda, “Prediction of pilot-in-the-loop oscillations due to rate saturation,” *Journal of Guidance, Control, and Dynamics*, vol. 20, no. 3, pp. 581–587, 1997.
- [10] J. S. Jang, *Nonlinear control using discrete-time dynamic inversion under input saturation: theory and experiment on the Stanford dragonfly UAVs*, 2004.
- [11] F. Kendoul, D. Lara, I. Fantoni, and R. Lozano, “Nonlinear control for systems with bounded inputs: Real-time embedded control applied to UAVs,” in *Proceedings of the 45th IEEE Conference on Decision and Control*. IEEE, 2006, pp. 5888–5893.

- [12] J. C. Monteiro, F. Lizarralde, and L. Hsu, "Optimal control allocation of quadrotor UAVs subject to actuator constraints," in *American Control Conference (ACC), 2016*. American Automatic Control Council (AACC), 2016, pp. 500–505.
- [13] A. Ailon, "Trajectory tracking for UAVs with bounded inputs and some related applications," *IFAC Proceedings Volumes*, vol. 42, no. 6, pp. 355–360, 2009.
- [14] W. Ren and R. W. Beard, "CLF-based tracking control for UAV kinematic models with saturation constraints," in *Decision and Control, 2003. Proceedings. 42nd IEEE Conference on*, vol. 4. IEEE, 2003, pp. 3924–3929.
- [15] J. R. Azinheira and A. Moutinho, "Hover control of an UAV with backstepping design including input saturations," *Control Systems Technology, IEEE Trans.*, vol. 16, no. 3, pp. 517–526, 2008.
- [16] S. Zhu, D. Wang, and C. B. Low, "Ground target tracking using UAV with input constraints," *Journal of Intelligent & Robotic Systems*, vol. 69, no. 1-4, pp. 417–429, 2013.
- [17] E. N. Johnson, M. A. Turbe, A. D. Wu, S. K. Kannan, and J. C. Neidhoefer, "Flight test results of autonomous fixed-wing UAV transitions to and from stationary hover," in *Proceedings of the AIAA Guidance, Navigation, and Control Conference Exhibit, Monterey, CO*, 2006.
- [18] E. Oland *et al.*, "Nonlinear control of fixed-wing unmanned aerial vehicles," 2014.
- [19] A. Pogromsky, B. Andrievsky, and J. Rooda, "Aircraft flight control with convergence-based anti-windup strategy," in *Proc. IFAC Workshop Aerospace Guidance, Navigation and Flight Control Systems (AGNFCS 09)*, 2009.
- [20] N. E. Kahveci and I. V. Kolmanovsky, "Constrained control of uavs using adaptive anti-windup compensation and reference governors," SAE Technical Paper, Tech. Rep., 2009.
- [21] N. Kahveci, P. Ioannou, and M. Mirmirani, "Adaptive LQ control with anti-windup augmentation to optimize UAV performance in autonomous soaring applications," *IEEE Transactions on Control Systems Technology*, vol. 16, no. 4, pp. 691–707, 2008.
- [22] O. Brieger, M. Kerr, D. Leibling, I. Postlethwaite, J. Sofrony, and M. C. Turner, "Anti-windup compensation of rate saturation in an experimental aircraft," in *2007 American Control Conference*. IEEE, 2007, pp. 924–929.
- [23] M. C. Turner, G. Herrmann, and I. Postlethwaite, "Incorporating robustness requirements into anti-windup design," *Automatic Control, IEEE Transactions on*, vol. 52, no. 10, pp. 1842–1855, 2007.
- [24] R. W. Beard, "Quadrotor dynamics and control," *Brigham Young University*, 2008.
- [25] M. C. Turner and I. Postlethwaite, "A new perspective on static and low order anti-windup synthesis," *International Journal of Control*, vol. 77, no. 1, pp. 27–44, 2004.
- [26] F. Tyan, D. S. Bernstein *et al.*, "Global stabilization of systems containing a double integrator using a saturated linear controller," *Int. J. Rob. and Nonlinear Contr.*, vol. 9, no. 15, pp. 1143–1156, 1999.

- [27] T. Hu, A. R. Teel, and L. Zaccarian, "Regional anti-windup compensation for linear systems with input saturation," in *Proceedings of the 2005, American Control Conference, 2005*. IEEE, 2005, pp. 3397–3402.
- [28] L. Rundquist and R. Hillgren, "Phase composition of rate limiters in JAS 39 Gripen," AIAA-96-3368-CP, Tech. Rep., 1996.
- [29] N. E. Kahveci, P. A. Ioannou, and M. D. Mirmirani, "Adaptive LQ control with anti-windup augmentation to optimize UAV performance in autonomous soaring applications," *IEEE Transactions on Control Systems Technology*, vol. 16, no. 4, pp. 691–707, 2008.
- [30] T. Lauvdal and R. M. Murray, "Stabilization of a pitch axis flight control experiment with input rate saturation," *Modeling Identification and Control*, vol. 20, no. 4, pp. 225–240, 1999.
- [31] R. M. Murray, "Geometric approaches to control in the presence of magnitude and rate saturations," *California Institute of Technology Authors Library*, 1999.
- [32] T. Lauvdal, R. M. Murray, and T. I. Fossen, "Stabilization of integrator chains in the presence of magnitude and rate saturations: a gain scheduling approach," in *Decision and Control, 1997., Proceedings of the 36th IEEE Conference on*, vol. 4. IEEE, 1997, pp. 4004–4005.
- [33] J. M. Berg, K. D. Hammett, C. A. Schwartz, and S. S. Banda, "An analysis of the destabilizing effect of daisy chained rate-limited actuators," *IEEE Transactions on Control Systems Technology*, vol. 4, no. 2, pp. 171–176, 1996.
- [34] H. A. Fertik and C. W. Ross, "Direct digital control algorithm with anti-windup feature," *ISA transactions*, vol. 6, no. 4, p. 317, 1967.
- [35] K. J. Åström, "Advanced control methods—survey and assessment of possibilities," in *Advanced control in computer integrated manufacturing. Proceedings of the thirteenth annual Advanced Control Conference*, 1987.
- [36] J. C. Doyle, R. S. Smith, and D. F. Enns, "Control of plants with input saturation nonlinearities," in *American Control Conference, 1987*. IEEE, 1987, pp. 1034–1039.
- [37] R. Hanus *et al.*, "Antiwindup and bumpless transfer: a survey," in *Proceedings of the 12th IMACS world congress*, vol. 2, 1988, pp. 59–65.
- [38] R. Hanus, M. Kinnaert, and J.-L. Henrotte, "Conditioning technique, a general anti-windup and bumpless transfer method," *Automatica*, vol. 23, no. 6, pp. 729–739, 1987.
- [39] K. Walgama, S. Ronnback, and J. Sternby, "Generalisation of conditioning technique for anti-windup compensators," in *Control Theory and Applications, IEE Proceedings D*, vol. 139, no. 2. IET, 1992, pp. 109–118.
- [40] M. V. Kothare, P. J. Campo, M. Morari, and C. N. Nett, "A unified framework for the study of anti-windup designs," *Automatica*, vol. 30, no. 12, pp. 1869–1883, 1994.

- [41] L. Rundquist and K. Aström, “Integrator windup and how to avoid it,” *Proc. of ACC, Pittsburg*, vol. 2, pp. 1693–1698, 1989.
- [42] P. Campo, M. Morari, and C. Nett, “Multivariable anti-windup and bumpless transfer: A general theory,” in *American Control Conference, 1989*. IEEE, 1989, pp. 1706–1711.
- [43] E. F. Mulder, M. V. Kothare, and M. Morari, “Multivariable anti-windup controller synthesis using linear matrix inequalities,” *Automatica*, vol. 37, no. 9, pp. 1407–1416, 2001.
- [44] M. T. Tham, “Internal model control,” *Chemical and Proc*, 2002.
- [45] C. E. Garcia and M. Morari, “Internal model control. a unifying review and some new results,” *Industrial & Engineering Chemistry Process Design and Development*, vol. 21, no. 2, pp. 308–323, 1982.
- [46] M. Morari and E. Zafriou, *Robust process control*. Prentice hall Englewood Cliffs, NJ, 1989, vol. 488.
- [47] G. Goodwin, S. Graebe, and W. Levine, “Internal model control of linear systems with saturating actuators,” in *Proc. ACC*, 1993.
- [48] R. M. Morales, W. P. Heath, and G. Li, “Robustness preserving anti-windup for siso systems,” in *2011 50th IEEE Conference on Decision and Control and European Control Conference*. IEEE, 2011, pp. 639–644.
- [49] F. J. Doyle III, “An anti-windup input–output linearization scheme for siso systems,” *Journal of process control*, vol. 9, no. 3, pp. 213–220, 1999.
- [50] A. R. King-Hans, W. P. Heath, and R. Alli-Oke, “Two-stage multivariable IMC antiwindup (tmia) control of a quadruple tank process using a plc,” in *2014 IEEE Conference on Control Applications (CCA)*. IEEE, 2014, pp. 1681–1686.
- [51] W. Wu and S. Jayasuriya, “An internal model control based anti-windup scheme for stable uncertain plants with input saturation,” in *Proceedings of the 45th IEEE Conference on Decision and Control*. IEEE, 2006, pp. 5424–5428.
- [52] A. Glattfelder and W. Schaufelberger, *Control systems with input and output constraints*. Springer, London, 2003.
- [53] S. Tarbouriech, G. Garcia, J. M. Gomes da Silva Jr., and I. Queinnec, *Stability and Stabilization of Linear Systems with Saturating Actuators*. Springer, 2011.
- [54] L. Zaccarian and A. Teel, *Modern Anti-windup Synthesis: Control Augmentation for Actuator Saturation*. New Jersey: Princeton University Press, 2011.
- [55] S. Galeani, S. Tarbouriech, M. Turner, and L. Zaccarian, “A tutorial on modern anti-windup design,” *European Journal of Control*, vol. 15, no. 3, pp. 418–440, 2009.
- [56] S. Tarbouriech and M. Turner, “Anti-windup design: an overview of some recent advances and open problems,” *IET control theory & applications*, vol. 3, no. 1, pp. 1–19, 2009.

- [57] J. A. De Doná, G. C. Goodwin, and M. M. Seron, “Anti-windup and model predictive control: Reflections and connections,” *European Journal of Control*, vol. 6, no. 5, pp. 467–477, 2000.
- [58] M. C. Turner, G. Herrmann, and I. Postlethwaite, “Accounting for uncertainty in anti-windup synthesis,” in *American Control Conference, 2004. Proceedings of the 2004*, vol. 6. IEEE, 2004, pp. 5292–5297.
- [59] J. Sofrony, M. C. Turner, and I. Postlethwaite, “Anti-windup synthesis using riccati equations,” *International Journal of Control*, vol. 80, no. 1, pp. 112–128, 2007.
- [60] M. L. Kerr, M. C. Turner, and I. Postlethwaite, “Practical approaches to low-order anti-windup compensator design: a flight control comparison,” in *IFAC World Congress, Seoul, Korea*, 2008.
- [61] G. Grimm, J. Hatfield, I. Postlethwaite, A. R. Teel, M. C. Turner, and L. Zaccarian, “Anti-windup for stable linear systems with input saturation: an LMI-based synthesis,” *Automatic Control, IEEE Transactions on*, vol. 48, no. 9, pp. 1509–1525, 2003.
- [62] G. Herrmann, M. C. Turner, and I. Postlethwaite, “Discrete-time and sampled-data anti-windup synthesis: stability and performance,” *International Journal of Systems Science*, vol. 37, no. 2, pp. 91–113, 2006.
- [63] G. Herrmann, B. Hredzak, M. C. Turner, I. Postlethwaite, and G. Guo, “Discrete robust anti-windup to improve a novel dual-stage large-span track-keep/following method,” *Control Systems Technology, IEEE Transactions on*, vol. 16, no. 6, pp. 1342–1351, 2008.
- [64] M. C. Turner, G. Herrmann, and I. Postlethwaite, “Discrete time anti-windup-part 1: stability and performance,” in *Proceedings of the European Control Conference*, 2003.
- [65] G. Herrmann, M. Turner, and I. Postlethwaite, “Discrete time anti-windup-part 2: extension to sampled data case,” in *Proceedings of the European control conference*, 2003.
- [66] G. Grimm, A. R. Teel, and L. Zaccarian, “Linear LMI-based external anti-windup augmentation for stable linear systems,” *Automatica*, vol. 40, no. 11, pp. 1987–1996, 2004.
- [67] T. Hu, A. R. Teel, and L. Zaccarian, “Anti-windup synthesis for linear control systems with input saturation: Achieving regional, nonlinear performance,” *Automatica*, vol. 44, no. 2, pp. 512–519, 2008.
- [68] L. Zaccarian, Y. Li, E. Weyer, M. Cantoni, and A. R. Teel, “Anti-windup for marginally stable plants and its application to open water channel control systems,” *Control Engineering Practice*, vol. 15, no. 2, pp. 261–272, 2007.
- [69] G. Herrmann, M. C. Turner, I. Postlethwaite, and G. Guo, “Practical implementation of a novel anti-windup scheme in a hdd-dual-stage servo-system,” *Mechatronics, IEEE/ASME Transactions on*, vol. 9, no. 3, pp. 580–592, 2004.
- [70] S. Galeani, A. R. Teel, and L. Zaccarian, “Constructive nonlinear anti-windup design for exponentially unstable linear plants,” *Systems & control letters*, vol. 56, no. 5, pp. 357–365, 2007.

- [71] F. Wu and B. Lu, "Anti-windup control design for exponentially unstable LTI systems with actuator saturation," *Systems & Control Letters*, vol. 52, no. 3, pp. 305–322, 2004.
- [72] A. R. Teel, "Anti-windup for exponentially unstable linear systems," *International Journal of Robust and Nonlinear Control*, vol. 9, no. 10, pp. 701–716, 1999.
- [73] C. Barbu, R. Reginatto, A. Teel, and L. Zaccarian, "Anti-windup for exponentially unstable linear systems with inputs limited in magnitude and rate," in *American Control Conference, 2000. Proceedings of the 2000*, vol. 2. IEEE, 2000, pp. 1230–1234.
- [74] G. Grimm, I. Postlethwaite, A. R. Teel, M. C. Turner, and L. Zaccarian, "Linear matrix inequalities for full and reduced order anti-windup synthesis," in *American Control Conference, 2001. Proceedings of the 2001*, vol. 5. IEEE, 2001, pp. 4134–4139.
- [75] K. P. Groves, A. Serrani, S. Yurkovich, M. A. Bolender, and D. B. Doman, *Anti-windup control for an air-breathing hypersonic vehicle model*. Defense Technical Information Center, 2005.
- [76] C. Burgat and S. Tarbouriech, "Intelligent anti-windup for systems with input magnitude saturation," *International Journal of Robust and Nonlinear Control*, vol. 8, no. 12, pp. 1085–1100, 1998.
- [77] A. R. Teel and N. Kapoor, "The L2 anti-windup problem: Its definition and solution," in *Proceedings of the European control conference*, 1997, pp. 1–4.
- [78] L. Zaccarian and A. R. Teel, "Nonlinear scheduled anti-windup design for linear systems," *Automatic Control, IEEE Transactions on*, vol. 49, no. 11, pp. 2055–2061, 2004.
- [79] C. Barbu, S. Galeani, A. Teel, and L. Zaccarian*, "Non-linear anti-windup for manual flight control," *International Journal of Control*, vol. 78, no. 14, pp. 1111–1129, 2005.
- [80] C. Edwards and I. Postlethwaite, "An anti-windup scheme with closed-loop stability considerations," *Automatica*, vol. 35, no. 4, pp. 761–765, 1999.
- [81] M. V. Kothare and M. Morari, "Multivariable anti-windup controller synthesis using multi-objective optimization," in *American Control Conference, 1997. Proceedings of the 1997*, vol. 5. IEEE, 1997, pp. 3093–3097.
- [82] M. Kothare and M. Morari, "Stability analysis of anti-windup control scheme: a review and some generalizations," in *European Control Conference, 1997*.
- [83] S. Miyamoto and G. Vinnicombe, "Robust control of plants with saturation nonlinearity based on coprime factor representations," in *Proceedings of the IEEE Conference on Decision and Control*, vol. 3, 1996, pp. 2355–3592.
- [84] C. Edwards and I. Postlethwaite, "Anti-windup and bumpless transfer schemes," 1996.
- [85] P. F. Weston and I. Postlethwaite, "Linear conditioning for systems containing saturating actuators," *Automatica*, vol. 36, no. 9, pp. 1347–1354, 2000.
- [86] M. C. Turner and I. Postlethwaite, "Further results on full-order anti-windup synthesis: exploiting the stability multiplier," *Nonlinear Control Systems 2004*, vol. 1, p. 1, 2005.

- [87] A. Das, K. Subbarao, and F. Lewis, "Dynamic inversion with zero-dynamics stabilisation for quadrotor control," *Control Theory & Applications, IET*, vol. 3, no. 3, pp. 303–314, 2009.
- [88] E. Altuğ, J. P. Ostrowski, and C. J. Taylor, "Control of a quadrotor helicopter using dual camera visual feedback," *The International Journal of Robotics Research*, vol. 24, no. 5, pp. 329–341, 2005.
- [89] A. Das, F. Lewis, and K. Subbarao, "Backstepping approach for controlling a quadrotor using lagrange form dynamics," *Journal of Intelligent and Robotic Systems*, vol. 56, no. 1-2, pp. 127–151, 2009.
- [90] I. D. Cowling, O. A. Yakimenko, J. F. Whidborne, and A. K. Cooke, "Direct method based control system for an autonomous quadrotor," *Journal of Intelligent & Robotic Systems*, vol. 60, no. 2, pp. 285–316, 2010.
- [91] R. Molero, S. Scherer, L. J. Chamberlain, and S. Singh, "Navigation and control for micro aerial vehicles in GPS-denied environments," 2011.
- [92] S. Bouabdallah and R. Siegwart, "Full control of a quadrotor," in *Intelligent robots and systems, 2007. IROS 2007. IEEE/RSJ international conference on*. IEEE, 2007, pp. 153–158.
- [93] T. Bresciani, "Modelling, identification and control of a quadrotor helicopter," *MSc Theses*, 2008.
- [94] M. De Lellis and C. De Oliveira, "Modeling, identification and control of a quadrotor aircraft," *Czech Technical University, Praga*, 2011.
- [95] T. L. Chow, *Classical mechanics*. CRC Press, 2013.
- [96] H. Goldstein, C. P. Poole, and J. L. Safko, *Classical Mechanics: Pearson New International Edition*. Pearson Higher Ed, 2014.
- [97] A. A. White and R. Bromley, "Dynamically consistent, quasi-hydrostatic equations for global models with a complete representation of the coriolis force," *Quarterly Journal of the Royal Meteorological Society*, vol. 121, no. 522, pp. 399–418, 1995.
- [98] F. D. Bianchi, R. J. Mantz, and H. De Battista, *The Wind and Wind Turbines*. Springer, 2007.
- [99] G. M. Hoffmann, H. Huang, S. L. Waslander, and C. J. Tomlin, "Quadrotor helicopter flight dynamics and control: Theory and experiment," in *Proc. of the AIAA Guidance, Navigation, and Control Conference*, vol. 2, 2007, p. 4.
- [100] UnmannedTech.co.uk. (2014) 2014 3DR quad kit. [Online]. Available: <http://www.unmannedtechshop.co.uk/arducopter-3dr-quad-diy-frame>
- [101] B. Erginer and E. Altug, "Modeling and PD control of a quadrotor vtol vehicle," in *Intelligent Vehicles Symposium, 2007 IEEE*. IEEE, 2007, pp. 894–899.

- [102] J. Stowers, M. Hayes, and A. Bainbridge-Smith, "Altitude control of a quadrotor helicopter using depth map from microsoft kinect sensor," in *Mechatronics (ICM), 2011 IEEE International Conference on*. IEEE, 2011, pp. 358–362.
- [103] J. Li and Y. Li, "Dynamic analysis and PID control for a quadrotor," in *Mechatronics and Automation (ICMA), 2011 International Conference on*. IEEE, 2011, pp. 573–578.
- [104] K. W. Weng and M. Abidin, "Design and control of a quad-rotor flying robot for aerial surveillance," in *Research and Development, 2006. SCORed 2006. 4th Student Conference on*. IEEE, 2006, pp. 173–177.
- [105] A. Tayebi and S. McGilvray, "Attitude stabilization of a vtol quadrotor aircraft," *Control Systems Technology, IEEE Transactions on*, vol. 14, no. 3, pp. 562–571, 2006.
- [106] P. Castillo, R. Lozano, and A. Dzul, "Stabilization of a mini rotorcraft with four rotors," *IEEE Control Systems Magazine*, vol. 25, no. 6, pp. 45–55, 2005.
- [107] I. D. Cowling, J. F. Whidborne, and A. K. Cooke, "Optimal trajectory planning and LQR control for a quadrotor uav," in *UKACC International Conference on Control*, 2006.
- [108] S. L. Waslander, G. M. Hoffmann, J. S. Jang, and C. J. Tomlin, "Multi-agent quadrotor testbed control design: Integral sliding mode vs. reinforcement learning," in *Intelligent Robots and Systems, 2005.(IROS 2005). 2005 IEEE/RSJ International Conference on*. IEEE, 2005, pp. 3712–3717.
- [109] E. Reyes-Valeria, R. Enriquez-Caldera, S. Camacho-Lara, and J. Guichard, "LQR control for a quadrotor using unit quaternions: Modeling and simulation," in *Electronics, Communications and Computing (CONIELECOMP), 2013 International Conference on*. IEEE, 2013, pp. 172–178.
- [110] T. Madani and A. Benallegue, "Backstepping control for a quadrotor helicopter," in *Intelligent Robots and Systems, 2006 IEEE/RSJ International Conference on*. IEEE, 2006, pp. 3255–3260.
- [111] H. Voos, "Nonlinear control of a quadrotor micro-UAV using feedback-linearization," in *Mechatronics, 2009. ICM 2009. IEEE International Conference on*. IEEE, 2009, pp. 1–6.
- [112] C. Nicol, C. Macnab, and A. Ramirez-Serrano, "Robust adaptive control of a quadrotor helicopter," *Mechatronics*, vol. 21, no. 6, pp. 927–938, 2011.
- [113] Z. T. Dydek, A. M. Annaswamy, and E. Lavretsky, "Adaptive control of quadrotor uavs: A design trade study with flight evaluations," *IEEE Transactions on control systems technology*, vol. 21, no. 4, pp. 1400–1406, 2013.
- [114] C. Coza and C. Macnab, "A new robust adaptive-fuzzy control method applied to quadrotor helicopter stabilization," in *Fuzzy Information Processing Society, 2006. NAFIPS 2006. Annual meeting of the North American*. IEEE, 2006, pp. 454–458.
- [115] Z. T. Dydek, A. M. Annaswamy, and E. Lavretsky, "Adaptive control of quadrotor uavs in the presence of actuator uncertainties," *AIAA Infotech Aerospace*, pp. 20–22, 2010.

- [116] N. A. Ofodile and M. C. Turner, "Decentralized approaches to antiwindup design with application to quadrotor unmanned aerial vehicles," *IEEE Transactions on Control Systems Technology*, vol. Volume:24, no. Issue: 6, pp. 1980–1992, November 2016.
- [117] C. Edwards and I. Postlethwaite, "Anti-windup and bumpless-transfer schemes," *Automatica*, vol. 34, no. 2, pp. 199–210, 1998.
- [118] N. A. Ofodile, M. C. Turner, and O. C. Ubadike, "Channel-by-channel anti-windup design for a class of multivariable systems," in *American Control Conference (ACC)*, 2015.
- [119] K.-P. Sondergeld, "A generalization of the routh-hurwitz stability criteria and an application to a problem in robust controller design," *IEEE transactions on automatic control*, vol. 28, no. 10, pp. 965–970, 1983.
- [120] A. G. MacFarlane and I. Postlethwaite, "The generalized nyquist stability criterion and multivariable root loci," *International Journal of Control*, vol. 25, no. 1, pp. 81–127, 1977.
- [121] F. Nori, "Bibo stability and asymptotic stability," *system*, vol. 1, p. x2.
- [122] R. W. Brockett *et al.*, "Asymptotic stability and feedback stabilization," *Differential geometric control theory*, vol. 27, no. 1, pp. 181–191, 1983.
- [123] C. A. Desoer, *Notes for a second course on linear systems*. Van Nostrand Reinhold, 1970.
- [124] R. Z. Khas' minskii, "Necessary and sufficient conditions for the asymptotic stability of linear stochastic systems," *Theory of Probability & Its Applications*, vol. 12, no. 1, pp. 144–147, 1967.
- [125] H. K. Khalil, "Nonlinear systems, 3rd," *New Jersey, Prentice Hall*, vol. 9, 2002.
- [126] H. J. Marquez, *Nonlinear Control Systems: Analysis and Design*. John Wiley & Sons, Inc, 2003.
- [127] H. Nijmeijer and A. Van der Schaft, *Nonlinear dynamical control systems*. Springer Science & Business Media, 2013.
- [128] R. E. Kalman and J. E. Bertram, "Control system analysis and design via the second method of lyapunov: continuous-time systems," *Journal of Basic Engineering*, vol. 82, no. 2, pp. 371–393, 1960.
- [129] A. Teel, T. Georgiou, L. Praly, and E. Sontag, "Input-output stability," *The Control Handbook, CRC Press, Boca Raton, FL*, pp. 895–908, 1996.
- [130] A. Van der Schaft, *L2-gain and passivity techniques in nonlinear control*. Springer Science & Business Media, 2012.
- [131] H. K. Khalil and J. Grizzle, *Nonlinear systems*. Prentice hall New Jersey, 1996, vol. 3.
- [132] D. G. Bates and I. Postlethwaite, "The structured singular value and μ -analysis," in *Advanced Techniques for Clearance of Flight Control Laws*. Springer, 2002, pp. 37–55.
- [133] K. Michels, F. Klawonn, R. Kruse, and A. Nürnberger, *Fuzzy control: fundamentals, stability and design of fuzzy controllers*. Springer, 2007, vol. 200.

- [134] S. P. Buerger, “Stable, high-force, low-impedance robotic actuators for human-interactive machines,” Ph.D. dissertation, Massachusetts Institute of Technology, 2005.
- [135] W. M. Haddad and D. S. Bernstein, “Explicit construction of quadratic lyapunov functions for the small gain, positivity, circle, and popov theorems and their application to robust stability. part i: Continuous-time theory,” *International Journal of Robust and Nonlinear Control*, vol. 3, no. 4, pp. 313–339, 1993.
- [136] V. A. Yakubovich, “S-procedure in nonlinear control theory,” *Vestnik Leningrad University*, vol. 1, pp. 62–77, 1971.
- [137] O. Brieger, M. Kerr, I. Postlethwaite, J. Sofrony, and M. C. Turner, “Flight testing of low-order anti-windup compensators for improved handling and PIO suppression,” in *American Control Conf.*, 2008, pp. 1776–1781.
- [138] S. Gayadeen and S. Duncan, “Anti-windup compensation for electron beam stabilisation control systems on synchrotrons with rate constrained actuators,” in *European Control Conf.*, 2013, pp. 2752–2757.
- [139] S. Bouabdallah, P. Murrieri, and R. Siegwart, “Design and control of an indoor micro quadrotor,” in *Robotics and Automation, 2004. Proceedings. ICRA'04. 2004 IEEE International Conference on*, vol. 5. IEEE, 2004, pp. 4393–4398.
- [140] M. Cutler, N. K. Ure, B. Michini, and J. P. How, “Comparison of fixed and variable pitch actuators for agile quadrotors,” in *AIAA Conf. on Guidance, Navigation and Control, Portland, OR*, 2011.
- [141] M. Orsag, M. Poropat, and S. Bogdan, “Hybrid fly-by-wire quadrotor controller,” in *2010 IEEE International Symposium on Industrial Electronics (ISIE)*, 2010, pp. 202–207.
- [142] A. Adegbege and W. Heath, “Internal model control design for input-constrained multi-variable processes,” *AIChE Journal*, vol. 57, pp. 3459–3472, 2011.
- [143] C. F. V. Loan, “The ubiquitous kronecker product,” *Journal of computational and applied mathematics*, vol. 123, no. 1, pp. 85–100, 2000.
- [144] G. Li, G. Herrmann, D. P. Stoten, J. Tu, and M. C. Turner, “Application of robust anti-windup techniques to dynamically substructured systems,” *Mechatronics, IEEE/ASME Transactions on*, vol. 18, no. 1, pp. 263–272, 2013.
- [145] P. M. Dower, C. M. Kellett, and H. Zhang, “A weak L_2 -gain property for nonlinear systems,” in *Decision and Control (CDC), 2012 IEEE 51st Annual Conference on*. IEEE, 2012, pp. 2286–2291.
- [146] R. W. Beard and T. W. McLain, *Small unmanned aircraft: Theory and practice*. Princeton university press, 2012.
- [147] M. V. Cook, *Flight dynamics principles: a linear systems approach to aircraft stability and control*. Butterworth-Heinemann, 2012.

- [148] P. C. Garcia, R. Lozano, and A. E. Dzul, *Modelling and control of mini-flying machines*. Springer Science & Business Media, 2006.
- [149] S. Farokhi, *Aircraft propulsion*. John Wiley & Sons, 2014.
- [150] B. L. Stevens, F. L. Lewis, and E. N. Johnson, *Aircraft Control and Simulation: Dynamics, Controls Design, and Autonomous Systems*. John Wiley & Sons, 2015.
- [151] H. Goldstein, *Classical mechanics*. Pearson Education India, 1965.
- [152] R. J. Adams, J. M. Buffington, A. G. Sparks, and S. S. Banda, *Robust multivariable flight control*. Springer Science & Business Media, 2012.
- [153] J. F. Whidborne, *AVMS- The Aerosonde Model*, Cranfield University, January 2010.
- [154] J. Y.-C. Hung, “Investigation of methods for increasing the energy efficiency on unmanned aerial vehicles (UAVs),” 2011.
- [155] F. Bateman, H. Noura, and M. Ouladsine, “Fault diagnosis and fault-tolerant control strategy for the aerosonde uav,” *IEEE Transactions on Aerospace and Electronic Systems*, vol. 47, no. 3, pp. 2119–2137, 2011.
- [156] M. S. Anon, “Flying qualities of piloted airplanes,” *Department of Defense Handbook Flying Qualities of Piloted Aircraft*, 1980.
- [157] J. S. Jang and C. Tomlin, “Longitudinal stability augmentation system design for the dragonfly UAV using a single GPS receiver,” in *AIAA Guidance, Navigation, and Control Conference, AIAA*, vol. 5592, 2003.
- [158] D. Dusha, W. W. Boles, and R. Walker, “Fixed-wing attitude estimation using computer vision based horizon detection,” 2007.
- [159] S. A. Frost, B. R. Taylor, C. V. Jutte, J. J. Burken, K. V. Trinh, and M. Bodson, “A framework for optimal control allocation with structural load constraints,” in *AIAA Atmospheric Flight Mechanics Conference*, 2010, p. 8112.
- [160] E. N. Johnson and S. K. Kannan, “Adaptive flight control for an autonomous unmanned helicopter,” in *AIAA Guidance, Navigation and Control Conference*, vol. 11. Monterey, CA: AIAA, 2002.
- [161] A. Dorobantu, A. Murch, B. Mettler, and G. Balas, “System identification for small, low-cost, fixed-wing unmanned aircraft,” *Journal of Aircraft*, vol. 50, no. 4, pp. 1117–1130, 2013.
- [162] G. Chowdhary, E. N. Johnson, R. Chandramohan, M. S. Kimbrell, and A. Calise, “Guidance and control of airplanes under actuator failures and severe structural damage,” *Journal of Guidance, Control, and Dynamics*, vol. 36, no. 4, pp. 1093–1104, 2013.
- [163] Y. Shtessel, J. Buffington, and S. Banda, “Tailless aircraft flight control using multiple time scale reconfigurable sliding modes,” *IEEE Transactions on Control Systems Technology*, vol. 10, no. 2, pp. 288–296, 2002.

- [164] R. W. Beard, D. Kingston, M. Quigley, D. Snyder, R. Christiansen, W. Johnson, T. McLain, and M. Goodrich, "Autonomous vehicle technologies for small fixed-wing UAVs," *Journal of Aerospace Computing, Information, and Communication*, vol. 2, no. 1, pp. 92–108, 2005.
- [165] M. C. Turner, G. Herrmann, and I. Postlethwaite, "Anti-windup compensation using a decoupling architecture," in *Advanced Strategies in Control Systems with Input and Output Constraints*. Springer, 2007, pp. 121–171.
- [166] M. C. Turner and D. G. Bates, "Mathematical methods for robust and nonlinear control," *Book series on control systems*. Springer, Berlin, 2007.
- [167] A. Lekka, M. C. Turner, and P. P. Menon, "Full and reduced order IMC anti-windup compensators for a class of nonlinear systems with application to wave energy converter control," in *2013 American Control Conference*. IEEE, 2013, pp. 4861–4866.
- [168] P. March and M. C. Turner, "Anti-windup compensator designs for nonsalient permanent-magnet synchronous motor speed regulators," *IEEE Transactions on Industry Applications*, vol. 45, no. 5, pp. 1598–1609, 2009.
- [169] B. Kada and Y. Ghazzawi, "Robust PID controller design for an UAV flight control system," in *Proceedings of the World Congress on Engineering and Computer Science*, vol. 2, 2011, pp. 19–21.
- [170] S. Park, D. Won, M. Kang, T. Kim, H. Lee, and S. Kwon, "RIC (robust internal-loop compensator) based flight control of a quad-rotor type uav," in *2005 IEEE/RSJ International Conference on Intelligent Robots and Systems*. IEEE, 2005, pp. 3542–3547.
- [171] S. Sieberling, Q. Chu, and J. Mulder, "Robust flight control using incremental nonlinear dynamic inversion and angular acceleration prediction," *Journal of Guidance, Control, and Dynamics*, vol. 33, no. 6, pp. 1732–1742, 2010.
- [172] J. Kim, M.-S. Kang, and S. Park, "Accurate modeling and robust hovering control for a quad-rotor vtol aircraft," in *Selected papers from the 2nd International Symposium on UAVs, Reno, Nevada, USA June 8–10, 2009*. Springer, 2009, pp. 9–26.
- [173] R. M. Morales, G. Li, and W. P. Heath, "Anti-windup and the preservation of robustness against structured norm-bounded uncertainty," *IFAC Proceedings Volumes*, vol. 41, no. 2, pp. 14 144–14 149, 2008.
- [174] S. I. Al Swailem, "Application of robust control in unmanned vehicle flight control system design," 2004.
- [175] K. Rudin, M.-D. Hua, G. Ducard, and S. Bouabdallah, "A robust attitude controller and its application to quadrotor helicopters," *IFAC Proceedings Volumes*, vol. 44, no. 1, pp. 10 379–10 384, 2011.
- [176] W. Ren, R. W. Beard, and E. M. Atkins, "A survey of consensus problems in multi-agent coordination," in *Proceedings of the 2005, American Control Conference, 2005*. IEEE, 2005, pp. 1859–1864.

-
- [177] W. Ren and R. W. Beard, "Trajectory tracking for unmanned air vehicles with velocity and heading rate constraints," *IEEE Transactions on Control Systems Technology*, vol. 12, no. 5, pp. 706–716, 2004.
- [178] M. T. DeGarmo, "Issues concerning integration of unmanned aerial vehicles in civil airspace," *The MITRE Corporation Center for Advanced Aviation System Development*, 2004.